ALBA

ALBA Synchrotron - Carrer de la Llum 2-26
08290 Cerdanyola del Vallès, Barcelona, Spain - Tel: +34 93 592 43 00 - www.albasynchrotron.es

2015 ACTIVITY REPORT ALBA

ALBA

2015
ACTIVITY REPORT

2015

ACTIVITY REPORT

ALBA Synchrotron
Carrer de la Llum 2-26
08290 Cerdanyola del Vallès (Barcelona)
Spain
Tel. +34 93 592 4300

Editors: Salvador Ferrer and Ana Belén Martínez

We'd like to thank the contributors who participate in this publication: Lucía Aballe, Marta Ávila, Olivier Boulle, Josep Campmany, Carles Colldelram, François Fauth, David Fernández, Salvador Ferrer, Michael Foerster, Mª José García, Laura García, Maria José García, José Luis García-Muñoz, Jorge Gascon, Javier Herrero-Martín, Jordi Juanhuix, José López Carrascosa, Jordi Marcos, Rubén Martínez Buey, Cristina Massa, Valentí Massana, Óscar Matilla, Jairo Moldes, Lionel Mourey, Josep Nicolàs, Ángel Olmos, Maria Rosa Palacín, Francis Pérez, Montse Pont, Trinitat Pradell, Jordi Puiggalí, Claude Ruget, Alejandro Sánchez, Xavier Serra, Massimo Tallarida, Núria Valls, Lada Yashina, Ibraheem Yousef.

Graphic design: Lucas Wainer

Printing: JM Gràfic

CONTENTS

FOREWORD

Dear reader,

You will find in this report a brief extract of the many activities in which the ALBA team and its users have been involved during 2015.

The operation of the facility is now consolidated. A new group of Floor Coordinators has joined the operation team, reinforcing the user support capabilities. The accelerator availability is still increasing, and 97% in excess has been reached. We are still operating at an electron current lower than the nominal one: still struggling with the radio frequency power IOTs reliability we have chosen to privilege the stability with respect to the current. Nevertheless, during the year the peak current has been increased by 50%.

Two user calls have been published, and the recurrent calendar of our user activity has been defined for the future. We have now statistics enough to start looking at evolution trends, and we can say that the international representation has doubled from the first beamtime in 2012, and that the number of our industrial users has more than doubled with respect to 2014.

We have extracted a few scientific highlights as a representation of the results obtained by the one thousand user visits that we received. Among them you can find investigations opening the way to new therapies, carried out at the macromolecular crystallography beamline XALOC and at the soft X-ray microscope MISTRAL, studies for the design of new catalysts carried out at the absorption and emission spectroscopy beamline CLÆSS, projects devoted to magnetic properties of different materials at MISTRAL, at the photoemission spectroscopy beamline CIRCE and using the dichroism techniques of BOREAS, research on the chemical properties of materials related to alternative energy sources and batteries at CIRCE and at the powder diffraction beamline MSPD, and of biodegradable polyesters at the SAXS beamline NCD. Conservation of historic grisailles is the aim of the investigation carried out at MSPD.

While exploiting the Phase-I beamlines, Phase-II is progressing: the installation of the ALBA eighth beamline, MIRAS, devoted to infrared spectroscopy, has been almost completed during the Christmas shutdown, and will be ready to start operation in fall 2016. The design of LOREA, low-energy angular resolved photoemission with ultra-high resolution, is ready and first calls for tender have been launched.

The decision of starting the first beamline of Phase-III has been taken at the end of the year. It will be a microfocus macromolecular crystallography beamline which will expand the capacity in terms of resolution for very small crystals of the large structural biology national community.

Participation to national and international projects, very often in collaboration with other institutions, is enriching our capacities and increasing our staff. I want to mention here the recent incorporation of nine young people in different areas of the infrastructure thanks to a program from MINECO for young employment. And speaking of young people at ALBA, let me express my satisfaction as I witness the student program progressing year by year, with a group of undergraduate, vocational training and PhD students sharing our activities and preparing themselves for the future.

Health and Safety group activity, on top of every day control on safety issues for staff, users and visitors, has continued developing the protocols, best practices, and an intensive training program for all staff on the many different aspects of the safety rules and their compliance.

2015 was designated by the UNESCO as the International Year of Light and Light-based Technologies to show the society how light directly affects every aspect of our lives. ALBA has been participating to several outreach activities in Spain and in international events, increasing the awareness of many people on the necessity of supporting the research for a sustainable and solidary world.

I wish you to enjoy the reading,
Sincerely

Caterina Biscari
Director

THE ALBA SYNCHROTRON

ALBA is the Spanish 3rd generation synchrotron light source, located in Cerdanyola del Vallès, near Barcelona, and constitutes the largest scientific infrastructure in the country. The facility consists of the accelerator systems providing 3 GeV electron beam and several experimental beamlines, with photon energies currently ranging from infrared up to hard X-rays of tens of KeV. Different synchrotron radiation techniques are available including diffraction, spectroscopies and imaging.

The ALBA project was approved in 2003 and funded in equal parts by the Spanish and Catalan governments. It is managed by CELLS (Consortium for the Construction, Equipping and Exploitation of the Synchrotron Light Source).

ALBA was built on a green field next to the Universitat Autònoma de Barcelona and several research centres in the Bellaterra campus. The construction began in 2006, after few years dedicated to the design and to the training of a new team of experts, coming from Spain and abroad. The building and the services were ready by 2009, when the accelerator installation started. The whole accelerator was ready and commissioned by 2011, and the seven first beamlines were installed and commissioned in 2011-12. First official users were hosted in May 2012, and in February 2013 all the Phase I beamlines were operational.

The accelerators

The accelerator system consists of a linear accelerator (Linac) - where electrons reach 100 MeV-, a low-emittance, full-energy Booster - where electrons are accelerated to 3GeV-, and the Storage Ring - where electrons are injected in top-up operation mode-. The Booster (250 m of circumference) and the Storage Ring (269 m) are both hosted in the same tunnel. The lattice is optimized for high photon flux density, with a nominal current of 250 mA. There is a large number of straight sections (24) available, despite the relatively short circumference, thanks to the very compact lattice design, which incorporates quadrupolar field component in the dipoles.

The vacuum chamber has up to 34 windows for the light extraction. Eleven of them are presently used (2 for accelerator diagnostics, 9 for the Phase-I and Phase-II Beamlines), and the others witness the large potentiality of ALBA for the future.

The beamlines

ALBA is in operation since May 2012 with seven beamlines dedicated to different scientific fields, mainly physics, chemistry, life sciences, materials science, cultural heritage, biology, nanotechnology. Two new beamlines were initiated in 2014, devoted to infrared microspectroscopy and angle-resolved photoemission spectroscopy. These beamlines are expected to receive users by the end of 2016 and 2018, respectively.

Below, the list of Phase-I and Phase-II beamlines describing the number of endstations, the experimental techniques and their scientific applications is shown.

PORT	BEAMLINE	ENDSTATIONS	EXPERIMENTAL TECHNIQUES	SCIENTIFIC APPLICATIONS
4	MSPD	2	High resolution powder diffraction Microdiffraction including high pressure	Structure of materials, Time resolved diffraction Quantitative phase analysis
9	MISTRAL	1	Soft X-ray full field transmission X-ray microscopy. Optimized on the 'water window'	Cryogenic tomography of biological objects. Spatially resolved spectroscopy
11	NCD	1	High resolution small and high angle X-ray scattering/diffraction	Structure and phase transformations of biological fibres, polymers, solutions. Time resolved X-ray studies
13	XALOC	1	X-ray diffraction from crystals of biological macromolecules	Macromolecular crystallography, with particular emphasis on large unit cell crystals
22	CLÆSS	2	EXAFS, XANES, Quick-EXAFS, XES	Material science, chemistry, time resolved studies
24	CIRCE	2	Photoemission microscopy (PEEM) Near atmospheric pressure photo-emission (NAPP)	Nano-science and magnetic domain imaging (PEEM). Surface chemistry (NAPP)
29	BOREAS	2	Circular Magnetic Dichroism Resonant Magnetic Diffraction	Magnetism, surface magnetism and magnetic structures
01	MIRAS	1	Infrared microspectroscopy	Life sciences, Food sciences, Materials science
20	LOREA	1	Angle-resolved photoemission spectroscopy	Polarized electron spectroscopies, band structure determination

BIOSCIENCES

Scientific activities in bioscience-related beamlines at ALBA are well consolidated in the macromolecular crystallography (BL13-XALOC) and the Soft X-ray microscopy (BL9-MISTRAL) beamlines, and are also growing in the Non-crystalline diffraction beamline (BL11-NCD).

Two examples come from the structural biology field. One is the study of the structure of a key enzyme, Uhgb_MP, required for the degradation of the sugars containing nitrogen and the dietary fibres. Failure of the correct degradation may lead to Crohn's disease and other problems. The enzyme structure was solved with and without the substrate, leading to a better understanding of the mechanism. Interestingly, this enzyme may also be used in the process of converting hemicellulose into compounds with high added value. The second example is the elucidation of the regulation mechanism of the purine nucleotide metabolism. A key enzyme involved in this process, the IMPDH, is widely studied as a therapeutic target, but little was known about its regulation until now. Unravelling the mechanism will allow differentiating the target eukaryotic and prokaryotic IMPDHs. Moreover, the molecular basis of several mutations has been found, paving the way to new therapeutic approaches to related diseases, such as human retinopathies.

One more example shows the science on biology that cryo-soft X-ray microscopy technique may offer at the MISTRAL beamline. Nanoparticles are becoming important in nano-biotechnology and nanomedicine for hyperthermia treatment against tumours, drug delivery and image diagnosis. We refer to an experiment in which quantitative information is extracted from superparamagnetic iron oxide nanoparticles attached to acidic vesicles in breast cancer cells. The spatial distribution, number and size of these vesicles were monitored in 3D at 60 nm resolution in close-to-native conditions. The accurate determination of the intracellular mass and density of the nanoparticles was also possible by calculating the differential absorption before and in an iron absorption edge. Overall, the system could only be studied using cryo-soft X-ray tomography, electron and light microscopy techniques.

The beamlines dedicated to biosciences will continue to provide efficient, flexible and world-class service to our diverse user community. In addition to the currently implemented capabilities, the activities in biosciences will nevertheless be boosted in 2016 by the forthcoming user operation of the infrared beamline (BL1-MIRAS).

X-ray structure of the mannoside-phosphorylase Uhgb_MP: an enzyme related with N-glycan processing

Structural bases for N-glycan processing by mannoside-phosphorylase.
***Acta Crystallographica Section* D 71:1335-46 (2015)**

Simon Ladevèze[1,2,3], Gianluca Cioci[1,2,3], Pierre Roblin[4], Lionel Mourey[5,6], Samuel Tranier[5,6]* and Gabrielle Potocki-Véronèse[1,2,3]*

Researchers conducted metagenomic studies on the human gut microbiota and characterized a new carbohydrate active enzyme involved in N-glycan as well as dietary fibres degradation. They solved the X-ray structures of this protein alone and in complex with mannose and/or N-acetylglucosamine.

N-linked glycans are present in many living organisms and play a key role in cell signalling and recognition, protein stability and activity tuning. In eukaryotes, the common core structure of N-glycans is composed of the β-D-Manp-1,4-β-D-Glc*p*NAc-1,4-D-Glc*p*NAc (Man-GlcNAc2) trisaccharide. To date, little is known about the degradation pathway of human N-glycans, especially by bacteria or fungi. Huge efforts have been made in recent years to understand exactly how this hydrolytic process takes place, particularly among gut inhabitants, as the alteration of host glycans by microbes is thought to be related to intestinal disorders such as Crohn's disease and other inflammatory bowel diseases (IBDs).

In order to metabolize both dietary fibre constituent carbohydrates and host glycans lining the intestinal epithelium, gut bacteria produce a wide range of carbohydrate active enzymes, of which glycoside hydrolases are the main components. Among them, Uhgb_MP is a mannoside phosphorylase catalyzing the phosphorolysis (i.e. the attack by inorganic phosphate) of the terminal mannosyl residue of the β-D-Manp-1,4-β-D-Glc*p*NAc-1,4-D-Glc*p*NAc core of N-glycans. This enzyme, belonging to the GH130_2 subfamily of glycoside hydrolases according to the CAZY classification (http://www.cazy.org/; [1]), is also highly efficient to catalyze the synthesis of this N-glycan core trisaccharide by reverse-phosphorolysis.

Its crystal structure was solved by X-ray crystallography in the presence of inorganic phosphate alone or in complex with, mannose and/or N-acetylglucosamine. Diffraction data were collected to a resolution between 1.6 and 1.94 Å either at the ESRF synchrotron (ESRF, Grenoble, France) for the native structure or at the XALOC beamline of the ALBA Synchrotron (Cerdanyola del Vallès, Spain) for all the complexes. The overall structure of Uhgb-MP revealed a five-bladed β-propeller fold of each protomer with a homohexameric organization consisting of a trimer of dimers (Figure 1A). This hexameric organization was confirmed in solution by SEC-MALS and SAXS experiments without detecting any lower oligomeric state.

Interestingly, a large conformational change was observed in the Uhgb_MP structures upon mannose binding in the -1 subsite. This allows Asn44 to flip in order to allow direct interaction of its side chain with the C3 and C4 hydroxyls of the mannose which is stabilized in a stressed $B_{2,5}$ boat conformation (Figure 1B). The side chain of the catalytic residue Asp104 is also moved towards mannose and stabilized by the flipped Asn44 in

order to interact with the mannose C3 hydroxyl, which acts as a proton relay from the catalytic Asp104 to the *N*-acetylglucosamine O4 during catalysis (Figure 1C), as previously described by Nakae et al. for the *Bf*MGP protein which belongs to the GH130_1 subfamily [2].

The structure of Uhgb-MP is the first structure of a phosphorolytic enzyme participating in N-glycan degradation, in its apo form and in complex with mannose and N-acetylglucosamine, and the first structure of a characterized enzyme belonging to the GH130_2 subfamily.

As previously shown, genes coding for GH130_2 enzymes are highly prevalent in the gut metagenomes of IBD patients. This makes these enzymes promising targets to develop new drugs and these three-dimensional structures are a first stage in the structure-based drug design of potential specific GH130_2 inhibitors.

This work is also of great biotechnological interest, as it provides insight into the conversion of hemicellulose into compounds with high added value.

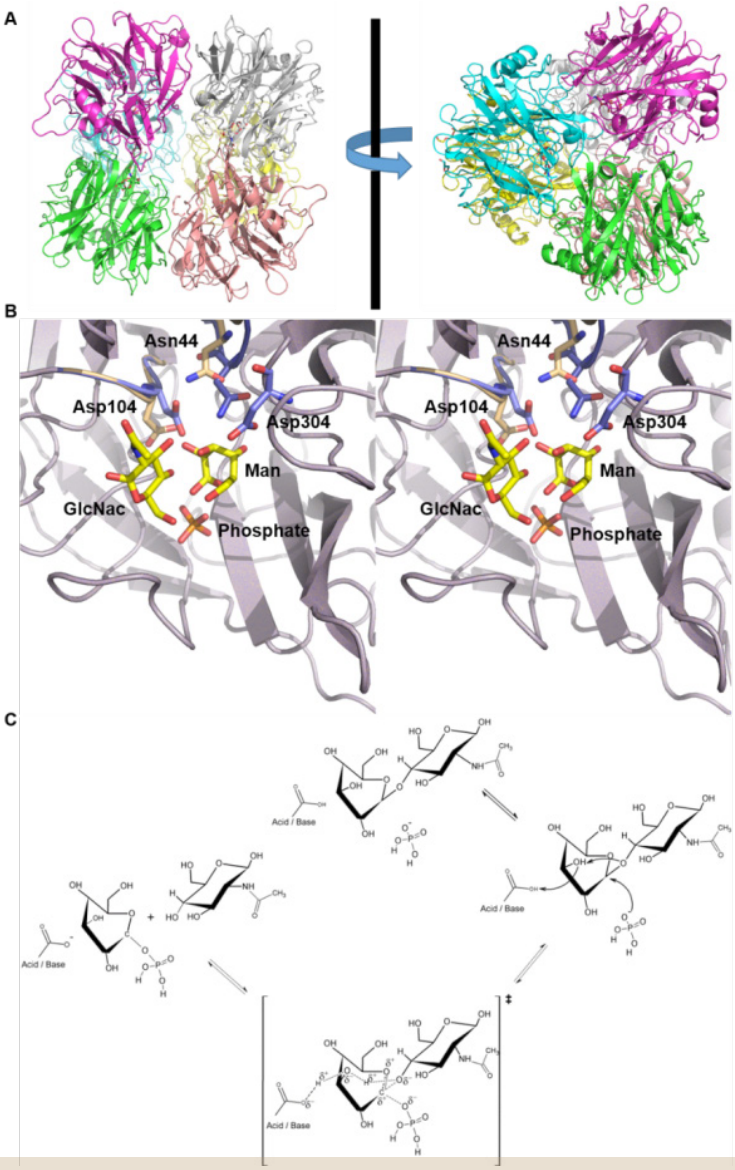

Figure 1: A/ Ribbon representation of Uhgb_MP homohexameric quaternary structure. B/ Stereoview of the alternative conformations of Asn44, and the catalytic Asp104 upon mannose (Man) binding in the -1 subsite. The catalytic site also contains a N-acetylglucosamine (GlcNac) molecule in the +1 subsite and the phosphate ion responsible for the phosphorolysis reaction. C/ Catalytic mechanism proposed for β-D-Manp-1,4-D-GlcpNAc phosphorolysis by Uhgb_MP.

ACKNOWLEDGEMENTS

This work was supported by the French Ministry of Higher Education and Research and by the French National Institute for Agricultural Research.

OTHER REFERENCES

[1] Lombard, V., Golaconda Ramulu, H., Drula, E., Coutinho, P. M. & Henrissat, B. (2014). ***Nucleic Acids Res.*** 42:D490–95.

[2] Nakae, S., Ito, S., Higa, M., Senoura, T., Wasaki, J., Hijikata, A.,Shionyu, M., Ito, S. & Shirai, T. (2013). ***J. Mol. Biol.*** 425:4468–78.

AFFILIATION:

1. Université de Toulouse; INSA, UPS, INP; LISBP, 135 Avenue de Rangueil, 31077 Toulouse, France,
2. CNRS, UMR5504, 31400 Toulouse, France
3. INRA, UMR792 Ingénierie des Systèmes Biologiques et des Procédés, 31400 Toulouse, France
4. Synchrotron SOLEIL, L'Orme des Merisiers, BP 48, Saint Aubin, 91192 Gif-sur-Yvette CEDEX, France
5. Institut de Pharmacologie et de Biologie Structurale (IPBS), Centre National de la Recherche Scientifique (CNRS), 205 Route de Narbonne, BP 64182, 31077 Toulouse, France
6. Université de Toulouse, Université Paul Sabatier, IPBS, 31077 Toulouse, France

Deciphering the allosteric regulation mechanisms of IMP dehydrogenases

Guanine nucleotide binding to the Bateman domain mediates the allosteric inhibition of eukaryotic IMP dehydrogenases. *Nature Communications* 6, 8923 (2015)

Rubén M. Buey[1], Rodrigo Ledesma-Amaro[1], Adrián Velázquez-Campoy[2], Mónica Balsera[3], Mónica Chagoyen[4], José M. de Pereda[5] and José L. Revuelta[1]

This work sheds light on the mechanisms of the allosteric regulation of enzymes mediated by Bateman domains and provides a molecular basis for certain retinopathies, opening the door to new therapeutic approaches.

Inosine-5'-monophosphate dehydrogenase (IMPDH) plays key roles in purine nucleotide metabolism and cell proliferation. Although IMPDH is a widely studied therapeutic target, there is limited information about its physiological regulation. Using the industrial fungus *Ashbya gossypii* as a model, researchers have deciphered the molecular mechanisms and the structural basis for the allosteric regulation of IMPDH by guanine nucleotides. Data suggest that eukaryotic and prokaryotic IMPDHs might have developed different regulatory mechanisms, opening the door to a promising unexplored strategy to differentially target eukaryotic and prokaryotic IMPDHs. Moreover, several mutations associated with human retinopathies map into the guanine nucleotide binding sites and disrupt allosteric inhibition. Therefore, the results provide a molecular basis for these pathologies and pave the road to new therapeutic approaches.

Purine nucleotides are essential molecules for the cell. They not only constitute the building blocks of nucleic acids but also play central roles in metabolism, become incorporated into enzyme cofactors, represent the energy source for translation and microtubule polymerization, and take part in signal transduction, angiogenesis and axon guidance.

Inosine 5´-monophosphate dehydrogenase (IMPDH) is a key enzyme in the regulation of the cellular pools of purine nucleotides. It catalyzes the oxidation of IMP into XMP with the concomitant reduction of NAD^+ to NADH, which is the rate-limiting step in the *de novo* guanine nucleotide biosynthesis. IMPDH plays crucial roles in cell division and viability and, in fact, is the target of a diverse number of drugs widely used at present in clinical chemotherapy as immunosupressors, antivirals, antitumorals or antibiotics [1].

IMPDHs have an archetypal structure composed of a catalytic TIM barrel and a regulatory domain; the latter inserted within a loop of the catalytic domain and representing a Bateman domain. Up to date, all drugs targeting IMPDH target the active site, either in the IMP or the NADPH binding sites and inhibit catalytic activity, limiting the *de novo* synthesis of guanine nucleotides. The immediate consequence is that the guanine nucleotide pool inside the cell is drastically reduced and cells enter into a quiescent state, accounting for its anti-proliferative effect [2].

Although IMPDH is a widely studied therapeutic target, there is limited information about its physiological regulation. Especially, there is essentially no knowledge regarding the molecular mechanisms responsible for the communication between the Bateman regulatory domain and the catalytic core of IMPDH.

In this work, using *Ashbya gossypii* as a model, the authors have used a structural biology approach, mainly involving X-ray crystallography as well as X-ray small-angle scattering methodologies to decipher the physiological allosteric molecular mechanisms of regulation of IMPDHs.

The authors report that IMPDH is allosterically inhibited by guanine nucleotides that bind to canonical as well as to new non-canonical sites within the Bateman domain, inducing octamers with compromised catalytic activity. This mechanism of allosteric regulation occurs only in eukaryotic IMPDHs, in contrast to prokaryotic IMPDHs whose catalytic activity is unaffected by GTP/GDP. The relevance of this regulatory mechanism is stressed by the fact that most of the mutations in IMPDH associated to severe retinopathies such as retinitis pigmentosa and Leber congenital amaurosis [3] map into the guanine nucleotide binding sites. Therefore, the authors propose that these mutations might deregulate the enzyme, resulting in constitutively activated enzymes. This is, indeed, in perfect agreement with the dominant character of these mutations.

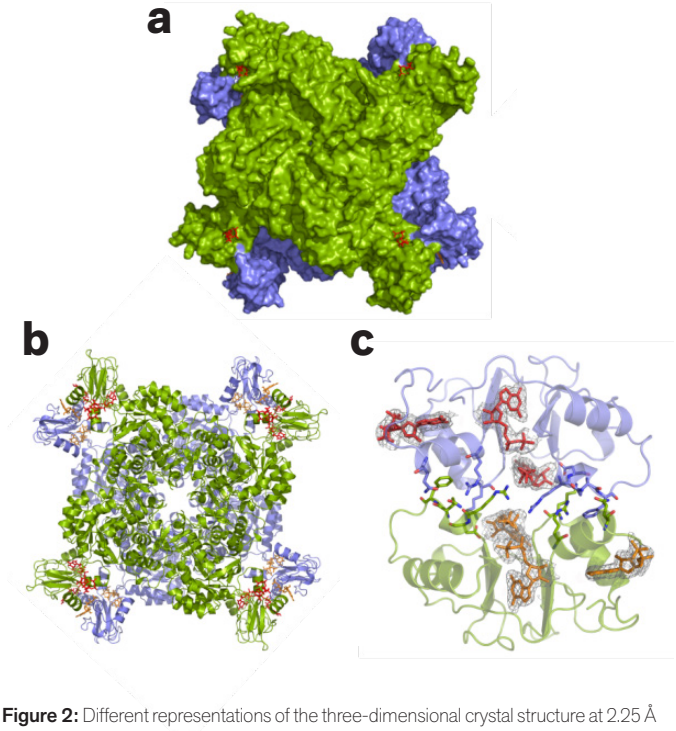

Figure 2: Different representations of the three-dimensional crystal structure at 2.25 Å resolution of the IMPDH enzyme of the fungus *Ashbya gossypii* (AgIMPDH) bound to GDP. A) Surface representation of the octamers, composed of two AgIMPDH tetramers, obtained in the presence of GDP (red and orange sticks). The two tetramers that pile up tail-to-tail are colored green and blue. B) Cartoon representation of the octamers shown in a). C) Detailed view of two interacting Bateman regulatory domains bound to three GDP molecules, using the same color code as in a) and b). The grey meshes around GDP molecules represent the simulated annealing omit 2mFo-DFc electron density maps contoured at the 1σ level.

OTHER REFERENCES

[1] Braun-Sand SB, Peetz M. Inosine monophosphate dehydrogenase as a target for antiviral, anticancer, antimicrobial and immunosuppressive therapeutics. ***Future Medicinal Chemistry* 2**, 81-92, (2010).

[2] Hedstrom L. IMP Dehydrogenase: Structure, Mechanism and Inhibition. ***Chem Rev.* 109**, 2903–2928, (2009).

[3] McGrew DA, Hedstrom L. Towards a pathological mechanism for IMPDH1-linked retinitis pigmentosa. ***Advances in Experimental Medicine and Biology* 723**, 539-545, (2012).

ACKNOWLEDGEMENTS

This work was supported by grant BIO2011-23901 (José Luis Revuelta) and BFU2013-47064-P (Adrián Velázquez-Campoy) from the Spanish Ministry of Economy and Competitiveness, grant B89/Protein Targets Group (Adrián Velázquez-Campoy) from the Government de Aragón and grant FP7-PEOPLE-2011-CIG-293831 (EB-SxIP; Rubén M Buey). Rubén M. Buey is supported by a "Ramón y Cajal" contract from the Spanish Ministry of Economy and Competitiveness. The authors thank María Dolores Sánchez and Silvia Domínguez for their excellent technical help. Protein crystallography experiments were performed at the PXIII (SLS, Switzerland) and XALOC (ALBA Synchrotron, Spain) beamlines with the collaboration of SLS and ALBA staff. X-ray scattering experiments were performed at the P12 beamline in Petra III synchrotron (Hamburg, Germany).

AFFILIATION:

1. Metabolic Engineering Group, Dpto. Microbiología y Genética, Universidad de Salamanca, Salamanca, Spain
2. Institute of Biocomputation and Physics of Complex Systems (BIFI), Joint Unit IQFR-CSIC-BIFI, Universidad de Zaragoza, Zaragoza, Spain; Dept. of Biochemistry and Molecular and Cell Biology, University of Zaragoza, Zaragoza, Spain; Instituto de Investigaciones Sanitarias de Aragón (IIS-A), Zaragoza, Spain; and Fundación ARAID, Government of Aragón, Zaragoza, Spain
3. Dept. Abiotic Stress, Instituto de Recursos Naturales y Agrobiología (IRNASA-CSIC), Salamanca, Spain
4. Computational Systems Biology Group, Centro Nacional de Biotecnología (CNB-CSIC), Madrid, Spain
5. Instituto de Biología Molecular y Celular del Cáncer (ICSIC-Universidad de Salamanca), Salamanca, Spain

Study of interaction of magnetic nanoparticles with cells by correlation of soft X-ray and near-edge absorption tomography

Intracellular nanoparticles mass quantification by near-edge absorption soft X-ray nanotomography. *Scientific Reports* 6; 22354 (2016)
Cryo-soft X-ray tomography as a quantitative three-dimensional tool to model nanoparticle-cell interaction. *Journal of Nanobiotechnology* 3;14(1):15 (2016)

Francisco Javier Chichón[1], José Javier Conesa[1], Joaquín Otón[1], Michele Chiappi[2], Carlos Oscar S. Sorzano[1], Maria Josefa Rodríguez[1], Eva Pereiro[3], and José L. Carrascosa[1,4]

A comprehensive quantitative study has been done on the interaction of magnetic nanoparticles with breast cancer cells using cryo-soft X-ray nanotomography.

Nanoparticles have a great potential in nano-biotechnology and nanomedicine. The authors have studied the interaction of superparamagnetic iron oxide nanoparticles (SPION) with a breast cancer cell line (MCF-7) by cryo-soft X-ray tomography (cryo-SXT). Vitrified samples of cells incubated with SPION were tested by correlative cryo-epifluorescent microscopy showing SPION accumulation into acidic vesicles related to the endocytic pathway. The unique possibility of cryo-SXT to obtain three-dimensional (3D) information from whole cells in close-to-native conditions allows quantitative analysis of SPION-containing vesicle (SCV) accumulation inside cells. Statistical analysis showed SCV increase in number and size concomitant with longer incubation times, and therefore an increase in their accumulated volume within the cell. To quantify the mass of iron oxide SPIONs within whole cells, the authors used near-edge absorption soft X-ray nanotomography (NEASXT) by exploiting the iron oxide differential absorption contrast. NEASXT combines whole-cell 3D structure determination at 50 nm resolution, with 3D elemental mapping and high throughput. The multimodal 3D SXT approach results in a comprehensive quantitative description of SPION: cell interaction, which will serve as a basis for metal-based nanoparticle design and for the selection of those best suited for hyperthermia treatment, drug delivery and image diagnosis in nanobiomedicine.

MCF7 cells were grown on gold grids coated with quantifoil R2/2 and incubated with SPION. Internalized nanoparticles were localized into acidic vesicles revealed by LysoTracker. Vitrified cells were cryo-preserved by plunge freezing and imaged by epifluorescence microscopy to localize areas of interest. Cryo-SXT allowed the authors to visualize at 60 nm resolution in close to native conditions, and in 3D, whole cells incubated with SPIONs for different periods (0 to 24 hours). 68 tilted series were acquired at exposure times ranged 1-4 seconds, (-65º to 60º every 1 degree), using the 40 nm zone plate at a pixel size of 11.56 nm (Figure 3). Using the 3D volumes reconstructed for the different incubation times, the authors extracted quantitative information including vesicle number and size, distances between vesicles, and their distance from the nucleus. Statistical analysis showed that SPION containing vesicles (SCV) increase in number and size concomitant with longer incubation times, yielding an increase in their accumulated volume within the cell.

For an accurate determination of the intracellular mass and density of the SPION (composed by maghemite), the authors set up Near Edge Absorption Soft X-ray Tomography. Cultured MCF-7 cells where incubated on grids as in cryo-SXT and imaged by epifluorescent optical microscopy. Nevertheless, and due to the high oxygen absorption at the iron L3 absorption edge, grid cultured cells were prepared by critical point drying to remove the water. They simultaneously obtained a pair of tilted series, one at 700 eV (just below the L3 iron edge) and the other at 709 eV in the same area. As the absorption corresponding to cellular components remained constant at these two energies, the differential projection images specifically detect the iron oxide signal changes corresponding to the differential absorption before and in the iron L3 absorption edge. 32 data series were collected (64 tilted series with the corresponding 64 cell mosaics at the two photon energies) using the 25 nm zone plate at a pixel size of 11.56 nm and 25 data series (50 tilted series with the corresponding cell mosaics) at a pixel size of 14.44 nm. Following this approach the authors succeed to generate three-dimensional quantitative maps corresponding to the iron signal. Within the reconstructed volume, SPION clusters showed internal substructures (Figure 4) with a mean iron oxide density of 0.9 g/cm3 and a maximum diameter of 1.2 µm. This method allowed us to estimate the total SPION mass within a cell volume of ~90 µm3 as 11.5 pg.

The correlation of cryo-soft X-ray tomography, electron and light microscopy allows a detailed and comprehensive quantitative analysis of the interaction of magnetic nanoparticles with cells.

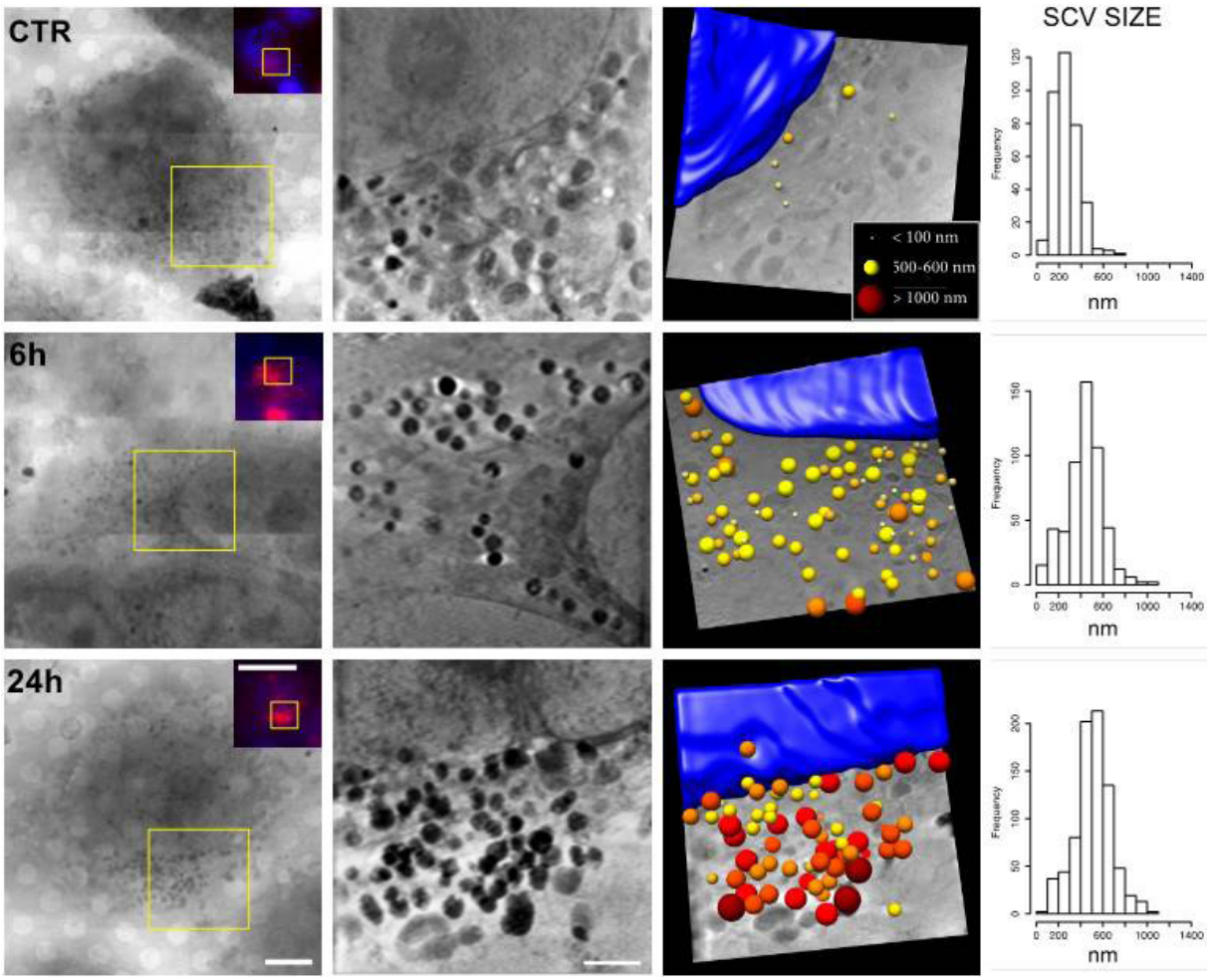

Figure 3: Cryo-SXT correlative workflow at the MISTRAL beamline at ALBA, tomogram-derived colour-coded volumetric representation of SCV and diameter histogram for SPION-incubated MCF-7 cells. Images correspond to MCF-7 cell line incubated with SPION (0.25 mg ml−1) for 0, 6 and 24 h. Left column, cryo-soft X-ray projection mosaic of the area marked by a yellow square in the fluorescent inset. Bar, 5 µm. Inset, cryo-epifluorescence micrograph LysoTracker Red- and DAPI-labelled cells. Bar, 20 µm. Central-left column, central sections of reconstructed tomograms of the area marked by a yellow square in the left column. Bar, 2 µm. Central-right column, colour-coded volumetric representation of SCV where the nucleus is segmented in blue. Field of view, 11.5 µm x 11.5 µm. Right column, histograms showing distributions of SPION-containing vesicle (SCV) size, at different incubation times.

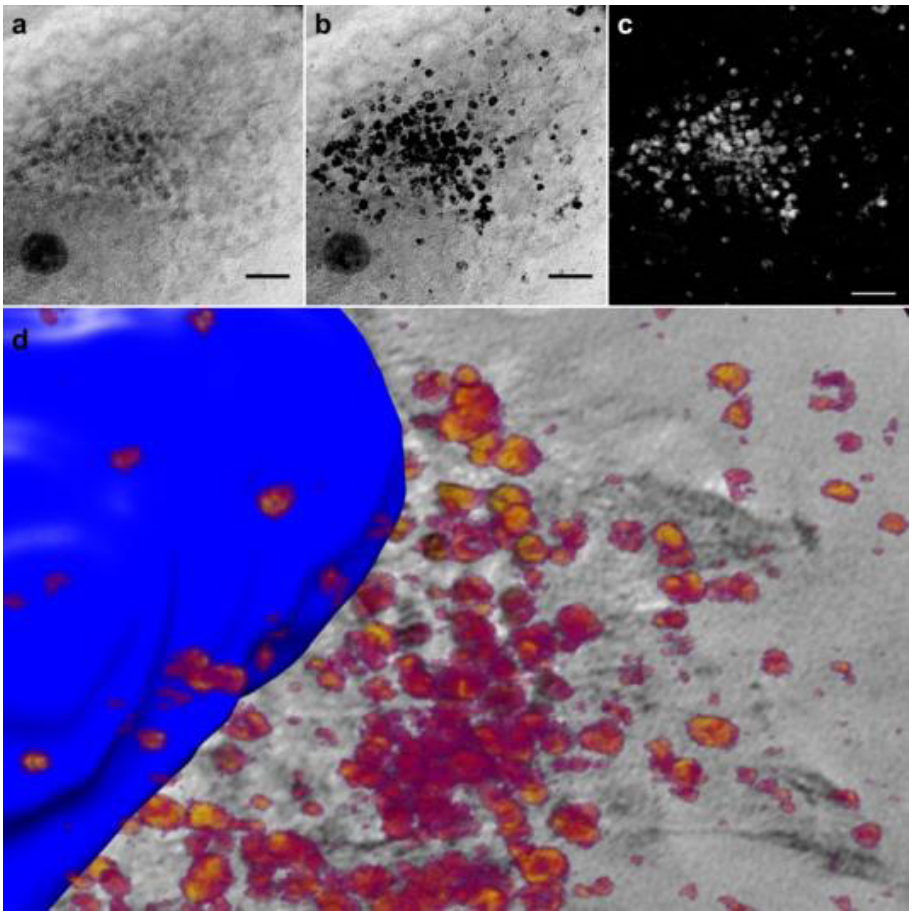

Figure 4: Differential tilt-series generation and volumetric density representation. a, b) 0º projection images at 700 (a) and 709 eV (b). c) Differential 0º projection image containing the SPION signal. Bar, 2 µm. d) Volumetric representation of iron oxide densities within the cells, forming clusters with internal substructures near the nucleus.

Characterization and quantification of iron oxide nanoparticles internalized in intracellular vesicles was done using near-edge absorption soft X-ray nanotomography, which also provided their three-dimensional distribution within the cellular structure.

ACKNOWLEDGEMENTS

The authors acknowledge the collaboration with Gerd Schneider and the personnel at the U41-TXM beamline at Helmholtz Zentrum Berlin – BESSY II Synchrotron during the first steps of this work. We thank the confocal microscopy service at the CNB for their assistance, G. Salas from IMDEA Nanoscience and P. Morales from ICMM for SPION generation. JJC is supported by a predoctoral fellowship from the Spanish Ministry of Economy and Competitiveness (MINECO) and MC was a PhD fellow of the La Caixa Foundation International Fellowship Programme (La Caixa/CNB). This work was partially supported by grants from the European Seventh Framework Programme (FP7/2007-2013) under the project MULTIFUN (grant agreement no. 262943), and BioStructX (FP7-283570), MINECO (BFU2014-54181) and Madrid regional government (S2013/MIT-2850) to JLC.

AFFILIATION:

1. Departmento de Estructura de Macromoléculas, Centro Nacional de Biotecnología (CNB-CSIC). Madrid, Spain.
2. Imperial College London. National Hearth and Lung Institute. London, United Kingdom.
3. ALBA Syncrotron Light Source. Cerdanyola del Vallés, Barcelona, Spain.
4. Unidad Asociada CNB-Instituto Madrileño de Estudios Avanzados en Nanociencia (IMDEA Nanociencia). Madrid, Spain.

CATALYSIS

Heterogeneous catalysis is an active field of research at ALBA since the beginning of operation. Specially designed flow reactors developed by several user groups allow to precisely control the proportions of the reactants and catalyst temperatures while the reactions are taking place. The catalysts usually consist of metal nanoparticles dispersed on oxides that act as support that have been pressed forming pellets with large specific surface areas. At CLÆSS and MSPD beamlines, catalytic reactions at atmospheric pressures have been investigated in a number of occasions. Absorption spectroscopy and powder diffraction in operating catalytic conditions allow monitoring the evolution of the catalyst particles during the reaction. Additionally, at CIRCE, the NAPP instrument is also appropriate for studies of catalysis. In that case, the catalyst is interrogated using photoemission spectroscopy at pressures ranging from high vacuum to several mbars. In this case the electronic properties of the metallic particles, as their oxidation states, are monitored under chemically active conditions.

We have selected an example from a recent publication dealing with the Fischer Tropsch catalytic reaction, invented almost one hundred years ago, that is widely used to generate carburants from the reaction of carbon monoxide and hydrogen. The most commonly used catalyst of the reaction consist of widely dispersed iron carbide particles. In the article that follows, the authors describe a new route to achieve highly efficient and stable catalysts based on metal organic frameworks that allow preparing very dispersed iron nanoparticles in a carbon matrix.

Metal organic framework-mediated synthesis of highly active and stable Fischer-Tropsch catalysts

Metal organic framework-mediated synthesis of highly active and stable Fischer-Tropsch catalysts, *Nature Communications* 6, 6451 (2015)

Vera P. Santos[1,2], Tim A. Wezendonk[1], Juan José Delgado Jaén[3], A. Iulian Dugulan[4], Maxim A. Nasalevich[1], Husn-Ubayda Islam[5], Adam Chojecki[2], Sina Sartipi[1], Xiaohui Sun[1], Abrar A. Hakeem[1], Ard C.J. Koeken[6], Matthijs Ruitenbeek[6], Thomas Davidian[6], Garry R. Meima[2,6], Gopinathan Sankar[5], Freek Kapteijn[1],Michiel Makkee[1] and Jorge Gascon[1]

***In situ* X-ray absorption spectroscopy (XAS) studies together with Mössbauer spectroscopy demonstrate that the Metal Organic Framework-mediated synthesis is a promising route for the design of Fe-based Fischer-Tropsch synthesis catalysts.**

Depletion of crude oil resources and environmental concerns have driven a worldwide research on alternative processes for the production of commodity chemicals. Fischer–Tropsch synthesis is a process for flexible production of key chemicals from synthesis gas originating from non-petroleum-based sources. Although the use of iron-based catalysts would be preferred over the widely used cobalt, manufacturing methods that prevent their fast deactivation because of sintering, carbon deposition and phase changes have proven challenging. This work presents a strategy to produce highly dispersed iron carbides embedded in a matrix of porous carbon. Very high iron loadings (>40 wt %) are achieved while maintaining an optimal dispersion of the active iron carbide phase when a metal organic framework is used as catalyst precursor. The unique iron spatial confinement and the absence of large iron particles in the obtained solids minimize catalyst deactivation, resulting in a highly active and stable operation.

Fischer–Tropsch synthesis (FTS) is a heterogeneous catalysed polymerization reaction where syngas (a mixture of CO and H2), derived from natural gas, coal or biomass, is converted into a wide spectrum of hydrocarbon chains. Recently, metal organic frameworks (MOFs) have emerged as promising precursors for the synthesis of nano-materials, because of their unique structure, atomic metal dispersion and textural properties. This work reports a simple, tunable and scalable MOF-mediated synthesis (MOFMS) strategy for the preparation of exceptionally dispersed Fe nano-particles in a porous carbon matrix. The resulting solids display outstanding FTS performance, with high activity and stability.

The Fe-based MOF Basolite F300 was used as a template for the preparation of the different catalysts. Basolite F300 (Fe(BTC), C9H3FeO6; BTC¼1,3,5-benzenetricarboxylate) consists of oxo-centred trimers of Fe3+ cations connected by trimesate anions. The synthesized catalysts are denoted as 'Z-Fe@C', with Z representing the amount of Fe (wt%) in the catalyst.

The experimental observations from Mössbauer spectroscopy were supported by *in situ* X-ray absorption spectroscopy (XAS) studies. The spectrum of Fe@C is markedly different from Basolite F-300. X-ray absorption near-edge spectroscopy analysis on the pyrolysed solid reveals the reduction of Fe3+

centres of Basolite to Fe2+ (Fig. 5). Based on the fitting parameters and in line with the Mössbauer data, we conclude that Fe@C consists of a mixture of Wüstite and iron carbides. With this spectroscopic characterization together with the full set of data shown in the original article, the authors have demonstrated that the MOFMS is a promising route for the precise design of Fe-based FTS catalysts. Catalysts prepared following this approach display an intimate contact between Fe and C that facilitates the formation of iron carbides already during the synthesis of the material, which results in very high carbidization degrees.

In spite of high Fe loadings that can be realized through this preparation method, the high dispersion of the metal phase and its encapsulation in a highly porous carbon matrix result in an unrivalled activity and exceptional stability. The spatial restriction created by encapsulation seems to minimize sintering and oxidation of the active Hägg carbide phase. The high catalytic activity of the solids presented here is further highlighted when comparing their productivity with the available data from commercial benchmark catalysts, namely the well-known Ruhrchemie and Sasol catalysts for high-temperature FTS. The comparison demonstrates that MOF-derived solids display productivities, on a total catalyst weight basis, one order of magnitude higher than these benchmarks, even when the MOF-based catalysts contain a lower amount of iron. This simple and potentially universal design strategy opens the door to the controlled manufacture of highly dispersed and stable metal nanoparticles in porous matrices, one of the major challenges in materials science and industrial catalysis.

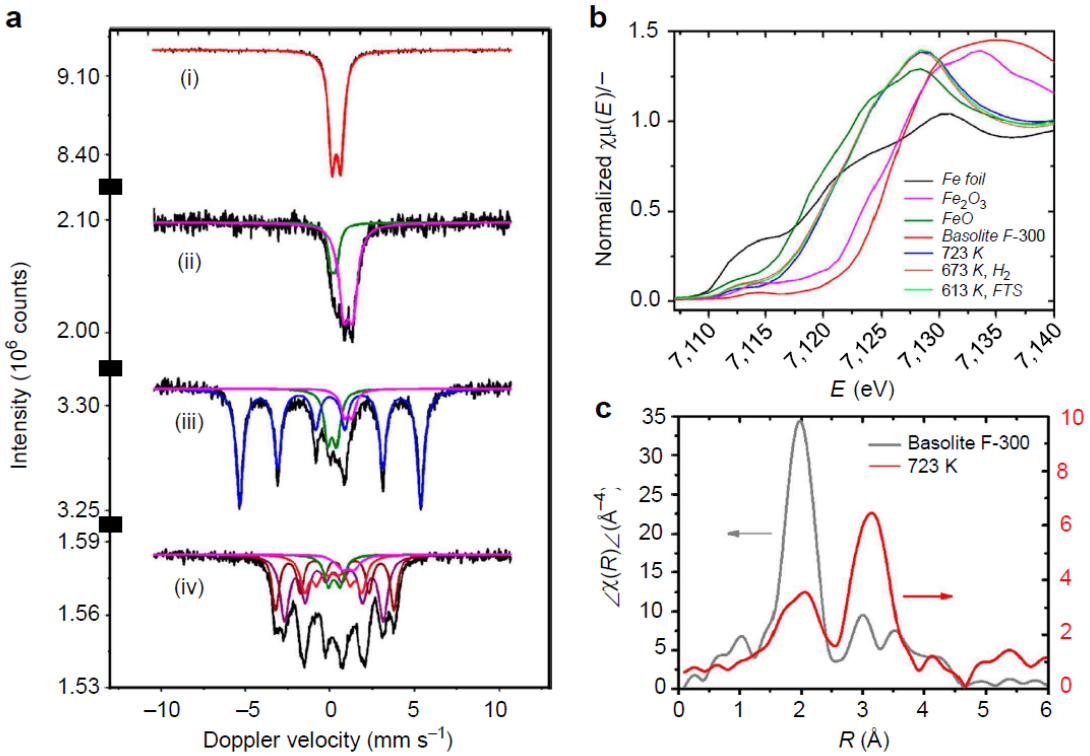

Figure 5: Spectroscopic characterization. (a) Mössbauer spectra obtained at 300 K after different successive treatments at 1 bar: (i) Fresh Basolite F-300; (ii) Fe@C obtained after pyrolysis in Ar atmosphere at 723 K (38-Fe@C); (iii) 38-Fe@C after reduction under H2 atmosphere at 673 K; and (iv) 38-Fe@C after exposure to syngas (H2/CO ¼ 1) at 613 K. (b) X-ray absorption near-edge spectra of iron foil (black); Fe2O3 (magenta); FeO (olive); Basolite F-300 at 298 K (red); Fe@C obtained after pyrolysis at 723 K (blue); Fe@C reduced at 673 K by H2/He (10 vol. %, 1 bar; orange); Fe@C after 5 h FTS reaction (613 K, CO/H2 ¼ 1, 1 bar; green). (c) EXAFS spectra of Basolite F-300 at 498 K and Fe@C at 723 K.

AFFILIATION:

1. Catalysis Engineering, Department of Chemical Engineering, Delft University of Technology, The Netherlands
2 Core R&D,Dow Benelux B.V., Terneuzen, The Netherlands
3 Departamento de Ciencia de los Materiales e Ingeniería Metalúrgica y Química Inorgánica, Facultad de Ciencias, Universidad de Cádiz, Cádiz, Spain
4 Fundamental Aspects of Materials and Energy Group, Delft University of Technology, Delft, The Netherlands
5 Department of Chemistry, University College London, London, UK
6 Hydrocarbons R&D, Dow Benelux B.V., Terneuzen, The Netherlands

MAGNETISM

Research in magnetism and magnetic materials is one of the major fields of activity at ALBA due to the fundamental and practical interest of nanomagnetic devices, which are the building blocks of spintronics applications.

The following three contributions are representative of the recent activity at the facility. The first two deal with imaging of magnetic singularities in magnetic domains using the circular magnetic dichroism as a magnetic contrast mechanism either at the X-ray microscope at MISTRAL or at the photoemission microscope at CIRCE. Magnetic singularities like skyrmions are stable magnetic structures considered to be promising candidates for the storage/transport of information. The first contribution shows how a type of singularities named merons, which are similar to ½ skyrmions, play a key role in the inversion of the magnetization. The second one visualized a skyrmion at room temperature.

The third contribution deals with the role of the spin orbit coupling in the magnetic properties of mixed cobalt oxides since their spin state influences their transport properties. The experiments were carried out at BOREAS using magnetic dichroism.

Viewing buried magnetic domains and singularities with the X-ray microscope

Nanoscale Imaging of Buried Topological Defects with Quantitative X-ray Magnetic Microscopy, *Nature Communications* 6, (2015)

C. Blanco-Roldán[1,2], C. Quirós[1,2], A. Sorrentino[3], A. Hierro-Rodríguez[4,5], L.M. Álvarez-Prado[1], R. Valcárcel[3], M. Duch[6], N. Torras[6], J. Esteve[6], J.I.Martín[1,2], M. Vélez[1,2], J.M. Alameda[1,2], E. Pereiro[3], S. Ferrer[3]

A group of researchers visualized and analysed in detail the properties and magnetic defects of materials at the nanoscale using an X-ray transmission microscope, based on the so-called dichroic contrast by using specific X-ray energies that match the electronic levels of the buried magnetic domains.

One of the key properties of magnetic storage media and magnetic devices of nanometric dimensions is the speed of change of the magnetization. Magnetic media for practical applications consist of alternate stacks of very thin films (few nm) of magnetic and non-magnetic materials that are cleverly designed to achieve specific purposes. The dynamics of the magnetization in these nanostructures is often controlled by the so-called magnetic singularities, which are local modifications of magnetization that are energetically stable. The determination of the nature of these singularities and of their characteristics is an active research area in nanomagnetism. Experimental methods to image magnetic domains and singularities are consequently appropriate. Some of them are based on optical phenomena as the magneto-optical Kerr effect, other rely on electron detection as photoemission microscopy (PEEM) and they are adequate to visualize the surface of magnetic materials (the topmost atoms within 1 or 2 nm in depth) but they are not suitable for inspecting buried layers several tens of nm below the surface as they exist in magnetic devices. The X-ray microscope of MISTRAL is a useful tool that overcomes this specific limitation since the penetration length of the X-rays with the selected energies is of tens of nm which in practice means that buried magnetic domains in layers as thick as 150 nm or more can be inspected. The magnetic contrast among domains of, for example, up and down magnetization relative to the surface of the films is based on the magnetic dichroic contrast (XMCD) that occurs when circularly polarized X-rays are tuned at energies to excite specific electronic transitions. The magnetic contrast depends on the angle θ between the direction of the photon beam and the magnetization as cos θ which gives +/- 1 for down and up magnetizations respectively.

Defining z as the direction normal to the surfaces of the films as indicated in figure 6, the white stripes in panel a have a magnetization with a positive z component. Additionally, one can also monitor the magnetization component along a direction x in the film plane. This is done by rotating the sample about the y axis located on the plane of the films. The image in panels a, b and d have a θ rotation angle of about 35º. The stripe domains in panels a, c and d arise from the magnetization of Fe on a permalloy (Ni80Fe20) film of 40 nm thickness grown on top of a ferromagnetic film of 120 nm.

At the centre of panel a there is a bifurcation of the stripes similar to an edge dislocation in a crystal. The two white branches of the bifurcation have different intensities. Careful analysis of the contrast allows to determine the in-plane magnetization indicated by the red (positive x component) and blue (negative x component) arrows. As shown by the curved arrow in panel a the magnetization rotates clockwise moving from the upper to the lower branch. Micromagnetic calculations and detailed quantitative analysis of the variation of the contrast with the angle allowed to identify the magnetic singularity at the edge of the dislocation as being a so-called meron that is a singularity similar to one half of a skyrmion as depicted in panel c. Merons in magnetic bifurcations drive the inversion of the magnetization as shown in panel d: the negative upper branch in blue has partially inverted the x component of the magnetization originating a Bloch point singularity B that moves away from the dislocation core as the in-plane magnetization is reversed.

As mentioned above, the microscope allows to image domains below the surface. This feature has been used to investigate how the merons at the surface propagate inside the film at the buried interfaces. Propagation selection rules have been experimentally found indicating that the propagation of merons to different interfaces depends on the intrinsic parameters of the merons such as chirality and polarity. These results are being analyzed and illustrate how the dynamics of topological defects is determined by their intrinsic topological characteristics.

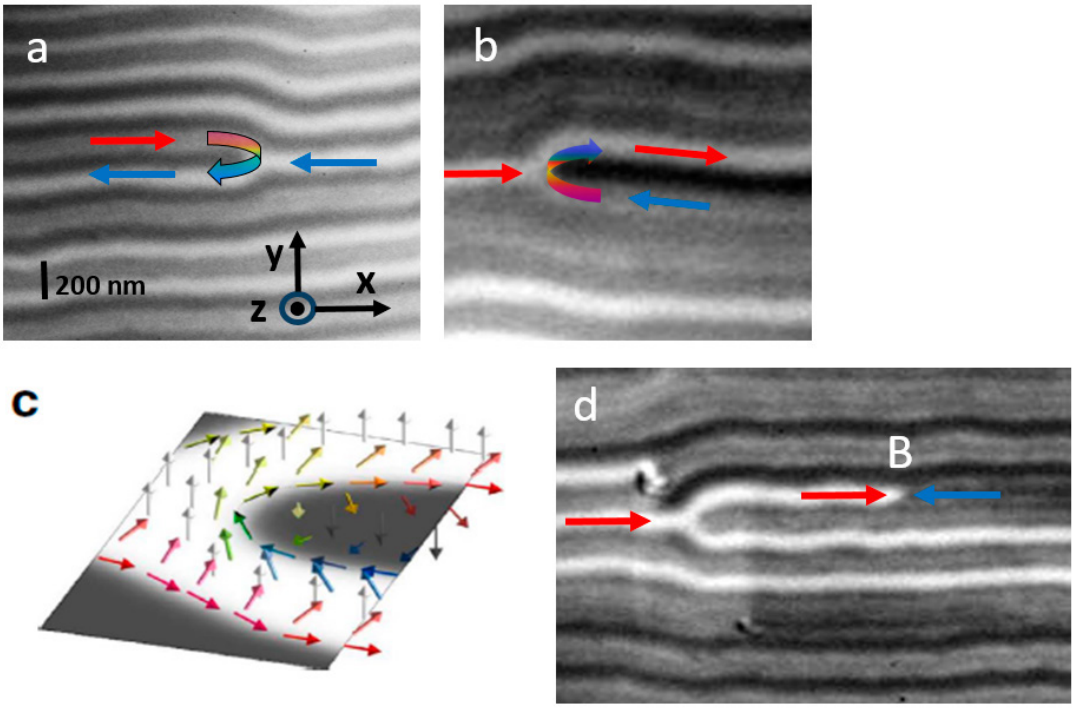

Figure 6: Magnetic domains in a permalloy film grown on top of a ferromagnetic substrate. The images are acquired at the L3 absorption edge of Fe (photon energy = 706.8 eV) using right circularly polarized X-rays. In panels a and b the merons have respectively counter-clockwise and clockwise chiralities. Panel c schematically shows the results of micromagnetic calculations describing the magnetization of the meron. In panel d, the upper branch of the dislocation has inverted in-plane magnetization until the Bloch point B.

AFFILIATION:
1. Departamento de Física, Universidad de Oviedo, Spain
2. Centro de Investigación en Nanomateriales y Nanotecnología, CINN (CSIC—Universidad de Oviedo), Spain
3. ALBA Synchrotron, Cerdanyola del Vallès, Spain
4. Departamento de Física e Astronomia, IN-IFIMUP, Universidade do Porto, Portugal
5. Departamento de Física e Astronomia, INESC-TEC (Coordinated by INESC-Porto), Universidade do Porto, Portugal
6. Centro Nacional de Microelectrónica, IMB–CNM, CSIC, Bellaterra, Spain

Magnetic skyrmions observed at room temperature

Room-temperature chiral magnetic skyrmions in ultrathin magnetic nanostructures, *Nature Nanotechnology* (2016)

Olivier Boulle[1,2,3], Jan Vogel[4,5], Hongxin Yang[1,2,3],Stefania Pizzini[4,5], Dayane de Souza Chaves[4,5], Andrea Locatelli[6], Tevfik OnurMentes[6], Alessandro Sala[6], Liliana D. Buda-Prejbeanu[1,2,3], Olivier Klein[1,2,3], Mohamed Belmeguenai[7], Yves Roussigné[7], Andrey Stashkevich[7], Salim Mourad Chérif[7], Lucia Aballe[8], Michael Foerster[8], Maïrbek Chshiev[1,2,3], Stéphane Auffret[1,2,3], Ioan Mihai Miron[1,2,3] and Gilles Gaudin[1,2,3]

Magnetic skyrmions, which are nanoscale spin textures, have been observed at room temperature in materials compatible with the microelectronics industry. Part of the experiments were carried out using the Photoemission Electron Microscope of the CIRCE beamline. These results break an important barrier for the use of skyrmions as nanoscale information carriers in our computers.

These structures are currently fascinating many research groups around the world, as they offer a new pathway to potentially store and process information in our computers more efficiently. These nanoscale objects are composed of elementary nanomagnets ("spins") that wind to form a stable spiral magnetic texture, like a well tightened knot. Although predicted in the 80's, magnetic skyrmions were not observed until 2009. Three years later, two research teams demonstrated that magnetic skyrmions can be manipulated by very low electrical currents, opening the path for their use as information carriers in computing devices. Several groundbreaking memory and logic devices based on the manipulation of skyrmions in nanotracks have since been proposed, promising very large information density and low power consumption. However, integration of skyrmions in devices still remained distant as they had been observed only at low temperature, in the presence of large magnetic fields and/or in exotic materials, unsuitable for practical applications.

By demonstrating isolated skyrmions stable at room temperature and in the absence of an external magnetic field, the authors have thus broken a major barrier. To reach this result, they deposited an ultrathin magnetic layer of cobalt (a few atoms thick) in a sandwich between a layer of a heavy metal (platinum) and a layer of magnesium oxide. In this sandwich, the Dzyaloshinskii-Moriya interaction (DMI) arising at the interfaces of cobalt with the heavy metal and the oxide, which is at the origin of the helical shape of the skyrmion, is strongly enhanced. In addition, the deposition technique used –sputtering-, has the advantage of being fast and is commonly used in the microelectronics industry.

Once the right material stack was identified, the next step was to acquire magnetic images in order to resolve the internal spiral spin texture of the skyrmions. For attaining this objective, a technique with high spatial resolution and high magnetic sensitivity is needed: the combination of polarized synchrotron X-rays with PhotoEmission Electron Microscopy (XMCD-PEEM). Figure 7 shows images of magnetic skyrmions taken with such

magnetic microscopes at the ALBA Synchrotron in Barcelona (Spain) and the Elettra synchrotron in Trieste (Italy). In XMCD-PEEM images, the intensity reflects the direction of the magnetization in each location. For example in Figure 7b, a small circular structure is visible within a larger Co dot with uniform light-gray intensity. The contrast sequence in the small circular structure is indicative of the helical spin arrangement within the skyrmion. The next step will be to move these skyrmions using electrical current, a further step towards the use of these particles to code and manipulate the information at the nanoscale in computing devices.

These results were obtained through a collaboration between several French laboratories: Spintec and Institut Néel in Grenoble, the Laboratory of Process and Material Sciences, Paris 13 University. The XMCD-PEEM magnetic imaging experiments were carried out in ALBA Synchrotron in Barcelona (Spain) and in Elettra synchrotron in Trieste (Italy).

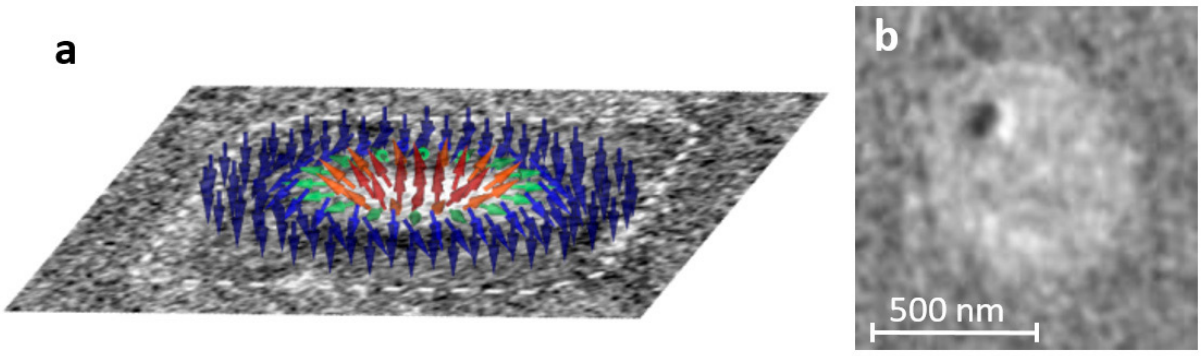

Figure 7: (a) XMCD-PEEM magnetic image of a magnetic skyrmion in a 420 nm squared magnetic dot (black and white figure) with the corresponding skyrmion magnetic configuration superimposed (coloured arrows). (b) XMCD-PEEM magnetic image of a 80 nm diameter skyrmion in a 630 nm diameter circular dot.

OTHER REFERENCES

[1] Skyrmion on the tracks, A. Fert et al., ***Nature Nanotechnology,* 8**, 152 (2016)

ACKNOWLEDGEMENTS

For their contribution at the CIRCE beamline of the ALBA Synchrotron, authors would like to thank C. Escudero, V. Perez-Dieste, E. Pellegrin, J. Nicolas and S. Ferrer.

AFFILIATION:

1. Univ. Grenoble Alpes, SPINTEC, Grenoble, France
2. CNRS, SPINTEC, Grenoble, France
3. CEA, INAC-SPINTEC, Grenoble, France
4. CNRS, Institut Néel, Grenoble, France
5. Univ. Grenoble Alpes, Institut Néel, Grenoble, France
6. Elettra-Sincrotrone, Trieste,Italy
7. LSPM (CNRS-UPR 3407), Université Paris 13, Villetaneuse, France
8. ALBA Synchrotron, Cerdanyola del Vallés, Barcelona, Spain

Spin-orbit coupling and magnetostructural changes in metallic $Pr_{0.50}Sr_{0.50}CoO_3$ investigated by soft XMCD

Spin-lattice coupling across the singular magnetostructural transition in $Pr_{0.50}Sr_{0.50}CoO_3$ by X-ray magnetic circular dichroism, *Physical Review B* **92**, 245136 [7pp] (2015)

J. Padilla-Pantoja [1], J. Herrero-Martín [2,*], E. Pellegrin[2], P. Gargiani [2], S.M. Valvidares [2], A. Barla [3] and J. L. García-Muñoz [1,*]

The singular properties of some cobalt oxides are often driven by the competition between structural and magnetic degrees of freedom, including here the rare ability of cobalt to change its atomic magnetic moment and electronic configuration (spin-state). Following the extensive investigations on the nature of the spin-state changes in undoped $LnCoO_3$ compounds (*Ln:* lanthanide), the spin-state of trivalent cobalt is being examined in a variety of cobaltites because of its proved ability to condition their transport, magnetic and electronic properties. Some $(Pr,Ln)_{0.50}A_{0.50}CoO_3$ perovskites exhibit exceptional photoresponse capabilities of potential interest for ultrafast optical switching devices, which are promoted by electronic and spin state instabilities [1].

In half-doped $Pr_{0.50}A_{0.50}CoO_3$ metallic perovskites, the spin-lattice coupling brings about distinct magnetostructural transitions for A=Ca and A=Sr at temperatures close to ~100 K. However, the ground magnetic and electronic properties of $Pr_{0.50}Sr_{0.50}CoO_3$ (PSCO) strongly differ from $Pr_{0.50}Ca_{0.50}CoO_3$ ones, where a partial Pr^{3+} to Pr^{4+} valence shift and simultaneous Co^{3+} spin state transition produces an exotic metal-insulator transition [2]. Here the authors have investigated the relevance of the spin-orbit coupling for the magnetic and electronic properties of $Pr_{0.50}Sr_{0.50}CoO_3$ (always metallic, and ferromagnetic below T_C ~ 230 K) across the unexpected magnetostructural transition at T_{S1} ~120 K, which separates two distinct FM metallic phases (FM1-FM2) [3-6] and has not been observed in samples with lanthanides other than praseodymium. The authors performed temperature dependent X-ray magnetic circular dichroism (XMCD) on ferromagnetic $Pr_{0.5}Sr_{0.5}CoO_3$ (PSCO) at the Co $L_{2,3}$ edges, to analyze the evolution and correlation between the spin and orbital components of the magnetization across the unforeseen *Imma→I4/mcm* symmetry change at T_{S1} ~120 K [7]. The magnetization around T_{S1} exhibits a step-like behaviour [3-5], whose amplitude and sign (positive or negative) shows a strong dependence on the external applied field (Figure 8). The studied sample was *in-situ* cut under ultrahigh vacuum conditions. The data were collected by means of surface-sensitive TEY detection, and the XAS spectrum of a reference CoO single crystal was used for energy calibration. The XMCD spectra were recorded from 40 K to 300 K using alternatively left and right circularly polarized X-rays at the HECTOR

endstation, where the superconducting split-coil setup allowed generating the required magnetic fields up to 5 T, parallel to the X-ray propagation direction. In order to avoid a possible photoreduction of Co ions, photon flux and exposure time were controlled. Charge transfer multiplet calculations of the XMCD spectra were performed to model the electronic configuration of Co^{3+} and Co^{4+} species in the system.

The authors used the orbital and spin sum rules to obtain the orbital m_L and spin m_S moments (the intra-atomic spin dipole contribution is negligible for octahedral metallic systems characterized by reduced exchange fields). From Co $L_{2,3}$ XMCD spectra at 50 K and 5T applied field it was obtained m_S= 0.297(6) μ_B/3*d* hole and m_L= 0.095(2) μ_B/3d hole, and consequently m_L/m_S= 0.32. The net moment of 1.77(4) μ_B/Co ion obtained from XMCD data is in excellent agreement with the magnitude of the ferromagnetic component found by neutron diffraction. The evolution of m_S and m_L as a function of temperature at 0.1 T is shown in the Figure 9. Three remarkable features must be underlined here: (i) the spin moment projection along the external field follows the same step-like behaviour shown by the magnetization under the same magnetic field, (ii) the projected orbital momentum m_L is sizeable (about one third of m_S), and –most importantly- (iii) it also presents a positive step on cooling the sample across the orthorhombic-tetragonal transition. In addition, the charge transfer multiplet calculations do not support a picture based on Co^{3+} ions in an intermediate spin (IS) state. Furthermore, they indicate that the IS state is realized in a fraction of low spin (LS) state-believed Co^{4+} ions, their electronic configuration thus being $t_{2g}^4 e_g^1$ instead of t_{2g}^5.

Using XMCD in PSCO the authors have found a sizeable orbital contribution m_L to the cobalt magnetization of around 1/3 of the spin component. Its projection over the applied magnetic field axis follows a temperature dependence that shows an abrupt jump that couples it to the ordering of the electronic spins, indicating the importance of the spin-orbital coupling term in the material. Thus, m_L and m_S exhibit the same original step–like behaviour through the magnetostructural transition. This reveals a strong tendency of the orbital and spin moments to be parallel. In the absence of an external field, a very likely reorientation of the orbital moment is provoked by the symmetry changes at the *Imma→I4/mcm* transformation [7]. By virtue of the spin-orbit coupling, the authors deduce that the spontaneous rotation of ordered Co spins between the FM1 and FM2 ferromagnetic phases (i.e. across T_{S1}) is driven by the rotation of the orbital moment easy-axis. This model has been just confirmed by the group using neutron diffraction [4], describing the details of the distinct magnetic orderings above (FM2) and below (FM1) the transition, and the spontaneous spin rotation by 45º at T_{S1} in this ferromagnetic metal. The origin of this intriguing magnetic behaviour has been thus univocally determined.

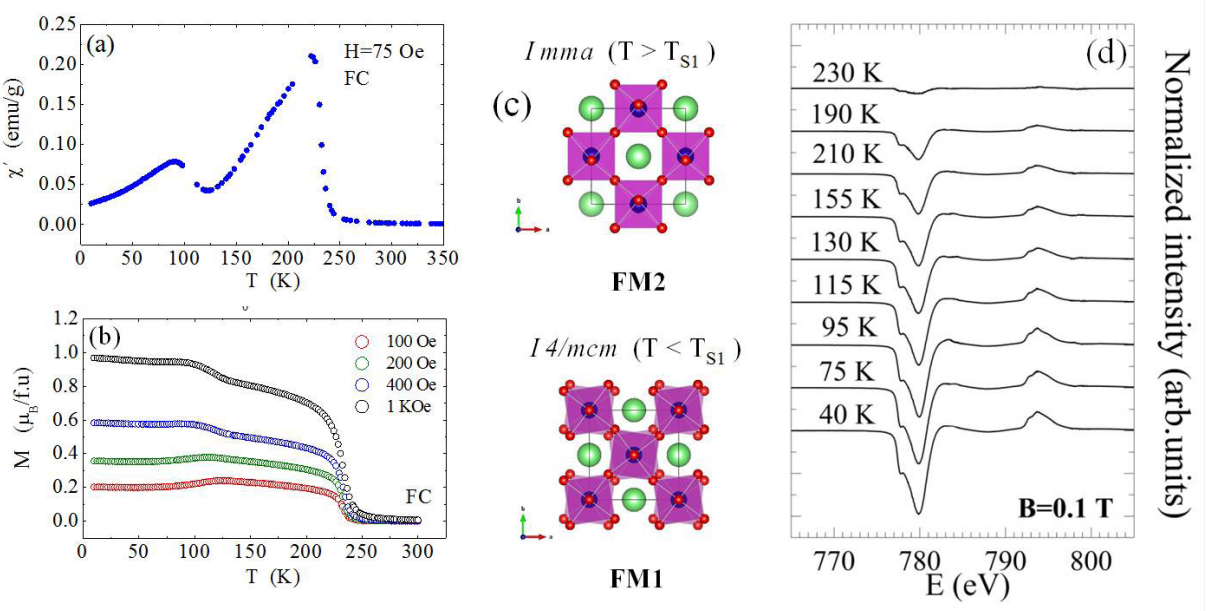

Figure 8: (a) ac susceptibility (h=10 Oe, f=13Hz) measured in PSCO using a dc field of 75 Oe (FC). (b) Temperature dependence of the magnetization (FC) measured at different fields. (c) Structures of PSCO at both sides of T_{s1}. (d) Temperature dependence of the Co $L_{2,3}$ XMCD signal at 0.1 T.

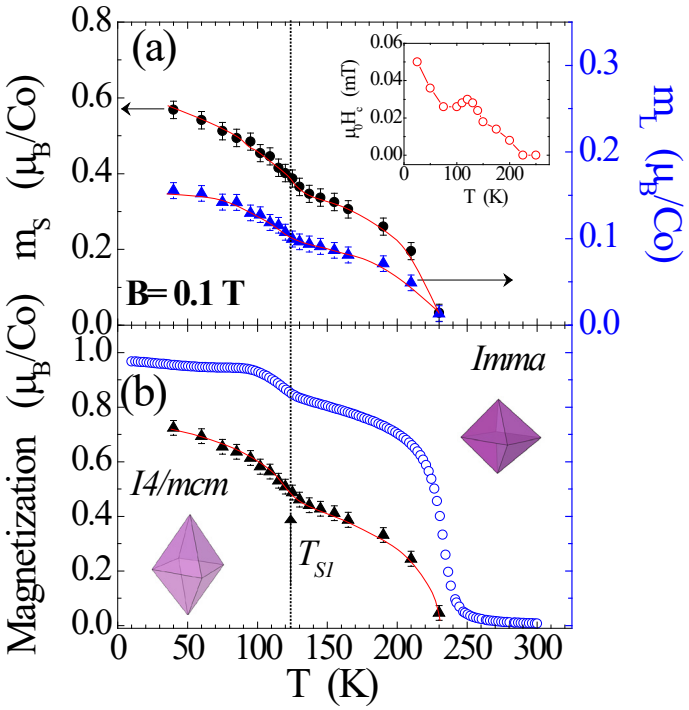

Figure 9: (a) Temperature dependence of the spin magnetic moment m_S (solid black circles) and the orbital magnetic moment m_L (solid blue triangles) derived from XMCD spectra of PSCO at 0.1 T. Inset: coercive field ($\mu_0 H_c$) vs T. (b) Temperature dependence of $m_L + m_S$ (solid black triangles), and dc magnetization (open blue circles) measured at 0.1 T. The solid red line is an eye-guide. Assuming 4.5 as the average number of Co 3*d* holes yields a net moment in excellent agreement with neutron results. The shape of CoO_6 octahedra in each structural phase is schematically represented.

OTHER REFERENCES

[1] Y. Okimoto, X. Peng, M. Tamura, T. Morita, K. Onda, T. Ishikawa, S. Koshihara, N. Todoroki, T. Kyomen, and M. Itoh, ***Phys. Rev. Lett.* 103**, 027402 (2009).

[2] J. Herrero-Martín, J. L. García-Muñoz, K. Kvashnina, E. Gallo, G. Subías, J. A. Alonso, and A. J. Barón-González, ***Phys. Rev. B* 86,** 125106 (2012) and refs. therein.

[3] R. Mahendiran and P. Schiffer, ***Phys. Rev. B* 68**, 024427 (2003).

[4] J.L. García-Muñoz, J. Padilla-Pantoja, X. Torrelles, J. Blasco, J. Herrero-Martín, B. Bozzo, J.A. Rodríguez-Velamazán, "Magnetostructural coupling, magnetic ordering and cobalt spin reorientation in metallic $Pr_{0.50}Sr_{0.50}CoO_3$ cobaltite", ***Phys. Rev. B 2016, submitted.***

[5] C. Leighton, D. D. Stauffer, Q. Huang, Y. Ren, S. El-Khatib, M. A. Torija, J. Wu, J. W. Lynn, L. Wang, N. A. Frey, H. Srikanth, J. E. Davies, Kai Liu, and J. F. Mitchell, ***Phys. Rev. B* 79**, 214420 (2009).

[6] N. A. Frey Huls, N. S. Bingham, M. H. Phan, H. Srikanth, D. D. Stauffer and C. Leighton, ***Phys. Rev. B* 83**, 024406 (2011).

[7] J. Padilla-Pantoja, J.L. García-Muñoz, B. Bozzo, Z. Jirák and J. Herrero-Martín, ***Inorganic Chemistry* 53**, 12297 (2014).

ACKNOWLEDGEMENTS

The authors thank the financial support from the Spanish Government (MINECO) and the European Community (ERDF) through project MAT2012-38213-C02-02. X-ray measurements were performed at the BL29-BOREAS beamline of the ALBA Synchrotron Light Source with the collaboration of ALBA staff. J. P.-P. thanks CSIC for a JAE-Predoc contract.

AFFILIATION:

1. Institut de Ciència de Materials de Barcelona, ICMAB-CSIC, Bellaterra, Barcelona, Spain
2. ALBA Synchrotron, Cerdanyola del Vallès, Barcelona, Spain
3. Istituto di Struttura della Materia, ISM CNR, Trieste, Italy

MATERIALS SCIENCE

Materials science deals with the study of the matter whether in condensed, soft or liquid form. At first glance, it is intended to determine the exact positions of the atoms in everyday materials and, based on this, to explain or deduce the origin of their physical and/or chemical properties. Synchrotron X-ray radiation directly interacts with the electrons of the probed material, so it is an ideal tool to extract information on the material's properties. In two of the following examples, X-rays interact with the electrons cloud surrounding each atom; one can then extract the structure – the atom arrangement – of the material. Such experiments are performed on powder form materials at the BL04-MSPD beamline. In soft matter, atoms are loosely bound to each other inducing flexibility/plasticity of the material. In this case, X-ray radiation is sensitive to the variation in electron density within the probed material and the non-negligible interaction between atoms can be deduced. This kind of measurements are performed at the BL11-NCD beamline dedicated to small/wide angle X-ray scattering (SAXS/WAXS). This technique typically allows determining the arrangement (stacking and folding) of polymer chains in commonly named "plastic"-like materials. Finally, X-ray photons can exchange energy with the electrons of the probed material, providing a direct insight into electron energy levels: the electronic structure. Such experiments are performed at BL22-CLÆSS at high energies within bulk materials or at BL24-CIRCE at very low photon energies, the latter technique being surface-sensitive only.

Three of the presented examples focus on a functional material with direct technological impact. The last one, classified as "Cultural Heritage", aims at a better understanding of the making of ancient art works. In their study, Pradell *et al.* used the small beam size (20 microns) offered by one of the BL04-MSPD endstations to map different parts of stained glass "grisailles" produced over the last four centuries. In their contribution, Palacín *et al.* discovered a possible way of producing portable rechargeable batteries using the naturally abundant calcium material instead of lithium or sodium. This discovery may have a huge technological impact since most of the batteries in our cell phones are made of lithium, which is costly and environmentally hazardous. The increasing development of electric vehicles further reinforces the need for alternative materials in battery production. Using the SAXS techniques offered by BL11-NCD, Puiggalí *et al.* aimed at finding the optimal chemical recipe in order to ensure an improved biodegradability of polymer materials. Everybody knows the impact of plastic bags in our environment and though it is our individual responsibility to minimize our waste, technology might also help our efforts. The last contribution, from Yashina *et al.,* is more scientifically oriented. Here the authors studied clathrates which are a kind of materials exhibiting large "holes" in their structure, allowing the storage of various kinds of gases depending on the so-called cages size. These cages can as well accommodate electrically charged molecules hence inducing –by compensation– strong thermo-electric effects.

Chemical Bonding and Electronic Structure of Thermoelectric Clathrate Compounds in the Sn–In–As–I System

Experimental and Computational Insight into the Chemical Bonding and Electronic Structure of Clathrate Compounds in the Sn–In–As–I System *Inorganic Chemistry* 54 11542–11549 (2015)

Lada V. Yashina[1,*], Andrey A. Volykhov[1], Elmar Yu. Kataev[1], Alina I. Belova[1], Virginia Pérez-Dieste[2], Carlos Escudero[2], Denis V. Vyalikh[3], and Andrei V. Shevelkov[1]

The chemical bonding and electronic properties of thermoelectric clathrate compounds have been studied by means of photoemission spectroscopy and theoretical modelling in the search for alternative energy conversion systems.

Nowadays, the growing need for alternative energy sources initiates a new quest for materials for energy generation, storage, and conversion. Under these circumstances, advanced thermoelectric materials with high electrical conductivity, low thermal conductivity, and, hence, good thermoelectric figures of merit are of high interest owing to their potential application in freon-free refrigerators, waste-heat converters, and direct solar thermal energy converters [1,2]. A possible way to decrease thermal conductivity is to exploit the unique structural features of inorganic/intermetallic clathrate materials. Their architecture includes a nanoscale framework of ordered cages, with large electropositive or electronegative atoms filling them and therefore compensating the framework charge [3]. The unique feature of clathrates is their abnormally low thermal conductivity because of the localized motion, so-called “rattling”, of the guest atoms inside the oversized cavities of the framework, which leads to either scattering or low

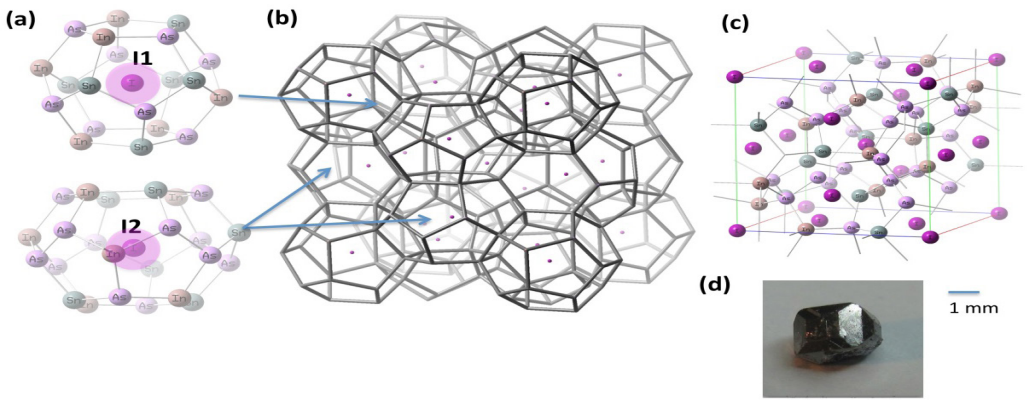

Figure 10: Crystal structure of the $Sn_{24-x}In_xAs_{22-y}I_8$ clathrates: a) two types of the iodine guest atom coordination in idealized polyhedral cages, b) polyhedral presentation of the crystal structure, c) a view of the unit cell, d) photo of a crystal grown for XPS experiments.

group velocity of heat-carrying phonons [4-7]. The lattice thermal conductivity can be optimized by tuning the host-guest mismatch and by increasing the atomic mass of the atoms composing the clathrate framework as well as guest species [8,9]. Symmetrically, transport of charge carriers can be optimized without compromising low thermal conductivity [3,4,6].

The authors focus on the experimental study of the band structure and chemical bonding for the $Sn_{24-x-\delta}In_xAs_{22-y}I_8$ clathrates (Fig.10) as probed by valence band and core-level photoemission for the first time, supplemented by the complementary quantum modelling.

To probe the charge state of the atoms in the $Sn_{24-x-\delta}In_xAs_{22-y}I_8$ clathrates of different composition, the authors analyzed the respective photoemission core level peak, and in particular its line shape and binding energy (*BE*) position. They modelled the core-level shifts that were calculated in the initial state approximation. To figure out the contribution of the final state effect, they calculated the relaxation energy using the so-called Wagner Auger parameter *α'* obtained from the corresponding Auger lines, thus providing quantitative correspondence of experimental and calculated data. The experimental In 3*d* chemical shifts in the initial state for the clathrate are typical for covalent compounds of formal In^{2+} InSe and In^{+3} in In_2Te_3. For the Sn 3*d* the chemical shifts correspond to Sn^{2+} in relatively covalent compounds like SnS, SnSe and SnTe. The As 3*d* peak position is close to that for covalent GaAs. As for iodine, the chemical shifts show the effective negative charge, which is even higher than that typical for ionic compounds like LiI and KI; this proves the electrostatic nature of the host-guest chemical bonds.

The authors studied the band structure both experimentally by photoemission spectroscopy and by quantum modelling using the Green function method. They used different excitation energies from 60 to 150 eV as well as 727 eV (which is more bulk sensitive) to check whether the possible surface contribution to the valence band spectrum can be revealed. As the

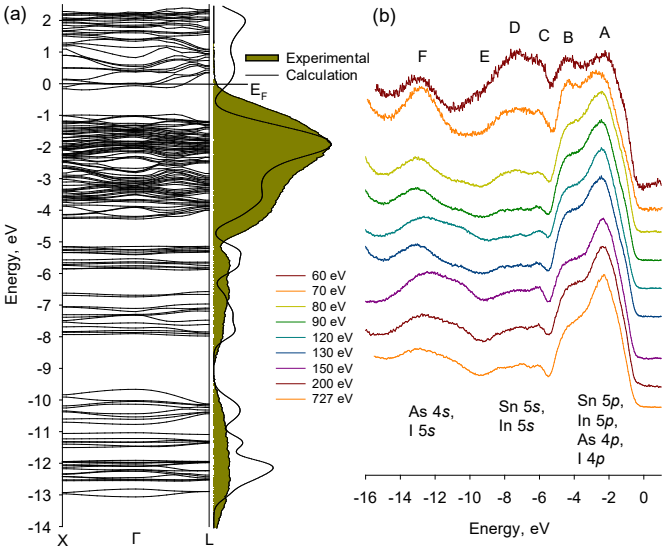

Figure 11: Band structure of $Sn_{24-x-\delta}In_xAs_{22-y}I_8$ for x=12: a) calculated band dispersion and total DOS; the Fermi level is set at zero energy, b) photon energy variation of the valence band spectrum (experimental data).

lattice constant is quite large, the contribution of the *k* perpendicular variation cannot be resolved. Indeed, all spectra show the same features, but with different intensity ratio. In addition, the spectrum obtained at high photon energy is in good agreement with the calculated DOS for the bulk crystal.

According to the calculations, ideally ordered and defect-free $Sn_{12}In_{12}As_{22}I_8$ is a degenerate semiconductor with an indirect band gap of 0.79 eV. The bands positioned at binding energies up to −5 eV in Fig. 11 are presumably composed of *p*-orbitals which are strongly mixed both due to the covalent nature of the bonds in the cage and to their overlapping in the energy scale. Introducing an As vacancy strongly modifies the electronic structure of the clathrate - a new energy level appears in the vicinity of the valence band in the gap resulting in the band gap of 0.07 eV. This is in line with the experimental observation of the charge carrier activation energy for different compositions of clathrates of the Sn–In–As–I series.

The chemical bonding and electronic properties of the clathrates $Sn_{24-x-\delta}In_xAs_{22-y}I_8$ of different *x* were explored by means of photoemission spectroscopy and theoretical modelling. Using the Auger parameter concept, the initial state chemical shifts were determined and compared with those simulated by DFT calculations. From this comparison one can deduce a covalent chemical bonding in the cages composed of Sn, In, and As and strongly ionic bonds between host and guest atoms, with clear charge

transfer from the framework atoms to the guest iodine orbitals. The defect-free $Sn_{24-x-\delta}In_xAs_{22-y}I_8$ clathrate crystals are *n*-type semiconductors with the estimated band gap of 0.3–0.8 eV, but if arsenic vacancies are taken into account; then the band structure essentially modifies owing to a new energy level appearing in the gap that makes the gap width ~0.05 eV and closer to the experimental data. The chemical modification of the surface reveals the contribution of I 5*p* orbitals in DOS in the vicinity of the Fermi level. This is in line with the calculations, according to which the valence band is composed by shallow mixed I 5*p*, As 4*p*, In 5*p* and Sn 5*p* orbitals and two lower bands of presumably *s*-character.

OTHER REFERENCES

[1] Snyder, G. J.; Toberer, ***E. S. Nat. Mater.*** **2008**, 7, 105–114.

[2] Kanatzidis, M. G. In ***Recent trends in thermoelectric materials research I***; Semiconductors and semimetals; Academic Press, 2000; Vol. 69, pp 51–100.

[3] Shevelkov, A. V.; Kovnir, K. A.; Zaikina, J. V. In ***The Physics and Chemistry of Inorganic Clathrates***; Nolas, G. S., Ed.; Springer Netherlands: Dordrecht, 2014; Vol. 199, pp 125–167.

[4] Paschen, S.; Pacheco, V.; Bentien, A.; Sanchez, A.; Carrillo-Cabrera, W.; Baenitz, M.; Iversen, B. B.; Grin, Y.; Steglich, ***F. Phys. B Condens. Matter*** **2003**, 328, 39–43.

[5] Christensen, M.; Abrahamsen, A. B.; Christensen, N. B.; Juranyi, F.; Andersen, N. H.; Lefmann, K.; Andreasson, J.; Bahl, C. R. H.; Iversen, B. B. ***Nat. Mater.*** **2008**, 7, 811–815.

[6] Takabatake, T.; Suekuni, K.; Nakayama, T.; Kaneshita, E. ***Rev. Mod. Phys.*** **2014**, 86, 669–716.

[7] Kovnir, K.; Stockert, U.; Budnyk, S.; Prots, Y.; Baitinger, M.; Paschen, S.; Shevelkov, A. V.; Grin, Y. ***Inorg. Chem.*** **2011**, 50, 10387–10396.

[8] Fulmer, J.; Lebedev, O. I.; Roddatis, V. V.; Kaseman, D. C.; Sen, S.; Dolyniuk, J.-A.; Lee, K.; Olenev, A. V.; Kovnir, K. ***J. Am. Chem. Soc.*** **2013**, 135, 12313–12323.

[9] Prokofiev, A.; Sidorenko, A.; Hradil, K.; Ikeda, M.; Svagera, R.; Waas, M.; Winkler, H.; Neumaier, K.; Paschen, S. ***Nat. Mater.*** **2013**, 12, 1096–1101.

ACKNOWLEDGEMENTS

Authors are grateful to the Russian Foundation for Basic Research (grants 13-03-01187 and 13-03-00571). The calculations were performed using SKIF and "Lomonosov" supercomputers, Supercomputing Center of Lomonosov Moscow State University.

AFFILIATION:

1. Lomonosov Moscow State University, Moscow, Russia
2. ALBA Synchrotron, Cerdanyola del Vallès, Barcelona, Spain
3. Institute of Solid State Physics, Dresden University of Technology, Dresden, Germany

SAXS analysis of comonomer distribution between amorphous and crystalline phases of biodegradable copolyesters

Incorporation of azelate units into the crystalline phase of the copoly(alkylene dicarboxylate) derived from 1,9-nonanediol and an equimolar mixture of pimelic and azelaic acids, *Polymers*, 7(9), 1871-1894 (2015)

Angélica Díaz[1], María T. Casas[1], Luís J. del Valle[1], Lourdes Franco[1] and Jordi Puiggalí[1]

Properties of polymeric materials can be tuned by blending appropriate homopolymers and more precisely by synthesizing copolymers where different monomers are combined according to variable architectures. Properties such as degradability are strongly related to the way these constituent units are located in crystalline and amorphous phases. The present work is an example of the application of synchrotron radiation to address this problem.

Poly(alkylene dicarboxylate)s constitute a family of biodegradable polymers of growing interest because they may contribute to solve "white pollution" concerns and also because of their potential applications in the biomedical field.

Synthesis of copolymers offers a key opportunity to increase the range of degradable materials and even to get a set of new products with easily tuneable properties. Incorporation of comonomers should have a great influence on thermal and mechanical properties, sample crystallinity, and hydrolytic and enzymatic degradability [1-3].

Degradation of semicrystalline polymers preferably takes place in the amorphous phase but must also occur in the crystalline domains despite having a closely-packed structure. Lamellar crystals obtained by crystallization from dilute solutions are ideal systems to detect how this degradation takes place, finding that both molecular packing and the nature of molecular folds play a crucial role [4].

The present work has been focused on the study of the crystalline structure of bio-based poly(nonamethylene azelate), poly(nonamethylene pimelate) and the related copolymer having a similar ratio of the two dicarboxylate units. The main goal is nevertheless the comprehension of the distribution of comonomer units in the crystalline phase and the repercussion of this arrangement on the single-crystal morphology and the degradation behaviour.

The random copolyester (COPES 9,7/9) was able to crystallize from 1,6-hexanediol dilute solutions giving rise to large single crystals with a temperature-dependent pseudohexagonal morphology (Figures 12a and 12b). Azelate and pimelate units were incorporated into lamellae without

causing a significant distortion of crystalline lattice as supported from electron diffraction data (inset of Figure 12c). Nevertheless, comonomer units were differently distributed between the lamellar core and the lamellar surface. Thus, the crystalline part mainly corresponded to poly(nonamethylene azelate) (PES 9,9) as supported by the observed layer lines, the intensities of reflections in the fibre X-ray diffraction pattern (Figure 12c) and the crystalline absorption bands observed in the FTIR spectrum (data not shown). Lipase from *Rhizopus oryzae* was able to undertake an enzymatic attack, which was clearly initiated in the lamellar surfaces. Lamellar edges showed a major resistance as also observed in thermal annealing experiments (Figures 12d and 12e). The close-packed crystalline regions were therefore effectively degraded without being detected a preferential attack over the different crystalline sectors as would be presumable if a distinctive chain folding was produced.

Crystallization from the melt state rendered spherulitic morphologies and SAXS peaks that were indicative of a lamellar stacking. These peaks were analyzed by means of the correlation function which allowed to distinguish morphologic parameters like: long period, L_y, amorphous layer thickness, l_a, and crystalline lamellar thickness, l_c. Clear differences in lamellar thickness were found among the three studied samples (Figure 13a), the highest and lowest values corresponding to COPES 9,9/7 and PES 9,7, respectively. In addition, data obtained during crystallization revealed a significant decrease of L_y during primary crystallization, and a steady decrease during the secondary crystallization (Figure 13b) as a consequence of a lamellar insertion mechanism. Homopolymers showed differences in their amorphous layer thickness (i.e. from 4.25 to 6.24 nm), suggesting the existence of larger irregular molecular folds on the lamellar surface when the polymer was constituted by the slightly more rigid pimelate units. The greatest amorphous layer thickness (i.e. 7.17 nm) was observed in the copolymer, indicating that chain defects caused by the presence of comonomer units could be placed in these amorphous interlamellar regions.

Structural studies indicated that PES 9,7, PES 9,9 and COPES 9,7/9 crystallize according to an orthorhombic $P2_1ab$ space group and large unit cells that incorporate several molecular segments. These have an all-trans conformation and are arranged with a setting angle close to ± 50º. Morphology of lamellar crystals is variable, increasing their aspect ratio as the degree of supercooling decreases. Interestingly, copolymers are able to crystallize despite the high comonomer content giving rise to well-formed lamellae. Single crystals of the three

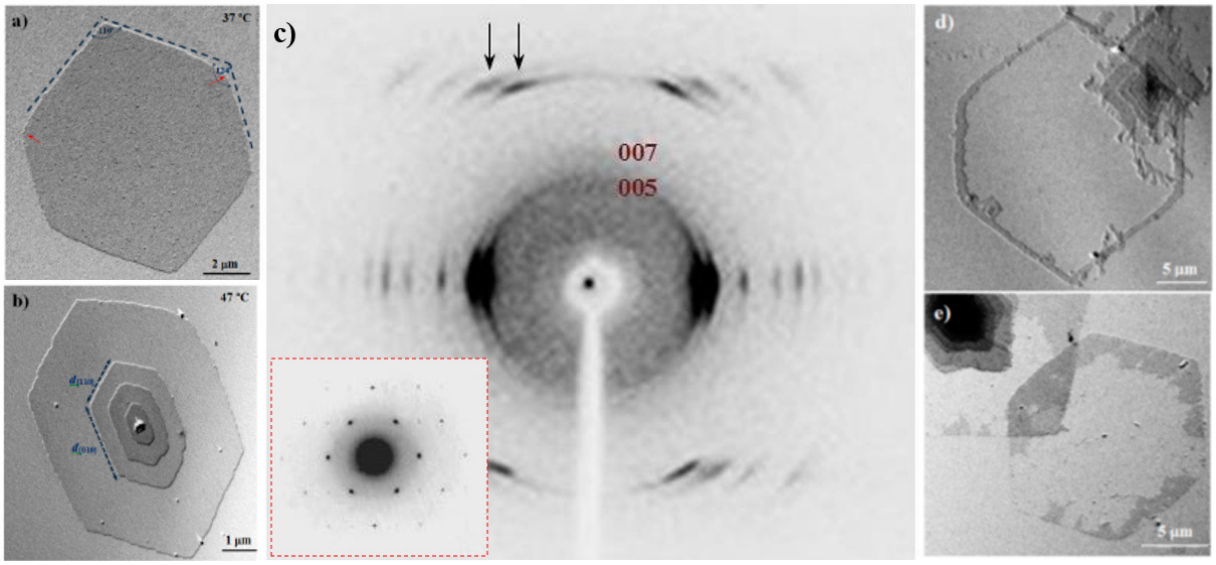

Figure 12: Lamellar single crystals of COPES 9,7/9 obtained at 37 ºC (a) and 47 ºC (b). Fibre X-ray and electron diffraction patterns (c) of COPES 9,7/9. Arrows indicate characteristic reflections of PES 9,9. Single crystal morphologies observed after thermal annealing (d) and enzymatic degradation (e) processes.

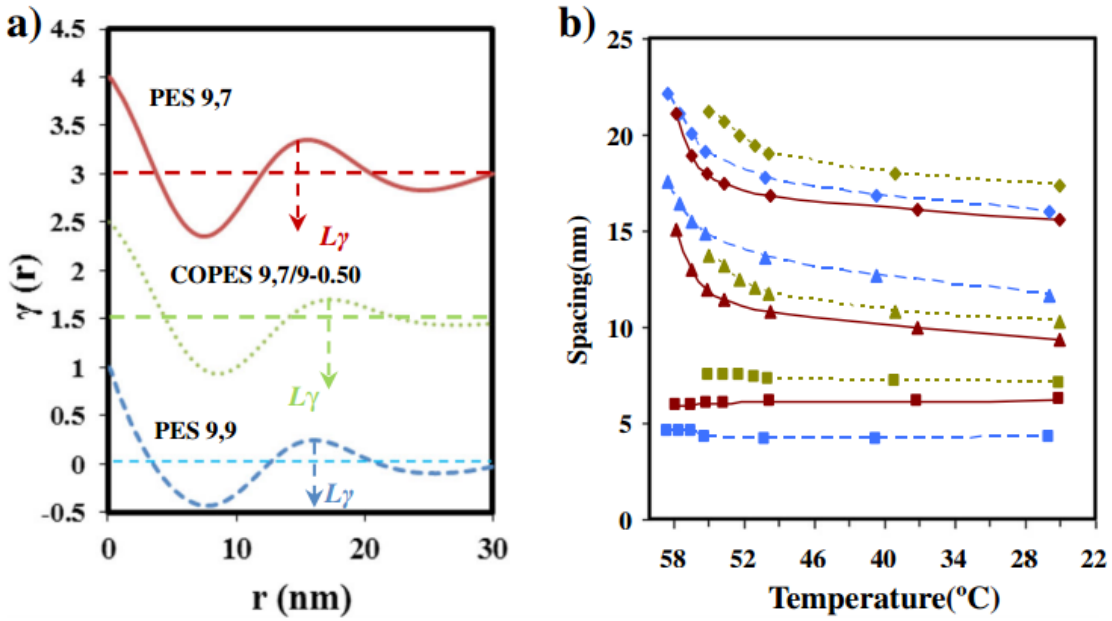

Figure 13: a) Correlation functions for non-isothermally crystallized PES 9,7, PES 9,9 and COPES 9,7/9 samples. b) Temperature evolution of L_γ (♦), l_c (▲), and l_a (■) during the nonisothermal crystallization (3 °C/min) of PES 9,9 (dashed lines), PES 9,7 (solid lines) and COPES 9,7/9 (dotted lines) samples.

samples are easily degraded by enzymes, which initiate the attack on the amorphous lamellar surfaces in such a way that crystals edges remain practically unaltered until the later stages of degradation.

X-ray diffraction data and FTIR spectra of the melt crystallized copolymer indicated a slight disorder along the chain axis and a preferential incorporation of azelate units in the crystalline phase. Pimelate units become therefore mainly located in the lamellar folding surface conditioning degradation and thermal annealing processes. An increase of both, the lamellar long period and the amorphous layer thickness as well as a significant decrease on the crystallinity of the lamellar stacks are characteristic features of the copolymer that were deduced by correlation function analysis of SAXS patterns.

OTHER REFERENCES

[1] Gan, Z.; Abe, H.; Doi, Y. Crystallization, melting, and enzymatic degradation of biodegradable poly(butylene succinate-co-14 mol% ethylene succinate) copolyester. ***Biomacromolecules* 2**, 313–321 (2001)

[2] Li, X.; Sun, J.; Huang, Y.; Geng, Y.; Wang, X.; Ma, Z.; Shao, C.G.; An, H.N.; Yan, T.Z.; Li, L.B. Inducing new crystal structures through random copolymerization of biodegradable aliphatic polyester. ***Macromolecules* 41**, 3162–3168 (2008)

[3] Liang, Z.; Pan, P.; Zhu, B.; Dong, T.; Hua, L.; Inoue, Y. Crystalline phase of isomorphic poly(hexamethylene sebacate-co-hexamethylene adipate) copolyester: Effects of comonomer composition and crystallization temperature. ***Macromolecules* 43**, 2925–2932 (2010)

[4] Casas, M.T.; Puiggalí, J. Enzymatic degradation of poly(octamethylene suberate) lamellar crystals. ***Polym. Degrad. Stab.* 94** , 1941–1947 (2009)

ACKNOWLEDGEMENTS

Authors are in debt to support from the Spanish Ministry of Economy and Competitiveness and the ERDF (MAT2015-69547-R) and the Government of Catalonia (2014SGR188). Diffraction experiments were performed at the NCD beamline of the ALBA Synchrotron with the collaboration of ALBA staff.

AFFILIATION:
1. Chemical Engineering Department, Polytechnic University of Catalonia, Barcelona, Spain

Towards a calcium-based rechargeable battery

Towards a calcium-based rechargeable battery, *Nature Materials* 15, 169-172 (published online October 2015)

A. Ponrouch[1], C. Frontera[1], F. Bardé[2] and M.R. Palacín[1]

X-ray diffraction has demonstrated the viability of calcium as electrode for rechargeable batteries, paving the way for the search of more sustainable energy storage technologies.

The development of a rechargeable battery technology using light electropositive metal anodes would bring in a breakthrough in energy density [1]. For multivalent charge carriers (M^{n+}), the number of ions that must react to achieve a certain electrochemical capacity is diminished by two (n=2) or three (n=3) when compared to Li^+ [2]. Calcium is especially attractive as it is the fifth most abundant element on earth crust and its standard reduction potential is only 170 mV above that of lithium, enabling significantly larger cell potential than that achievable with magnesium. The electrodeposition of calcium was thought to be impossible to date [3] and research restricted to non-rechargeable systems [4-7]. Considering the ideal properties of any electrolyte in terms of stability, viscosity and ability to dissociate salts, the authors decided to reinvestigate conventional polar aprotic solvents with high dielectric constants, such as alkyl carbonates used in commercial Li-ion batteries, as potential electrolytes to enable the development of calcium-based batteries. The feasibility of reversible calcium electrodeposition in such electrolytes containing salts with known stable anions was assessed at diverse temperatures in order to grasp the influence of ion pair formation.

The experiment consisted on assembling an electrochemical cell using a Cu disk as working electrode, an electrolyte made of a calcium salt in ethylene carbonate (EC) and propylene carbonate (PC) embedded in a fibre glass separator and Ca metal as counterelectrode. Cyclic voltammetry allowed to detect a reversible redox process when the $Ca(BF_4)_2$ salt was used, which could tentatively be assigned to calcium deposition. In order to assess this hypothesis, potentiostatic deposition was performed at -1.5 V vs Ca^{2+}/Ca at 75ºC-100ºC and an important reduction current was recorded.

The cell was disassembled inside an Ar filled glovebox and a grey and metallic like deposit was observed onto the Cu disk. This deposit was recovered and introduced inside a borosilicate glass capillary and sealed.

The capillary was brought to ALBA and its X-ray diffraction pattern was measured at BL04-MSPD beamline [8] using Mythen® bank of detectors. The sample was irradiated with a monochromatic beam focused on the detectors to enhance the resolution. Capillary was rotated during data collection to ensure a random orientation of the crystallites. The energy of the beam was selected at 20keV, which is the optimum for the detector used.

The pattern obtained was analyzed by the Rietveld method (Figure 15) after identifying the different crystalline phases present in the recovered material.

Based on the diffraction pattern analysis, the authors can assess that metallic Ca deposits on top of Cu. Besides Ca, they find CaF_2 resulting from the electrolyte salt decomposition, and minor amounts of Cu and Fe from the substrate and cell. Rietveld refinement allows the quantification of the crystalline phases and it shows equimolar amounts of Ca and CaF_2 and 6 and 3 wt-% of Cu and Fe respectively).

Thanks to the use of synchrotron diffraction the authors have been able to unquestionably confirm the deposition of Ca using $Ca(BF_4)_2$ in EC:PC as electrolyte and confirm the viability of such large potential window electrolytes for calcium plating-stripping.

These results thus open the way to exploratory screening and testing of potential cathode materials which would reversibly insert and deinsert calcium to assemble a full calcium based cell and achieve proof-of-concept. The authors are confident that these findings will serve as the basis to explore alternative far-reaching research avenues to explore the viability of a practical application.

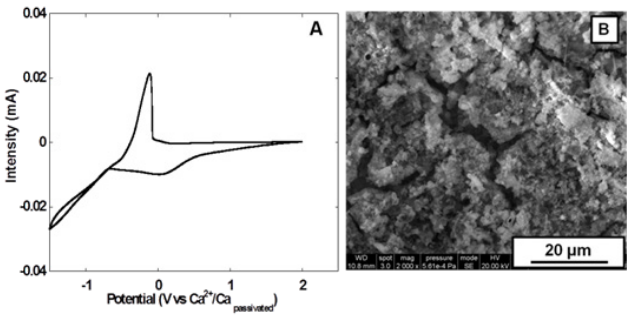

Figure 14: a) Cyclic voltammogram of 0.3 M $Ca(BF_4)_2$ in EC:PC based electrolytes (0.5 mV/s scan rate, 100ºC). b) Typical SEM micrographs of deposits (200h, 75ºC) obtained in 0.3 M $Ca(BF_4)_2$ in EC:PC at -1.5 V vs. $Ca^{2+}/Ca_{passivated}$.

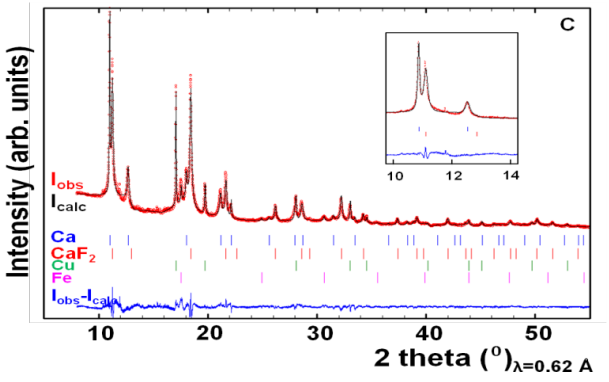

Figure 15: Rietveld refinement of measured pattern corresponding to the deposit achieved at 75 ºC with contributions from different crystalline phases found (indicated besides reflections coming from every phase). Inset: detail of the Ca most intense diffraction peaks.

OTHER REFERENCES

[1] Muldoon, J. Quest for Nonaqueous Multivalent Secondary Batteries: Magnesium and Beyond, ***Chem. Rev.* 114**, 11683-11720 (2014)

[2] Amatucci, G.G. et al. Investigation of Yttrium and Polyvalent Ion Intercalation into Nanocrystalline Vanadium Oxide. ***J. Electrochem. Soc* 148**, A940-A950 (2001)

[3] Aurbach,D., Skaletsky, R., Gofer, Y. The Electrochemical Behavior of Calcium Electrodes in a Few Organic Electrolytes. ***J. Electrochem. Soc.* 138**, 3536-3545 (1991)

[4] Sammells, A.F., Schumacher, B. Secondary Calcium Solid Electrolyte High Temperature Battery. ***J. Electrochem. Soc.* 133**, 235-236 (1986)

[5] Staniewicz, R.J. A Study of the Calcium-Thionyl Chloride Electrochemical System. ***J. Electrochem. Soc.* 127**,782-789 (1980)

[6] Hayashi, M., Arai, H., Ohtsuka, H., Sakurai, Y. Electrochemical characteristics of calcium in organic electrolyte solutions and vanadium oxides as calcium hosts. ***J. Power Sources* 119–121**, 617–620 (2003)

[7] See, K.A. et al. A High Capacity Calcium Primary Cell Based on the Ca-S System. ***Adv. Energy Mater.* 3**, 1056-1061 (2013)

[8] F. Fauth, I. Peral, C. Popescu, M. Knapp. The new Material Science Powder Diffraction beamline at ALBA Synchrotron. ***Powder Diffraction* 28 (S2)**, S360 (2013).

ACKNOWLEDGEMENTS

The authors thank the Toyota Battery Research division at Higashi Fuji (M6) for their funding, ALBA synchrotron for the beamtime, and Dr. F. Fauth for his support during data collection.

AFFILIATION:

1. Materials Science Institute of Barcelona (ICMAB-CSIC), Cerdanyola del Vallès, Barcelona, Spain.
2. Toyota Motor Europe, Zaventem, Belgium.

Materials, techniques and conservation of historic stained glass "grisailles"

Materials, Techniques, and Conservation of Historic Stained Glass "Grisailles".
***International Journal of Applied Glass Science* 7, 41-58 (2015)**

Trinitat Pradell[1], Gloria Molina[1], Sonia Murcia[2] and Rafael Ibàñez[2],
Chaoren Liu[1], Judit Molera[3], Andrew J. Shortland[4]

High-resolution X-ray diffraction studies to understand the differences in production and conservation of "grisailles" from the 16th, 17th, 19th and 20th centuries.

A grisaille is a black paint applied onto the inner surface of stained glass to draw the contours and details of figures and to produce the effect of shades and volumes (Fig.16).

Grisailles were traditionally made of finely ground oxides of iron but also of copper, lead, or manganese mixed with a flux such as lead ground glass and a binder and fixed onto the flat glass by firing. The grisailles of typical layer thickness between 10 and 100 μm are formed by a mixture of pigment particles, crystalline and amorphous reaction compounds, aging, and weathering compounds.

This work is part of a comprehensive program of restoration of the stained glass windows of the Cathedral of Segovia, which is being carried out the by studio Vetraria Muñoz de Pablos and particularly addressed the conservation of 17th century grisailles. A representative sample of glasses was used which included fragments from the Pierres master glaziers (16th century), see Fig. 16, Herranz (17th century), and Maumejan enterprise (20th century). Changes in the methods of production and materials in the different historical periods are obtained and related to the conservation state of the materials.

Polished cross sections of the glasses were studied by a set of complementary analytical techniques. The grisailles layer thickness, microstructure, vitrification degree and conservation state was studied by Scanning Electron Microscopy with an Energy Dispersive X-ray Spectroscopy detector attached to the microscope. Moreover, chemical analysis including trace elements of the glasses and grisailles was obtained by Laser Ablation Inductively Coupled Plasma Mass Spectrometry. Micro-XRD patterns of the microcrystallites present in the grisailles, i.e. the original pigment particles and reaction compounds formed during firing, as well as, aging and weathering compounds were obtained from thin cross sections (100-200 μm) of the grisailles, in transmission geometry, using a 0.4243Å wavelength, a 20 x 20 μm^2 spot size, and a CCD camera at MSPD beamline.

The stained glasses from the different epochs also show different compositions (16th century glasses are lime glasses, ~20% CaO; 17th century glasses are soda-potash, ~10% Na_2O and K_2O and 19th and 20th

Figure 16: Pierres de Holande and Pierres de Chiverri. Catedral de Segovia, 1544-1548.

century glasses are soda-lime, ~10 to 15% Na_2O and CaO). The thermal properties of the glasses and in particular the glass transition temperature was measured by Differential Scanning Calorimetry; 650ºC, 500ºC and 550ºC-600ºC for the 16th, 17th and 19th-20th century glasses respectively.

All the grisailles are basically formed by hematite (iron oxide) particles stuck together by a lead glass sometimes containing boron. The 16th century grisailles do not contain boron, show a thick glass-grisaille interaction layer and the formation of large a lead iron silicate microcrystallites (Fig. 17A) due to the reaction of the lead glass and the original hematite particles. On the contrary, the glass in the 17th century grisailles contain boron and higher amounts of lead and a large variety of microcrystallites, some formed by the reaction of the lead glass with the environment (lead phosphates, sulfates and carbonates) and others formed by the reaction between the lead glass and the hematite particles, and also lower temperature lead iron silicate (Fig. 17B). All this is indicative of a grisaille of unbalanced composition, heterogeneous nature and large particle size. Moreover, the lead-poor glass-grisaille interaction layer and cracks parallel to the glass surface are also indicative of a low firing temperature. Finally, the 19th and 20th century grisailles appear highly vitrified showing large porous related most probably to the large amount of boron present in the lead glass; they also show the presence of reaction microcrystallites and a well-developed interaction layer (Fig. 17C).

The addition of higher lead and boron glass in the grisailles was necessary to reduce the firing temperature to those acceptable to the base glasses; as a consequence, they appear more vitrified with lower opacity and more porous. The inadequate materials used in the 17th century are responsible for their dreadful conservation state.

The materials and firing conditions from the 16th century grisailles had to change in the 17th, 19th, and 20th centuries mainly due to the different composition of the glass which drastically reduced the acceptable firing temperature (about 650ºC, 500ºC and 550ºC-600ºC respectively); the addition of more fluxes (lead oxide and borax) in the grisailles allowed to fire them at lower temperatures. The grisailles, formed basically by hematite particles stuck together with glass, appear more vitrified although the firing temperature was lower. The 16th century grisailles do not contain boron show a good glass-grisaille interaction layer and large reaction microcrystallites. The 17th century grisailles contain boron and show the presence of crystallites of lead phosphates, sulfates, and carbonates formed by the reaction with the environment, as well as lower temperature reaction microcrystallites; they show a lead-poor glass-grisaille interaction layer and many cracks parallel to the glass surface; all this is indicative of a low firing temperature. The 19th and 20th-century grisailles appear highly vitrified showing large porosity related to the addition of boron, reaction compounds and a good interaction layer; the large porosity might, in time, give also conservation problems.

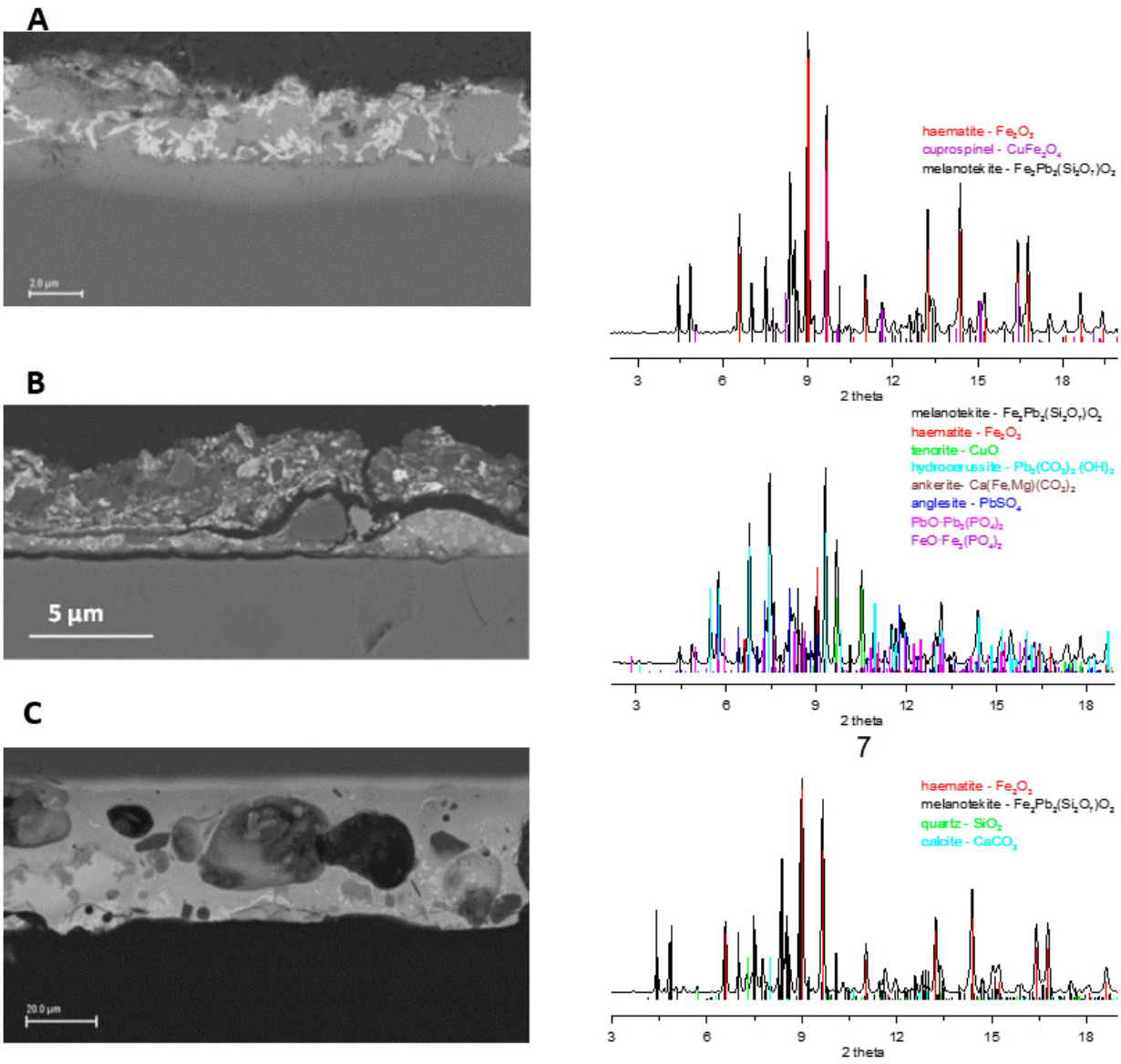

Figure 17: Typical A) 16th B) 17th and C) 19th-20th century grisaille microstructures and characteristic XRD patterns of the microcrystallites.

ACKNOWLEDGEMENTS

These experiments were performed at the MSPD-BL04 beamline of the ALBA Synchrotron with the collaboration of ALBA staff. The project is funded by CICYT grant MAT2010-20129-C02 and MAT2013-41127-R and Catalan Government grant 2014SGR-581. Vetraria Muñoz de Pablos S.L. and in particular Pablo and Alfonso, are especially thanked for providing the glass pieces studied and all their valuable comments and help.

AFFILIATION:

1. Physics Department and Centre for Research in NanoEngineering (CRNE) Universitat Politècnica de Catalunya, Barcelona, Spain
2. Institut de Ciència dels Materials, Universitat de València
3. GRTD, Escola Politècnica Superior, Universitat de Vic
4. Department of Materials and Medical Sciences, Cranfield University

INDUSTRIAL
LIAISON OFFICE

Relations with the industry

The Industrial Liaison Office, in charge of the relationships between ALBA and the industrial community, has progressively increased its activity during the last years. The 2015 period was enormously fruitful given the increase in industrial activities and the growing number of different companies that have been using the ALBA facility or that have been interested in our techniques and developments.

The main activity led by the Industrial Liaison Office is the proprietary access to the beamlines, which during 2015 has increased by more than twice with respect to the 2014 period (see industrial beamtime hours graph). Almost all the beamlines carried out industrial measurements during 2015. The beamlines that allocated more industrial beamtime were MSPD and XALOC followed by NCD. 16 different international and local companies came to perform studies at ALBA during 2015. Those companies belong to very different industrials sectors such as pharmaceutical, chemistry, automotive, catalysis, nanotechnology, etc.

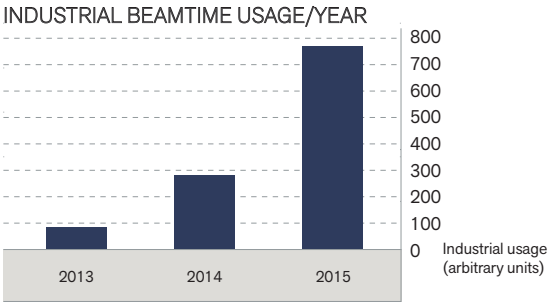

Pharmaceutical companies at ALBA

During 2015, the proprietary use of the MSPD and XALOC beamlines was mainly from pharmaceutical companies. In the MSPD beamline, most of the measurements at the powder diffraction endstation were focused on the detection of very low quantities of crystalline compounds present in drugs, like impurities or compounds that re-crystallize after the manufacturing process, as well as polymorphism studies. The higher resolution and detection levels compared to conventional powder diffraction make this beamline a really valuable tool for drug development as well as intellectual property protection in the pharmaceutical field. Proof of this is that, during 2015, six different companies have been using MSPD for these purposes and some of them are frequent users of the beamline.

The usage of macromolecular crystallography for drug discovery is also very well known among pharmaceutical companies. During 2015, XALOC has experienced the first industrial measurements with great success. Different pharmaceutical companies have been diffracting their crystals in XALOC to determine the structures of the target proteins with their inhibitors or drugs. It provides information at the atomic level on the interactions between the target and the drug and accelerates the long process of bringing a new pharmaceutical drug to the market.

Continuing with the pharmaceutical sector, in May 2015, ALBA celebrated an industrial workshop aiming to show to the pharmaceutical companies the applications of the state-of-the-art techniques and the advantages that synchrotron light might offer to their research and developments. It was a very successful event. More than 40 people from different companies attended to the workshop and were able to enjoy one day of presentations and networking with ALBA experts. Apart from the talks given by ALBA scientists, two different companies - Enantia and Almirall -

Networking during the Industrial Workshop for Pharmaceutical Companies celebrated at ALBA on the 7th of May 2015.

highlighted their experiences using the facility. Since the celebration of this event, the pharmaceutical usage of our beamlines has increased.

Diversity of industrial sectors benefiting from synchrotron light

In 2015, ALBA allocated beamtime to many different industrial sectors such as chemistry, nanotechnology, automotive, polymers, etc. For example, MSPD provided very interesting results in the area of batteries in the automotive industry as well as in the pigments sector. NCD beamline, devoted to small and wide angle X-ray scattering, was also a very useful tool for industries, mainly in the area of nanotechnology. This technique provides information on the size distribution. Comparison between different samples obtained at different conditions helps to find out the best manufacturing process. CLÆSS and BOREAS also dedicated beamtime to private companies. With those experiments, the companies benefited from the absorption techniques and acquired deeper knowledge about the local geometry of the samples as well as the electronic geometry and oxidation states. Also, surface studies on nanoparticles for catalysis and surface morphology were carried out at CIRCE.

These are some examples of the type of industrial studies that have been performed during 2015. It is expected to keep growing the industrial beamtime access in the years to come and for this purpose, ALBA will continue organizing specialized industrial workshops dedicated to specific industrial sectors.

Increasing commercial activity in the specialized laboratories of ALBA

In addition to beamtime access, ALBA has also increased the external usage of specialized laboratories such as the magnetic measurements and the radiofrequency laboratories and the optical and metrology laboratory also hosted its first commercial measurements. The main activity has been carried out by the ID-magnetic measurements lab, by testing with high precision different type of magnets such as dipoles, quadrupoles and bending magnets that want to be implemented in other accelerators and synchrotrons. The highly specialized personnel, their experience as well as the laboratory equipment have clearly strengthened the services provided in this lab and it is expected to keep increasing during 2016. Further information about that lab can be found in the following pages.

Technological transfer

ALBA is continuously developing new solutions to guarantee an optimal performance of the facility that may be of interest for the industrial community. In that direction, the Industrial Liaison Office is working together with ALBA scientists and engineers to establish the best approach to intellectually protect their own developments and, finally, to transfer them to the private sector for their commercial exploitation. During 2015, one new patent was registered for the X-ray mirror nanobender and one utility model for a new X-ray detector. Those developments were licensed to the private companies SENER and Alibava, respectively, for their commercialization.

The technological transfer is not only related to patenting and licensing ALBA developments but also to strengthening the relationships with private companies to find solutions together. In 2015, the AGAUR provided ALBA with funding for an industrial PhD. Part of this project is promoted by a private company that wants to increase the knowledge of optical surface cleaning by radiofrequency plasma sources and to implement it in its business. It is a three-year project that benefits both the private company and the interests of ALBA, and a significant success story for the public-private synergies and partnerships.

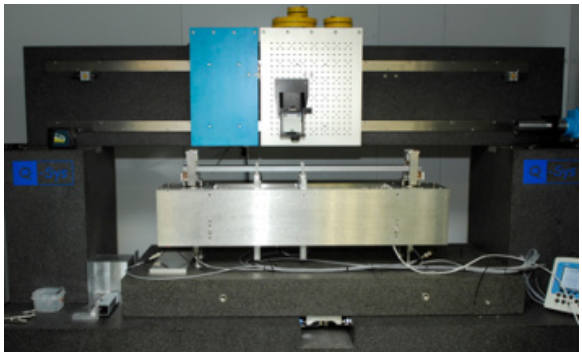

X-ray mirror nanobender licensed to SENER for its commercial exploitation.

TECHNOLOGY

During the year 2015, some projects of the facility have come to a successfully end, the implementation of a Fast Orbit Feedback for the Storage Ring and the extension of the synchronization timing capabilities to the beamlines. Also, in terms of collaboration, ALBA has measured -in the magnetic lab- the bending magnets of the SESAME project, the international synchrotron light source for the Middle East. And, already mentioned in the previous section, ALBA has developed new solutions that are also suitable for the industry, such as the X-ray mirror nanobender. For these reasons we dedicate this year's report to present in deep three developments and the magnetic lab.

The first article presents the Fast-Orbit FeedBack system, in charge of regulating the orbit of the electron beam with a correction frequency up to more than 100 Hz, which improves the stability of the beam below the micrometer level. It describes the system concept, the hardware implementation, the algorithms in soft real-time processes and the remarkable obtained results.

The second article presents the Timing System, which ensures the transmission of synchronization signals to accelerators and beamlines, with an accuracy of tens of picoseconds. The text also explains how the system was extended to broadcast interlock signals to any point in the installation -in a few microseconds- in order to ensure the safety operation of the accelerator equipment and how the beamlines got access to the synchronization capabilities of the Machine.

The third article explains in detail an advanced mirror bender, developed in-house, that includes, in addition to the usual bending mechanism, mechanical actuators that allow modifying the mirror surface by introducing a controlled deformation of the mirror substrate below the nanometer.

Finally, the fourth article explains the laboratory of magnetic measurements, its capabilities and how the team of physicists in charge of such measurements together with the mechanical, electronics and controls engineers put in place the tools and the appropriate benches to make the laboratory a reference of its kind, selling services to institutes all over the world.

The Fast Orbit Feedback System

Angel Olmos, Jairo Moldes, Xavier Serra

The Fast Orbit Feedback System (FOFB) is a hardware/software infrastructure developed at ALBA that aims to transversally stabilize the electron orbit using a feedback loop that evaluates the deviation of the beam position relative to the nominal one. A collection of beam position monitors provide the input values, which are computed via a specific mathematical algorithm to evaluate and apply the appropriate corrections to set the electrons to their nominal position. What follows is a brief description of the operating principles, technical characteristics and performances.

System description

One of the most important figure of merit of a modern synchrotron light source is the stability of the photon beam at the sample position. To achieve this, the position stability of the electrons in their orbit, that are the sources of the emitted photons, must be as high as possible. To achieve this goal, ALBA has developed a FOFB to reach sub-micron stability up to a frequency of 100 Hz.

The system is based on the reading of the beam orbit, computation of the correction values and final action on the beam through the corrector magnets, repeating this endless process in a feedback loop.

After investigation of possible system architectures, a decision was taken that exploits the available in-house hardware and 4-core processors. Future upgrade with dedicated electronics will enhance the FOFB system, in terms of performance and reliability.

Functional description can be summarized as a PI control loop. A PI is a controller that attempts to regulate a variable based on its current value (Proportional) and the previous ones (Integral). FOFB PI consists of 88/88 inputs/outputs for the horizontal plane and 89/88 for the vertical one:

- **Inputs:** the electron beam position measured at 88 Storage Ring eBPMs (electron Beam Position Monitors) plus the vertical photon beam measured at MISTRAL beamline xBPM (xRay Beam Position Monitor).

- **Algorithm:** core of the system that computes the necessary current change to be applied to the corrector power supplies to bring the beam position to the Golden Orbit (ideally established orbit of the electron beam).

- **Outputs:** the current values of the correctors.

The algorithm relies on the so-called Response Matrices Rx and Rz. These matrices are experimentally obtained by changing each corrector at a time and, then, measuring the position change on the BPMs, so that the effect of each corrector on the orbit is obtained.

From each plane, the algorithm computes the pseudo inverse matrices iRx and iRz. This is done using the SVD method (Single Value Decomposition). Once all done, the 88 correction values Cx and Cz are obtained by the following PI control implementation:

$$E(n) = iR * D$$

$$C(n) = C(n-1) + A1*E(n) + A2*E(n-1), \text{ for } A1 = (Ki * T/2) + Kp \text{ and } A2 = (Ki * T/2) - Kp$$

where the main variables are the difference between golden and measured orbits D, the error factors E, the proportional and integrative coefficients (Kp and Ki) and the correction loop period T (200us).

PI loops for horizontal and vertical plane are computed separately. This means that operators can tune Kp and Ki for horizontal and vertical planes separately, thus resulting in 4 different coefficients: Kpx, Kpz, Kix and Kiz.

The control of the 88x2 correctors (88 horizontal and 88 vertical) is spread around the 16 sectors of the ALBA Storage Ring. Other synchrotrons have a centralized orbit control where all calculations are done and then the correction values are distributed from the central node to the different correctors power supplies. At ALBA the system is distributed in 16 cPCI crates (compact PCI). As the problem is split in sectors, a given sector only has to compute its corrections with the advantage of less computation and, thus, higher speed.

The hardware

Figure 18 shows the global schematic hardware layout of the FOFB system. The system is composed of the following hardware elements:

- **BPMs (Beam Positon Monitors):** sensors that detect an electrical signal that is proportional to the electron or photon beam positions.

- **BPM electronics:** these devices are responsible for the calculation of the beam position. They transmit their own measured beam position and collect the position from all the other units at a 10 kHz rate. To do so, they are running a broadcasting firmware called Communication Controller (CC), developed at Diamond Light Source (DLS). There are currently 88 units connected to eBPMs and one unit connected to MISTRAL xBPM.

- **Sniffer cards:** 16 electronic cards that collect the data from the BPM electronics network. These boards are connected to the same network and hence can "sniff" the data flowing between the BPM electronics. This way these cards have all the X and Z beam positions from all the BPMs at a 10 kHz rate. The cards were originally purchased as event receivers for the Timing System, but since they have the necessary hardware components to act as Sniffers (suitable electronics and optical links), they were reused for this purpose.

- **CPUs:** 4-Core CPUs that calculate the needed correction for the beam. They run a soft real time program consisting of three steps: 1) Read data from the Sniffer card, 2) Compute the corrections to be applied to the corrector coils and 3) Apply these corrections to the power converter controllers through the IP carriers.

- **IP carriers:** these cards implement the interfaces that receive the setpoints from the CPUs and send them to the power converter controller through the so-called Transition Boards (Tx Boards).

- **Power converter controllers:** electronic devices that change the current of the correctors power converters (Correctors PC) according to the values sent by the IP modules.

- **Power converters:** AC-DC converters that feed current to the correction coils.

- **Correction Coils:** Extra wiring in the sextupole magnets, driven by the power converters that generate the magnetic field needed to correct the beam orbit.

The Sniffer cards, CPU and IP carriers are all seating in one cPCI chassis per sector.

Figure 19 shows the hardware layout of a sector. The BPM electronics are connected to each other to share their data within the sector. Then two of them are linked to the neighbouring sectors' electronics through the central node, where all sectors are interconnected. This way, all 88 BPM electronics share their position data. Two of the BPM electronics of each sector are wired to its sector Sniffer card, so that the positions from all BPM electronics are transferred to the 16 Sniffers.

The software

The software mainly consists of the following components:

***fofb* process:** this soft real time program runs on each of the 16 CPUs and is the core of the correction algorithm. The program is actually forked into 2 processes and uses a shared memory mechanism for external communication. One process (parent process) will take care of reading data from the Sniffer and then, when new data are available, it will signal that to the second process (child process)

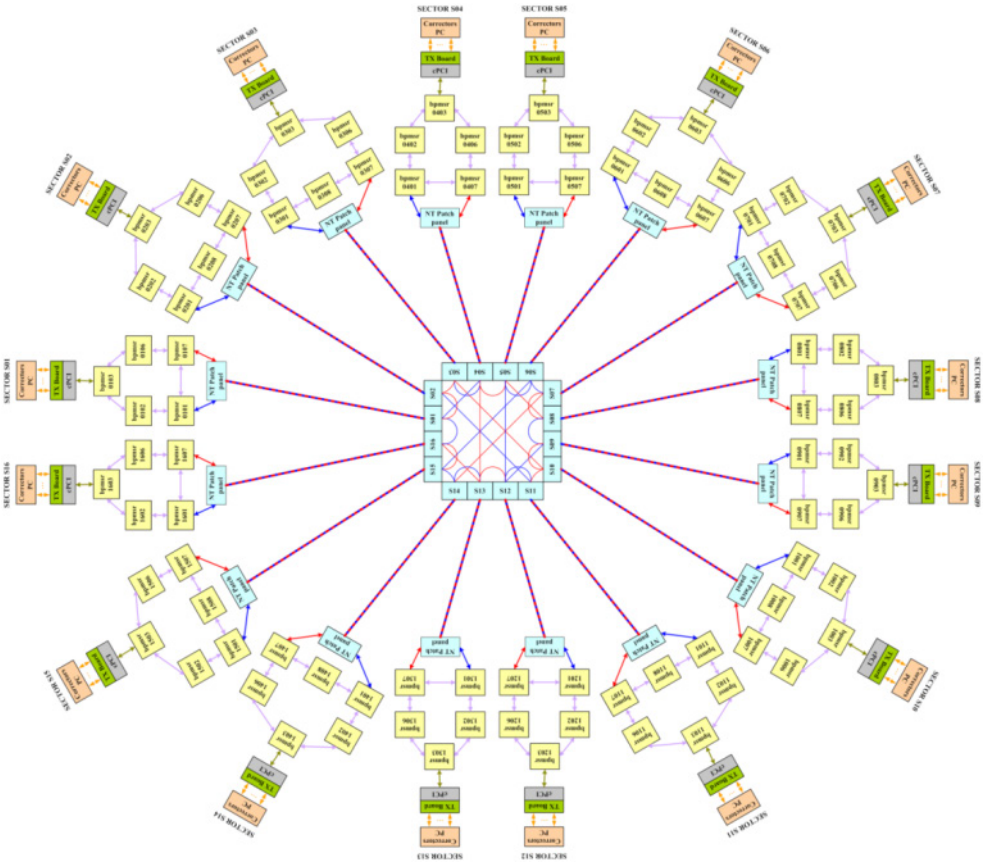

Figure 18: Global scheme of the FOFB system.

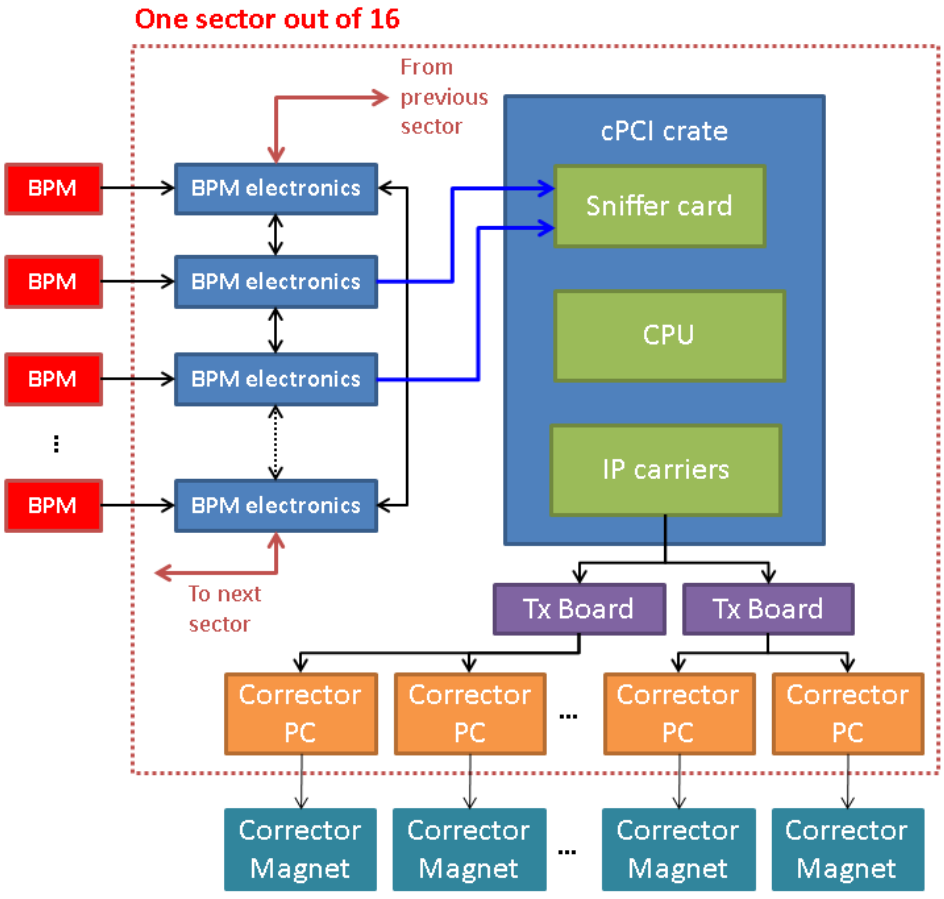

Figure 19: Hardware layout inside a sector.

and it will wait until new data from the Sniffer are available. Once signalled, the child process will compute the necessary corrections, apply them to the power supply and wait until it is signalled again.

TANGO device servers: the main task of these software layers is to provide a TANGO interface to the *fofb* programs, managing all the sectors' software in a single point, their configuration and the interfacing with the control room.

***ctfofb* GUI:** the GUI is the operators' control point of the whole FOFB system. It is a graphical front end to the TANGO device servers, presenting the more relevant attributes to the user.

Sniffer card and IP carrier drivers: modifications in these two drivers were necessary to properly access the hardware and guarantee the FOFB performance. The Sniffer driver was provided by DLS, who also shared with us the firmware to be run in the FPGA of the card.

FOFB performance

Correction of IDs perturbation. One of the main perturbations to the electron beam is caused by the magnetic field changes due to the movement of the Insertion Devices (IDs). Figure 20 shows the horizontal and vertical position of the 88 BPMs when moving XALOC in-vacuum undulator, at different FOFB status. One can see the proper position correction to zero when the FOFB is running, and also the noise reduction well below the micrometer level (on a slow rate time scale of 10 Hz).

Stability at different frequencies. Figure 21 shows a comparison of the integrated position FFT spectrum when FOFB is running (dashed lines) and when it is not (solid lines). FOFB specifications commonly refer to beam stability below 10% of the beam size. For ALBA, that means position stability below 13 um for the horizontal plane and 0.6 um in the vertical plane (generally speaking, because it actually depends on each beamline). When FOFB is running, beam stability specs are comfortably met even for high frequencies. For example at 1kHz, the frequency integrated rms horizontal and vertical amplitudes are respectively ~1,25 um and ~0,35 um, making the ALBA Storage Ring one of the most stable synchrotron light sources worldwide.

System limitations and future upgrades

- **Calculation speed:** the calculation loop can theoretically work at 10 kHz, but the system is currently working at 5 kHz due to data transfer limitations between the sniffer card and the CPU. That data transfer has to be done through 2 cPCI bridges that limit the transfer rate.

- **Redundancy:** the FOFB was originally designed to use sniffer cards with 2 optical links for redundancy in case a link goes down. Since existing sniffers with only 1 optical port were already reused, the redundancy is not accomplished and a full sector of correctors can be stopped if the link between its sniffer and the corresponding BPM is broken or not working.

- **Obsolescence:** BPM electronics and sniffer cards include already obsolete electronics inside. Spare modules have been purchased to cope with this problem.

- **Setpoints acknowledgment:** it was necessary to modify the IP carriers driver to make them able to send setpoints to the power converter controller at a high rate. With the regular driver, all the commands were checked to have been correctly understood by the controller. The mechanism used for acknowledgment was too slow to be compatible with FOFB needs. To solve that, the rewritten driver sends the command but does not wait for the acknowledgment. The problem with this is that it is not possible to know whether the command was correctly processed by the power converter controller, but that is the price to pay for high rate writings with the existing hardware.

Some of the limitations listed before are expected to be solved by the already acquired FOFB processors. The new boards will replace the existing sniffer and CPU cards. The intention is to migrate the data reading done by the sniffer and the correction calculation done by the CPU to a single board. There, the data transfer limitation will disappear and the correction calculation will run at 10kHz. Since it also has 2 optical ports, the expected FOFB redundancy will be met and the obsolescence problem of the current sniffer cards won't be a problem anymore.

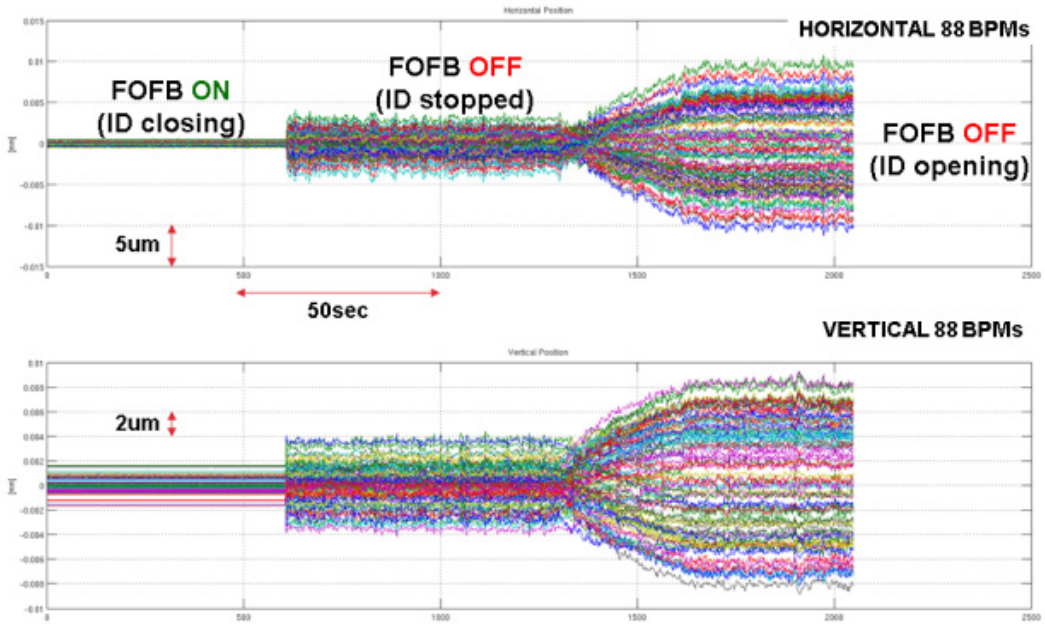

Figure 20: Correction of IDs perturbation.

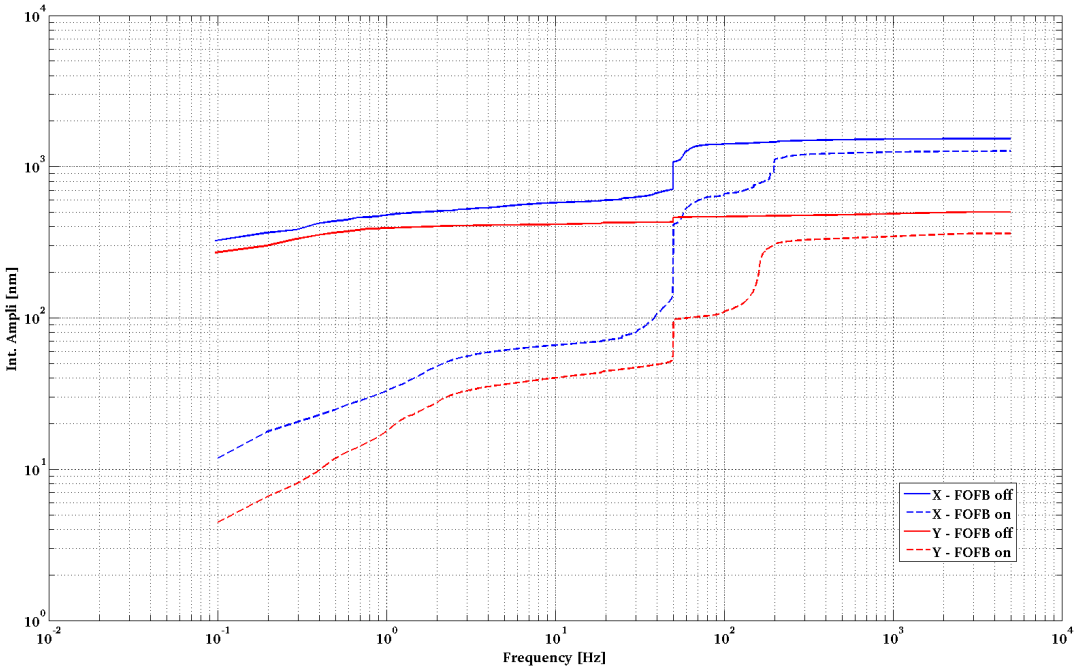

Figure 21: Comparison of the integrated position FFT spectrum (log scales).

Contributions

A. Olmos took the responsibility of the project and was in charge of the commissioning and the data analysis. J. Moldes developed the software for controls and data acquisition. X. Serra was in charge of the electronics. R. Petrocelli was responsible for power supplies. Z. Martí developed the machine physics. D. Yépez was committed to the commissioning of the project. G. Cuní, S. Rubio and S. Blanch were responsible for the controls software support. S. Pusó was responsible for the specific system administration. A. Gutiérrez, M. Muñoz and D. Beltrán were former contributors to this project. Special thanks to G. Rehm, M. Abbot and I. Uzun from the Diamond Light Source and A. Homs from the ESRF. A. Olmos, J. Moldes and X. Serra wrote the article.

Synchronization challenges in particle accelerators and why an independent Timing System is needed

Óscar Matilla, Jairo Moldes, Ángel Olmos, Michael Foerster, Lucía Aballe

The concept of "timing system" is widely used in the particle accelerators community. It refers to the system in charge of synchronizing the different parts of the accelerator (or what is also known as "sending the triggers"). In fact this generalization is somehow simplifying the need for time coherence in different locations, which allows the control and data acquisition systems to synchronize actions at a given time. This quite generic problem is in fact addressed very differently depending on the needs of each of the numerous subsystems.

Different types of timing systems

From a formal point of view the systems that are responsible of distributing time-coherent signals from one master to multiple receivers can be classified depending on the strategy used as:

- Signal-based systems – In this approach, a unique physical signal is connecting the master to each receiver where the trigger is needed, creating a typical tree diagram architecture often including further electronics to process and adapt the signals to the different applications. A typical example is a pulse trigger transmission from one point to two receivers via two independent cables in one of which a hardware delay is generated.

- Event-based systems – In contrast to the previous case, a common data bus is shared among all the receivers and the master. The master sends codes called events and the receivers are pre-programmed to react to certain events by generating actions with a certain delay. This approach enlarges the capabilities, the flexibility and provides better tools for commissioning, maintenance and troubleshooting. We can think of a typical example with three computers where one is sending commands via Ethernet to the other two and a concrete output is needed to be generated. In this example it is easy to realize the inherent flexibility of changing the delay of any response. Normally when time synchronization between receivers is high, an independent and exclusively used databus is needed.

- Time-based systems – In this case the master broadcasts messages to the receivers to generate triggers at certain timestamps. In parallel, they both share the same clock so the receiver can perform the proper action when the timestamp of the message coincides with the common clock.

It's all about time

When a new requirement for synchronization arises, the most critical factor to be determined is the precision needed to be guaranteed between the time base of the master and the receiver. The type, strategy and complexity of the system used will strongly depend on the order of magnitude of this factor:

- Milliseconds (and above) – There are innumerable time synchronization needs with this level of accuracy, being by far the most common in particle accelerators, its applications ranging from triggering or archiving to data acquisition. They are usually solved using time-based or event-based systems and implemented by software. When the accuracy needed is close to 1 ms, specific protocols such as Network Time Protocol (NTP) are used. Also multiple needs are solved using signal-based systems via PLCs or other input/output hardware that allows a very flexible implementation and tracking of all the signals. For this range the use of an independent transmission system to implement event-based or time-based systems is not usually needed unless there are specific safety requirements.

- Microseconds– When getting close to time ranges with an accuracy of microseconds a new problem needs to be addressed: the signal transmission time between the generator and the receiver gets close to the required accuracy that is needed. That means that the electronics in signal-based systems needs to be adapted. This electrical adaptation is usually very complex, discouraging

the use of event-based system architectures due to their inherent complexity and cost increase. On the other hand, the use of a time-based system is still possible with specific protocols such as the Precision Time Protocol (PTP).

- Nanoseconds and picoseconds accuracy – When getting close to an accuracy of nanoseconds the implementation of a signal-based system is much more complex. The electronics needed are very specific and temperature compensation needs to be deeply considered. The length of the signal paths needs to be calibrated and therefore a dedicated infrastructure is deployed. Independent event-based systems are starting to be used. They are commonly known as "Timing Systems". One of the main improvements implemented to reduce time jitter between receivers and master time bases is making each of the slaves capture the clock of the master. Following this same concept there are also some time-based developments as an evolution of PTP: for example the White Rabbit project being developed at CERN.

- Femtosecond accuracy – Increasing the accuracy to femtoseconds is not so common yet in synchrotrons, where the duration of electron bunches are typically in the order of ps. New developments led by Free Electron Lasers shorten the pulses down to 100 fs, creating new challenges. Achieving femtosecond accuracy is not directly possible using event-based or time-based systems alone: the electronics involved inherently have much more jitter and clock distribution, and recovery is almost impossible at those frequencies. To obtain an accuracy of this order of magnitude, very specific signal-based systems are designed based on lasers interferometry or other optic approaches.

The ALBA timing system

A known event-based architecture upgraded

When the ALBA project started, the initial synchronization requirements were fixed by the Accelerator Division. The main request was to distribute triggers synchronously with the RF master frequency (499.654 MHz) at different points of the machine with a very low jitter (bellow 100 ps), and to adjust the delay of triggers in steps lower than 16 ns. At some point, other requests regarding the transmission of fast interlock signals were made; the system needed to react synchronously, in the microsecond range, to interlock events at different locations of the machine. This was beyond the scope of the ALBA Equipment Protection System, which manages thousands of signals, is built on PLCs and deterministic ethernet technologies [1] and works with latencies of a few milliseconds.

In order to meet these requirements, different approaches were considered. The timing system that was being designed at that time already offered a platform to produce synchronous outputs and the transmission of the triggers was fast enough. Moreover its network already covered 106 different points all over the accelerator. Therefore, upgrading the timing system to manage a bidirectional communication link was considered to be the best possible option. Furthermore, there were different factors that reinforced the suitability of the project: the first one was the high flexibility that this architecture would provide, the second was that the diagnostic tools of event timestamps required by the timing system would also be reused for fast interlocks. Finally, regarding the cost, it appeared to be a very good solution as the timing network was composed of four fibre cables (following a "de facto" market standard) of which only one was used at that time.

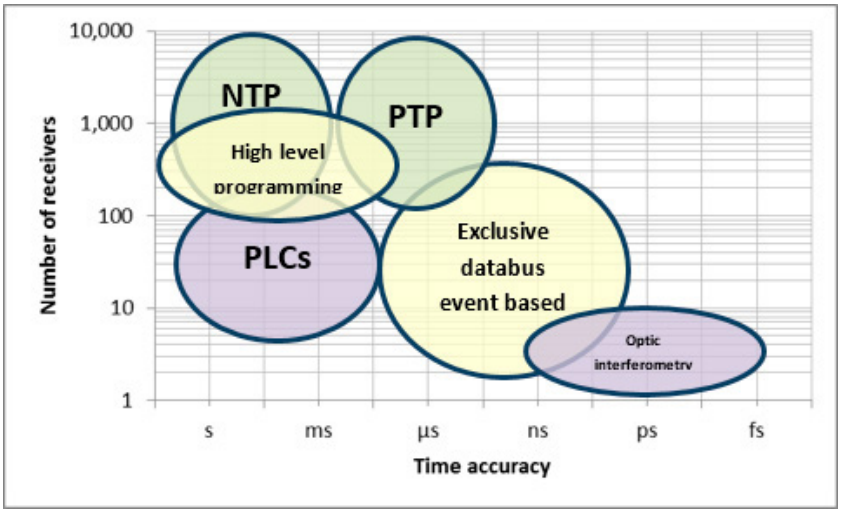

Figure 22: Diagram showing the different domains of basic synchronization techniques domain according to their time accuracy and number of receivers needed. PLC: Programmable Logic Controller, NTP: Network Time Protocol, PTP: Precision Time Protocol.

In conclusion, the Electronics and Controls Engineers at ALBA carried out the innovative project of extending the "traditional" mono-directional generator-to-receiver event-based Timing System already used in other synchrotrons to a bidirectional Synchronization and Fast Interlock System. ALBA was the first synchrotron where this functionality was implemented.

The basis of the receiver-to-generator link is enabling an independent event stream from the Event Receivers (EVR) towards the master called Event Generator (EVG) using the same infrastructure and the same protocol as the original Timing System. That stream of events is multiplexed in a new unit called "Fan Out Concentrator", which is one of the crucial parts of this new architecture as it manages event collision or saturation scenarios. Finally the interlock event stream arrives to the EVG, which dispatches the event so the interlock can arrive to all the points of the machine following the same path as the rest of the triggers generated by the EVG (Figure 23).

Implementation

The components of the timing system were purchased through two public calls for tenders. One was designed to purchase the electronics boards, generators, receivers and fan-outs, and the second one to purchase the fibre optics used for the timing network. More than 10 km of OM3 cable with 4 fibres were required with a very low dispersion in the fibre-optics length to minimize the thermal effects and the delay-adjustment procedures. In most cases the synchronization is carried out at the nanosecond range. However, in specific cases the system sets up delays fine-tuned in the order of tens of picoseconds, such as the trigger of the electron gun, the streak camera used for diagnostics and the storage ring injection kickers. For this purpose, a special 6U cPCI card manages delays at steps of 10 ps (EVRTG-300).

A cooperation with the company that manufactured the electronics was organised in order to carry out the fast interlock project. The results included new products such as a new electronics board, the FanOut Concentrator (cPCI-FCT-8) and a new firmware with the required functionalities

The response time from EVG to the EVRs in a typical event-based timing system is not a critical factor as far as all the trigger outputs are delivered synchronously and with the specified low jitter. But if the timing system is required to react to interlocks, its characterization becomes crucial. The hardware implementation at ALBA that codes and decodes the event stream uses 30 event clock cycles at 125 MHz adding up to a total time of 240 ns. Taking into account the number of stages, the total reaction time in the case of an interlock detection is:

$$\text{time} \approx 240\text{ns} \times 7 \text{ stages} + 5\,{}^{\text{ns}}/_{\text{m}} \times 450\text{m} \sim 3.8\mu\text{s}$$

To understand the real magnitude of this number we have to consider that in the interlock, codification, distribution, and decodification from any part to another of the machine, 60% of the time is used just for the signal propagation of the light over the optic fibre in order to transmit the signal to the different parts of the machine.

Timing Control System and User Interfaces

One of the main benefits of the event-based timing systems is their inherent big flexibility to configure trigger outputs, signals, delays and managing configurations. This flexibility, of course, extends to the Fast Interlock System.

The Control System is complex and physically distributed, and different layers of software components are needed in order to control the system:

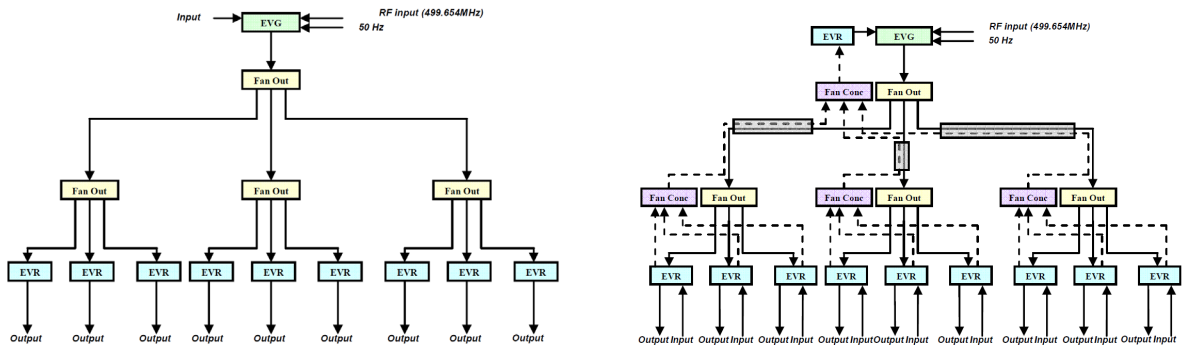

Figure 23: Traditional event-based block diagram based on Event Generator (EVG), Fan Outs and Event Receivers (EVR) (left) compared with upgraded block diagram implementing Fan-Out Concentrators (Fan Conc) (right).

- Drivers for interfacing the hardware with the linux operating system of the control machines.
- Low-level control software for interfacing with the ALBA general control system. ALBA uses tango[2] as the general control system and hence some pieces of software (known as device servers) had to be developed in order to configure and interface the hardware with the general control system.
- High level software. In this category we include both the user's direct control of the system and other applications that, amongst other things, need to manage the timing systems in order to perform their task (e.g. the top up feature).
- High level GUIs (graphical user interfaces). These are the user interface points with the whole system.

One of the challenges of the control system was to make the inherent complexity of the timing system transparent to the user by providing intuitive and easy-to-use tools. This was achieved by developing a general control GUI and a GUI for directly controlling the timing of the most basic injection elements (linac and kickers).

The users directly interact with the systems by using these GUIs. The timing manager GUI allows easy modification of the characteristics of any output signal of the whole system, configuration and easy log reporting of the fast interlock system.

Although the timing manager covers the whole system, a few purpose-specific graphical interfaces were developed in order to hide the inherent complexity of the timing system, such as the graphical interface for the configuration of the injection elements (linac and kickers), which is very frequently used by the operators.

Applications

The ALBA timing system is currently composed of 106 EVRs generating a total of 459 synchronized triggers.

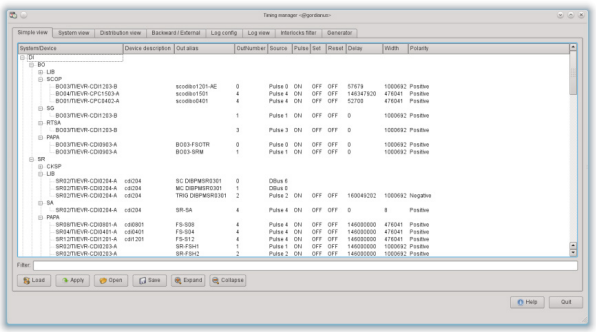

Figure 24: Timing manager Graphical User Interface.

Its event network based on OM3 optic fibre is longer than 10 km, and a total of 85 different event codes are being used. These numbers offer a clear overall picture of the extensive use of timing systems at ALBA.

This section presents two different applications that have been selected as examples of how the timing system is used in very different scenarios.

The use of a Fast Interlock System in the ALBA Machine Protection System

The Machine Protection System (MPS) ensures that the accelerator is not damaged by a number of hazards, such as the synchrotron radiation hitting the wrong place. There are many possible scenarios leading to an incorrect photon beam positioning that can cause damage to different machine components due to heat loading. To avoid this, the MPS monitors different machine parameters and interlocks the RF plants in case the beam has to be killed to prevent the damage.

The MPS has been built based on the redundancy accomplished by the use of the so-called Fast MPS through the Timing System (µs response time) and the Slow MPS through the Equipment Protection System EPS (ms response time). Figure 25 shows the different elements of the complete system. In red, the path for the Fast MPS over Timing, and in blue, the Slow one over EPS.

The MPS continuously checks that the following parameters are within their safe values:

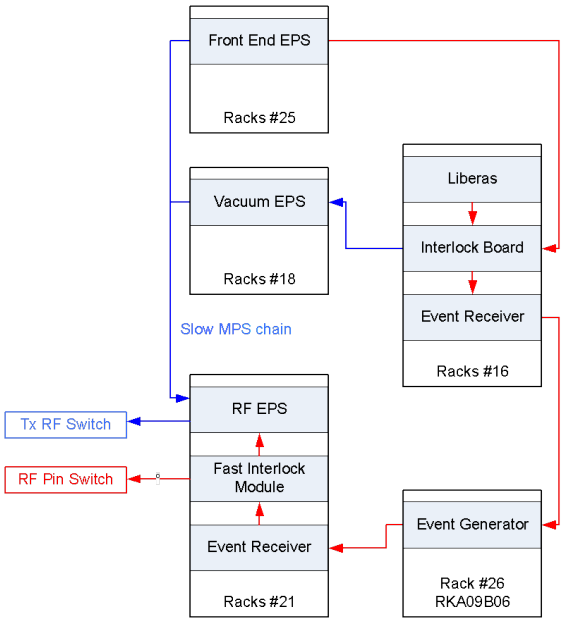

Figure 25: Elements of the Machine Protection System.

- Electron beam ***orbit*** within thresholds when the beam current is above 20 mA.
- Correct position of ***valves and photon shutters i***n the front ends.
- ***Temperature*** in the vacuum chamber and in-vacuum components.
- ***Water flow*** in the absorbers and in-vacuum components.
- ***Vacuum pressure*** in the storage ring and front ends.

When these parameters are detected to exceed certain thresholds the MPS acts on different components of RF plants to cut the RF power. Fast Interlock using the Timing System acts on the RF Pin switches, while the Slow MPS using the PLC deterministic Ethernet acts on the Transmitter RF switches.

The MPS over the Timing system allows the transmission of an interlock signal from any part of the machine (BPMs, front ends, …) to another (RF plants) in a fast way (less than 5 µs) whereas it timestamps these events both at the source points (BPMs EVRs) and at the destinations (RF EVRs). The analysis of such time stamps allows the accelerator experts to study the time sequence of the different events leading to the beam dump and thus better understand the machine behaviour and be able to design solutions to avoid recurrent problems. Figure 26 shows a snapshot of a series of events with their timestamps as a result of an orbit problem and consequent beam dump.

The timing system provides a timestamp resolution of 8 ns and provides a reaction time of 3,8 µs from the origin of the problem (sector S05) to the interlock action at the RF plants.

Another powerful diagnostic tool for beam loss analysis is the Post-Mortem beam position analysis (PM). The PM beam position data is stored at a turn-by-turn rate (~900 ns / turn) in a ring buffer in the BPM electronics. When a PM event is raised by the MPS, the timing system synchronously transmits that event to all receivers, which triggers the PM signal in all BPM electronics, freezing their buffers. The beam position data of thousands of turns before the interlock is kept in the buffers allows its readout and offline analysis. Figure 27 shows the horizontal position of all storage ring BPMs before and after a beam trip that happened around reference turn #1000. An off-centred BPM was identified (cyan) and a further analysis of even previous turns showed that it actually started to drift ~135 ms (150.000 turns) before the trip (see Figure 28).

Event	After	Unit	TotalTime	Logged On
1- SR05			2014-03-12 12:26:07	SR05/TI/EVR-CDI0501-A
2- RF14A	3.8147	usec	2014-03-12 12:26:07	SR14/TI/EVR-CRF1402-A
3- RF10B	0	nsec	2014-03-12 12:26:07	SR10/TI/EVR-CRF1002-A
4- RF10A	0	nsec	2014-03-12 12:26:07	SR10/TI/EVR-CRF1001-A
5- RF6B	0	nsec	2014-03-12 12:26:07	SR06/TI/EVR-CRF0601-A
6- RF14B	476.8372	nsec	2014-03-12 12:26:07	SR14/TI/EVR-CRF1401-A
7- RF6A	0	nsec	2014-03-12 12:26:07	SR06/TI/EVR-CRF0602-A
8- SR15	556.469	usec	2014-03-12 12:26:07	SR15/TI/EVR-CDI1501-A
9- SR06	8.5831	usec	2014-03-12 12:26:07	SR06/TI/EVR-CDI0601-A
10- SR11	1.9073	usec	2014-03-12 12:26:07	SR11/TI/EVR-CDI1101-A
11- SR01	2.861	usec	2014-03-12 12:26:07	SR01/TI/EVR-CDI0101-A
12- SR07	7.1526	usec	2014-03-12 12:26:07	SR07/TI/EVR-CDI0701-A
13- SR12	2.861	usec	2014-03-12 12:26:07	SR12/TI/EVR-CDI1201-A
14- SR03	476.8372	nsec	2014-03-12 12:26:07	SR03/TI/EVR-CDI0301-A
15- SR16	3.3379	usec	2014-03-12 12:26:07	SR16/TI/EVR-CDI1601-A
16- SR13	0	nsec	2014-03-12 12:26:07	SR13/TI/EVR-CDI1301-A
17- SR09	476.8372	nsec	2014-03-12 12:26:07	SR09/TI/EVR-CDI0901-A
18- SR10	3.3379	usec	2014-03-12 12:26:07	SR10/TI/EVR-CDI1001-A
19- SR08	1.4305	usec	2014-03-12 12:26:07	SR08/TI/EVR-CDI0801-A
20- SR02	1.9073	usec	2014-03-12 12:26:07	SR02/TI/EVR-CDI0201-A
21- SR04	4.2915	usec	2014-03-12 12:26:07	SR04/TI/EVR-CDI0401-A
22- SR14	581.7413	usec	2014-03-12 12:26:07	SR14/TI/EVR-CDI1401-A

Figure 26: Detected timestamped events.

Time-resolved experiments using reconstructed master RF clock at CIRCE-PEEM

The CIRCE photoemission electron microscope (PEEM) is a versatile tool to study surfaces, thin films and nanostructures. It combines high lateral (down to 20 nm) resolution imaging with spectroscopic and dichroic sensitivities, i.e. the ability to resolve by photon energy and polarization, or photoelectron energy, the sample's local chemical, structural, electronic and magnetic properties [3]. Typical measurements are made with the sample in a static condition, i.e. while it can respond to an external stimulus such as a magnetic field, the sample state is not changed during a single measurement. However, in many cases the sample response to an external excitation on a faster, intrinsic time scale is of great importance.

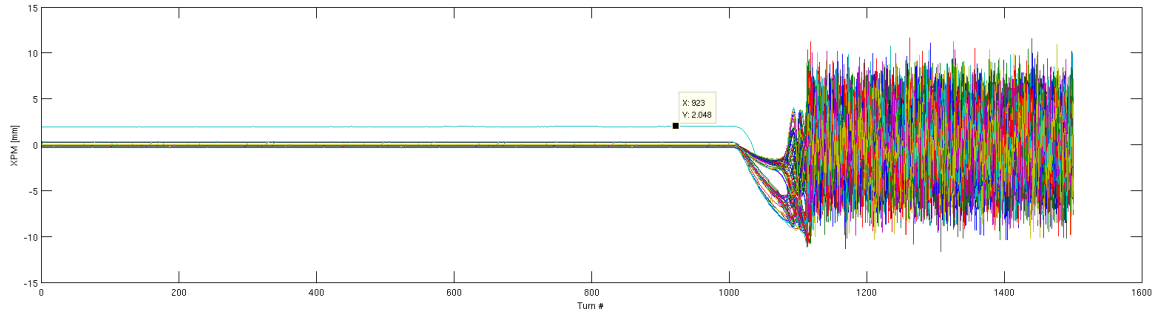

Figure 27: BPM horizontal position during beam trip.

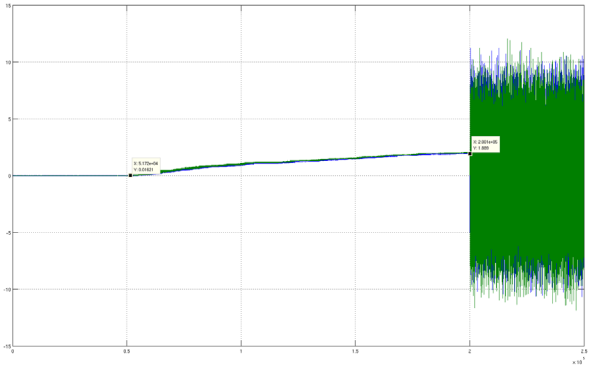

Figure 28: Previous turns to beam trip analysis.

For example, elastic deformations propagate in crystals at the speed of sound (in the order of thousands of meters per second), which for nanometric dimensions corresponds to a picosecond timescale. The ALBA PEEM team, together with collaborators Ferran Macia and Joan Hernandez from the University of Barcelona (Spain), Alberto Hernandez from the Paul Drude Institut (Germany) and Simone Finizio from the Paul Scherrer Institut (Switzerland) are interested in the dynamics of samples excited by elastic deformations on the subnanosecond timescale. Although the typical minimum integration time for a single PEEM image is above 1s and up to many minutes, a high time resolution for reproducible events can still be obtained by synchronizing the sample excitation (pump) to the stroboscopic light pulses (probe) of the synchrotron (30 ps every 2 ns).

The beamline scientists and the electronics engineers built a setup to excite samples in the PEEM by an electric RF signal of 499.654 MHz, synchronized with the RF of the storage ring (and thus the light) by a phase-locked loop (PLL), with adjustable amplitude and phase. A schematic of this setup and its components is shown in Figure 29. A jitter below 100 ps was achieved, which is an excellent result considering the constraints and complexity.

Figure 30 (a) shows a PEEM image of a propagating elastic deformation (surface acoustic wave or SAW) in a LiNbO3 crystal, accumulating over many billion light pulses. The wavelength is around 8 µm and it is only possible to detect the SAW because upon the arrival of every flash of light the phase of the wave is exactly the same at a given place. As the PEEM image is formed by X-ray photoemitted electrons with a selected energy (low energy Auger/secondary electrons), the contrast mechanism between the different phases of the SAW is the shift of the local, phase-dependent surface potential, due to the SAW electrical component in piezoelectric LiNbO3. The bright squares are magnetic micro-structures deposited on top of the LiNbO3. Figure 30(b+c) shows images of a wave intentionally detuned by 0.05 Hz (with respect to 500 MHz, i.e. relative 10^{-10}) at two different times. We can appreciate how, in 5 seconds, the position of the wave has advanced by a quarter wavelength when the light arrives.

This method can be used for different experiments in which the sub-nanosecond response of a sample to an elastic deformation is of interest. One example is the possibility to measure how the magnetic domain configuration in small structures can be changed upon elastic deformation, introducing an additional magnetic anisotropy term. The speed of this so-called magneto-elastic effect will be the ultimate limit of processing velocity for any device using it. Since new concepts for magnetic memory and logic devices for information technologies using the magneto-

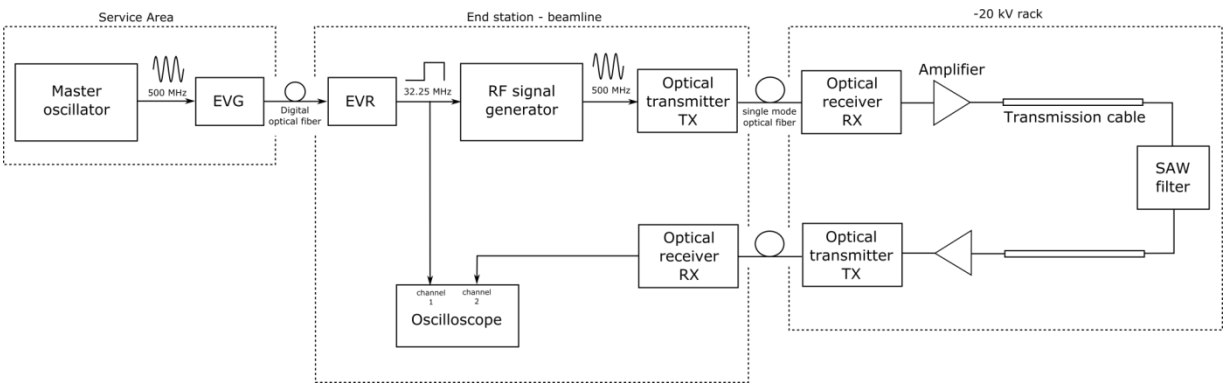

Figure 29: Schematic of the setup used for synchronized excitation: The digital timing signal is derived from the master oscillator by the event generator (EVG) and transmitted by optical fibre to the event receiver (EVR) at the beamline. A RF generator with phase-lock loop (PLL) produces a reconstructed 500 MHz signal. The phase with respect to the master oscillator and the amplitude of the signal can be adjusted as required by the experiment. As in the PEEM the sample is floating on high voltage, the analogue signal is then transmitted by optical fibre into the PEEM rack. Downstream of the optical receiver, only cheap components can be used, as they could be accidentally destroyed by arcs from inside the instrument.

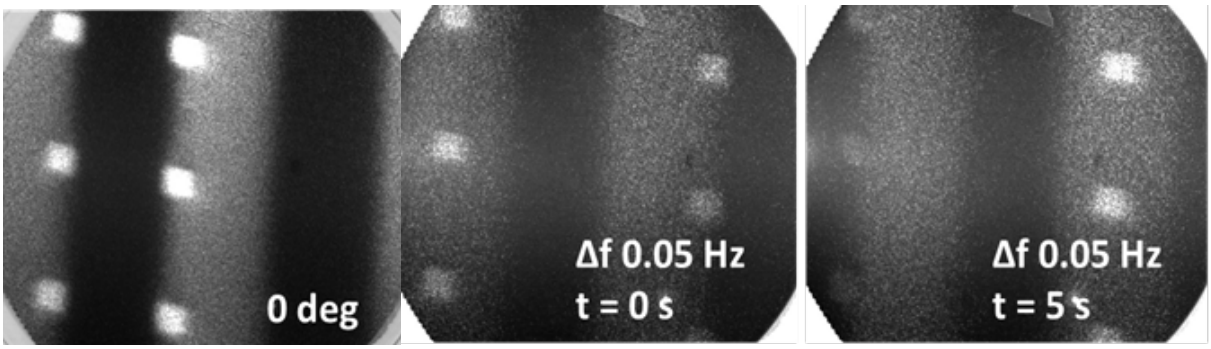

Figure 30: A propagating surface acoustic wave (SAW) imaged by PEEM (field of view 20 um) with Ni magnetic nanostructures. The SAW excitation is synchronized with the synchrotron master clock at 499.65 MHz. (a) a synchronized wave with approx. 8 um wavelength. (b) & (c) Images with the excitation intentionally detuned by 0.05 Hz, resulting in a shift of the wave by a quarter wavelength in 5 s.

elastic effect have been proposed, these studies are essential to evaluate their possible performance limits. Furthermore, the technique of time-resolved PEEM imaging through synchronized excitation can be used with magnetic field pulses, generated from microstriplines on the sample.

Conclusions

This article has provided a brief review of the main synchronization techniques and their inherent limits. It has demonstrated the necessity of having an independent synchronization system based on events for certain accelerator applications.

After its design and implementation, the ALBA Timing System has been used for more than six years. During this time, it has been one of the most reliable systems in operation, having no major incident.

To show its use in practice, two examples of applications have been described. In the Machine Protection System, the use of the Fast Interlock capabilities of the Timing System have helped to increase the speed of reaction in case of machine orbit interlock detection and also to ease diagnostics of orbit trips by accelerator scientists. In the second application at CIRCE-PEEM, the ALBA Timing System has been used to reconstruct the RF Master clock in order to be used in the first time-resolved experiment of the beamline in the picoseconds range.

The ALBA Timing System has proved to be a very good and stable basis to solve the new synchronization challenges that will appear at ALBA in the years to come.

OTHER REFERENCES

[1] D. Fernandez-Carreiras et al., "Personnel Protection, Equipment Protection and Fast Interlock Systems. Three different technologies to provide protection at three different levels", ICALEPCS'11

[2] http://www.tango-controls.org/

[3] L. Aballe, M. Foerster, E. Pellegrin, J. Nicolas, and S. Ferrer, The ALBA spectroscopic LEEM-PEEM experimental station: Layout and performance, J. Synchrotron Rad. 22, 745-752 (2015)

CONTRIBUTIONS

O. Matilla was the main person responsible for the project. R. Suñé and J. Moldes were in charge of the development of the control software. M. Foerster and L. Aballe were responsible for performing time-resolved experiments using the reconstructed master RF clock at the CIRCE-PEEM Beamline, and A. Fonseré and B. Molas developed the new specific electronics for this project. A. Olmos implemented the post-mortem use case described in the text. This was a large project, in which all the electronics technicians participated and to which most electronics engineers contributed to some extent. O. Matilla, J. Moldes, A. Olmos, M. Foerster and L. Aballe wrote the article.

Sub-nanometer mirror figure error using spring correctors developed at ALBA

Carles Colldelram, Josep Nicolàs, Claude Ruget

Here, we present an advanced mirror bender that includes, in addition to the usual bending mechanism, a number of mechanical actuators that allow modifying the mirror surface by introducing a controlled deformation of the mirror substrate below the nanometer. This system is an inexpensive mean to obtain extremely accurate mirror surfaces, flexible and stable implementation of active optics.

For modern light sources, such as ALBA, in which the photon source is in the order of few microns and collimated within few microradians, the quality of optical surfaces of the mirrors in a beamline has a direct impact on the beam delivered to the endstation.

For instance, a typical mirror with slope error of 0.5 µrad rms (root mean square), that focuses 1 m downstream, will produce a spot of 1 µm rms, at least. Moreover, besides a limit on spot size, slope error is usually the limit for the spectral resolution in soft X-ray beamlines. Slope error is also the cause of fringe structures that appear on the beam out of focus, which is critical in some diffraction beamlines. The appearing of diffraction limited X-ray sources, as multi-bend-achromat Storage Rings and free electron lasers is pushing the requirement on the surface quality of mirror to maximum deviations from ideal surfaces in the of one nanometer.

In the last years, there has been a great progress in the quality of optics installed on SR beamlines, associated to the improvement of metrology instruments and techniques, and to the development of deterministic polishing technologies, such as elastic emission machining and ion beam figuring. These techniques allow figuring mirrors with great accuracy, although they cannot control contributions to surface error induced by temperature, cooling, clamping or gravity. Also, very often, mirrors need to be installed on a mirror bender, which allows changing the curvature of the mirror for fine-tuning the focus, or for simply changing the focus position as part of the required functionality of the beamline.

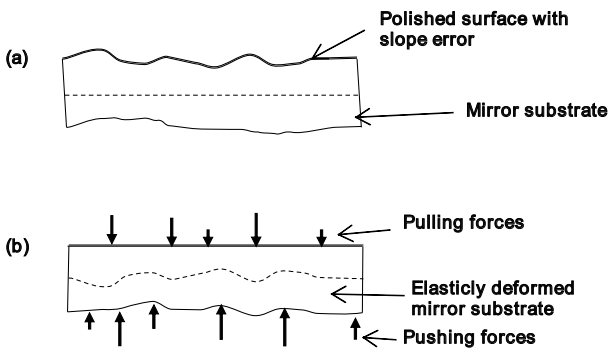

Figure 31: Working principle of surface correction by deformation of the substrate.

At ALBA we have developed an advanced mirror bender that includes, in addition to the usual bending mechanism, a number of mechanical actuators that allow modifying the mirror surface by introducing a controlled deformation of the mirror substrate. Such deformation can compensate residual errors, given by polishing defects, gravity sag, temperature, and others, to the level of one nanometer. Since the actuators are motorized, the system is actually an active optics system, capable also of introducing *in-situ* deformations of the mirror surface, for correcting wavefront deformations induced by other optical elements of the beamline, or for advanced functions such as shaping the beam out of focus.

In the system we have developed, the mirror surface deformation is controlled by the forces applied by the actuators situated at several positions along the mirror. This is, the actuators are designed to accurately control the force they apply onto the mirror. This is main difference with respect to other active optics systems, in which the correctors induce directly a high resolution displacement on the mirror. The main advantage of the approach we follow is the stability of the system, as the force introduced by the actuators is very robust to mechanical drifts. On the other hand, since the system is based on forces, we have built the numerical models that allow predicting the mirror figure as a function of the applied forces, and determining the forces required to correct a given mirror figure.

To achieve a control of the deformation below the nanometer, the actuators must provide forces up to about 20 N with resolution of 0.005 N, and more challenging, with stability of the same order. Moreover, to reach a correction independent of the bending radius, the crosstalk between actuators must be suppressed also to the millinewton level. The correctors included in the bender developed at ALBA, are designed to reach these performances. The applied force is controlled by adjusting the elongation of a weak spring, which works in extension, in order to achieve better stability still using very long springs. This allows reaching quite high forces still having a small spring constant, which is also a requirement to reach good resolution stability and low crosstalk.

The force is transmitted to the mirror by means of a mechanism that absorbs any force component not perpendicular to the mirror, which would induce parasitic deformations. In addition, it includes a mechanism that allows preserving the force applied to the mirror within 0.01 N for mirror height variations of up to 1 mm. Also, the system is also designed to minimize friction, so all articulations in the mechanism are rolled.

Besides the actuators, the mirror bender system has interesting features. Such as feedback on the applied forces, which allows determining the ellipse parameters with accuracies equivalent to a slope error below 15 nrad rms for a 1 m long mirror. Also the bender mechanics is designed to provide high stability, to cancel all parasitic forces, and to avoid every source of friction.

A prototype of the system has been built and has been characterized at the optics laboratory of ALBA. Both the actuators and bending mechanism have been found to reach the expected performances. The system has been used to correct a modest quality mirror. The surface error is reduced from 23.2 nm rms (0.87 µrad rms) to 0.86 nm rms (0.11 µrad rms). The discrepancy between theoretical prediction and actual measured surface is 0.083 nm rms (2.8 nrad rms).

The correction introduced by the correctors is independent of the bending radius, and has been tested for different radii of curvature. The variation of all the measurements is better than 0.25 nm rms, and is actually limited by the metrology. The development of such system, and the obtained results constitute a reference for the focusing systems of future beamlines at ALBA. For which the proposed system is a inexpensive mean to obtain extremely accurate mirror surfaces, flexible and stable implementation of active optics.

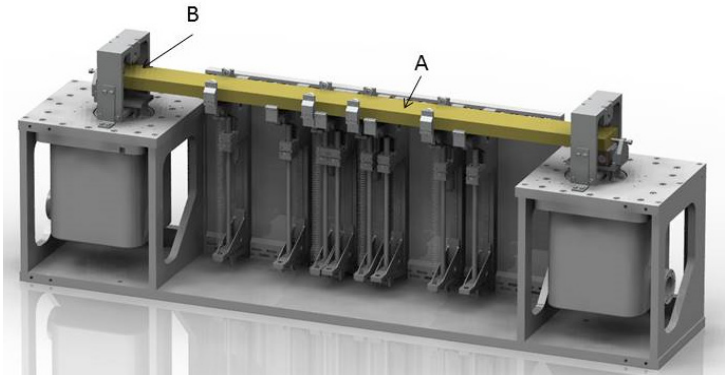

Figure 32: 3D model of the ALBA bender system.

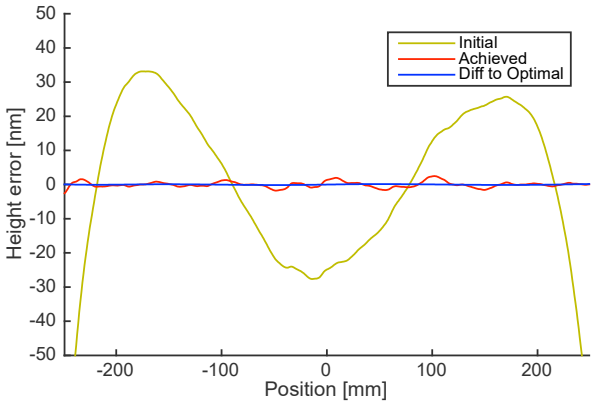

Figure 33: Compensation of the surface error below 1 nm rms. The starting figure of the mirror is 23.2nm rms (0.87µrad rms), and is optimized to 0.86 nm rms (0.11 µrad rms). The discrepancy with theoretical prediction of correction is 0.083 nm rms (2.8 nrad rms).

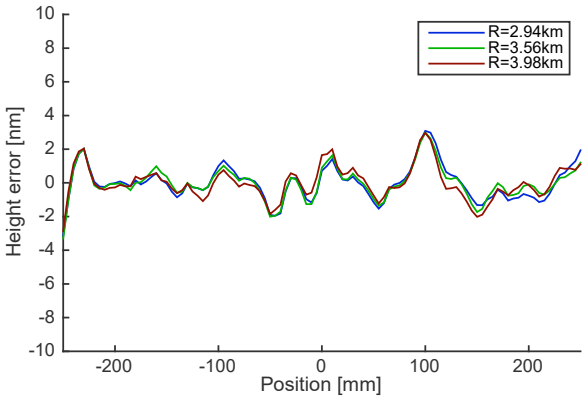

Figure 34: Residual figure profile for different radii of curvature, in all cases the system preserves the figure with error better than 0.25 nm rms.

CONTRIBUTIONS

The project has been the results of a joint effort between the Optics Group and the Engineering Division at ALBA. Claude Ruget, a former staff engineer provided the first initial key ideas.

The magnetic measurements laboratory: capabilities and developments

Josep Campmany, Jordi Marcos, Valentí Massana and Laura Garcia

In order to characterize the magnets to be installed in the accelerators of the ALBA Synchrotron, a fully equipped magnetic measurements laboratory was set up during the design and construction phase. It has the usual benches to measure different types of magnets used in accelerators: Hall probe bench for dipoles, rotating coil bench for quadrupoles and sextupoles and specific benches (Helmholtz coils, fixed stretched wire and flipping coil benches) for measuring pure permanent magnet blocks and their assemblies in order to build insertion devices. What follows is a description of the main characteristics and performances of the benches, illustrated with some examples.

Generalities: fieldmaps and integral measurements

In general, magnet characterization for accelerators is based on two approaches: fieldmaps and integral measurements.

Fieldmaps come from the measurement of magnetic induction vector B at nodes of a given grid that can be defined in a line, a plane or a volume. This kind of measurements are done to identify local variations of the magnetic field in a given volume, or to characterize the phase advance in the undulators.

The other type of characterization involves integral measurements, for instance those used to characterize the field integrals (accounting for the kicks received by a particle after crossing a magnet) or to measure the high order modes of multipole magnets (quadrupoles, sextupoles, etc.). Integral measurements are also used to determine the average or local magnetizations of pure permanent blocks used to build insertion devices.

In any case, measuring magnets in the accelerators' world requires dealing with high magnetic fields (~1 T or higher) confined in long volumes (~10^{-2} x 10^{-2} x 1 m^3) that should be mapped with an accuracy of 10^{-4} T and 10^{-5} m at least. Also, field integrals (the integral of the field along a trajectory) that account for the forces applied to accelerated particles should be determined with a relative accuracy of 0.1% with respect to the actual integral field value, or better.

The fulfilment of these requirements is a challenge that drives the measurement technologies to high accuracy mechanics and rapid and high precision data acquisition technologies.

Fieldmap measurements at ALBA

Fieldmap measurements at ALBA are done using a mechanical bench with 3D Hall probe sensors that was built several years ago. Its control software has been recently upgraded allowing on-the-fly

Figure 35: Hall probe bench at ALBA magnetic measurements laboratory.

measurements and the methodology has been improved to increase its accuracy. It can measure a volume of 2.5 m long, 0.5 m wide and 0.25 m high. The global accuracy of Hall probe positioning is ~30 µm, and repeatability of probe positioning is ~1 µm. The planarity, linearity and straightness of the Hall probe movement is within the ±50 µm and 50 µrad. Global accuracy of measured field is less than $1{\cdot}10^{-4}$ T in the range 0 – 2 T, and repeatability is < $0.5{\cdot}10^{-4}$ T.

To reach this accuracy in the magnetic field measurement using a 3D Hall probe we developed a new calibration methodology, accounting for the angular deviations of internal sensitive areas and resulting cross-talking, its non-linearity of the sensors as well as contributions such as the planar Hall effect, misalignment of sensor areas, and Hall probe offsets.

In this kind of measurements, fiducialization and alignment are an issue, because the geometrical grid measured by the Hall probe should be referred to the mechanical coordinates of the structure to be measured. To this end, a concept developed at SLAC was adopted, improving the portability and spatial resolution, changing from "magnetic needles" to a "cone system" approach. The accuracy of the position definition using this system is better than ±10 µm in all directions. Given that the translation of the magnetic structure to be measured is monitored with a laser-tracker with a maximum error of ±20 µm, the overall fiducialization error is ±23 µm. More details are given elsewhere [1].

SESAME magnets measurements as an example

This know-how was successfully applied to the measurement and characterization of SESAME bending magnets. SESAME is an international collaboration leaded by CERN for building a synchrotron light source in Jordan. Within this collaboration, ALBA had the mission of characterizing the bending magnets of the Storage Ring. Figure 36 presents the main characteristics of the magnet, and Figure 37 shows the characterization procedure followed for each magnet.

In addition to the presented Hall probe bench, a prototype bench to measure the magnetic field produced by «closed» devices has also been developed [3]. To this end, a number of mechanical solutions have been applied worldwide, but all of them are specific to each case. Instead, a more general approach has been developed. The bench design is presented in figure 38. The drawback of this design is that the object to be measured has to fit within the "C" aperture, and its length should be less than one third of that of "C".
In the design, the tape material is carbon fibre and,

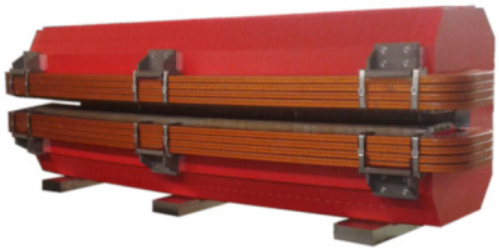

Dipole Characteristics	
Field B_0	1.455 Tesla
Gradient G_0	2.79 Tesla/m
Magnetic Length	2.25 m
Bending angle	22.5º
Nominal current	494 Amp

Figure 36: SESAME Storage Ring bending magnet.

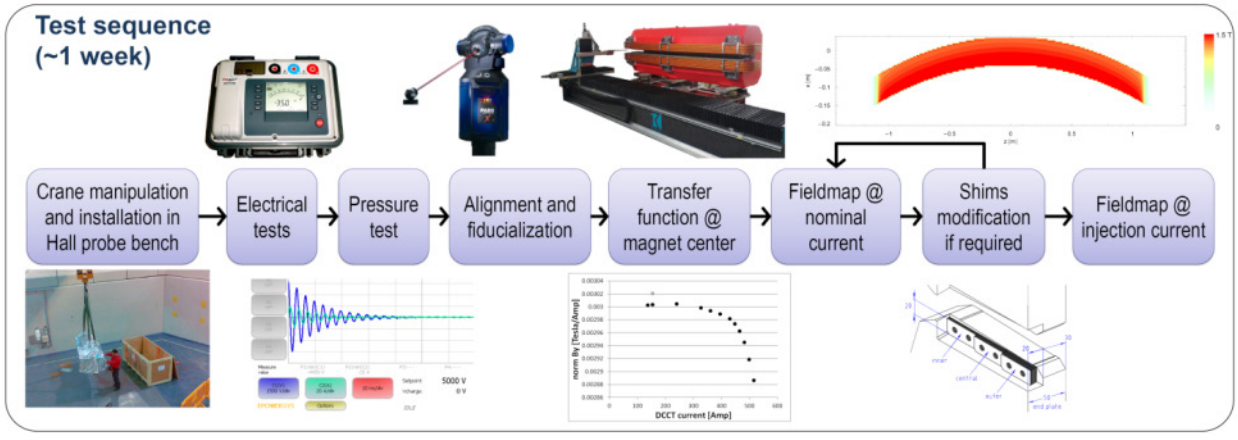

Figure 37: Characterization procedure followed for each magnet. It can take between 1 and 2 weeks.

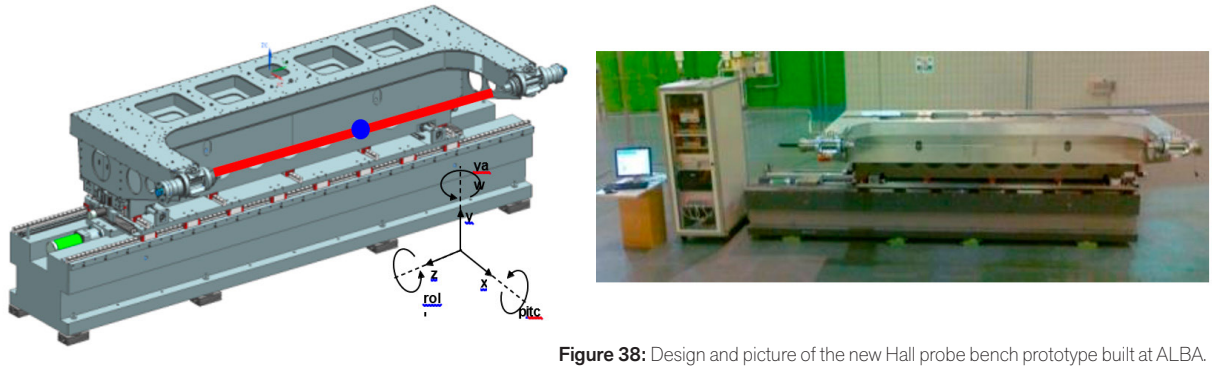

Figure 38: Design and picture of the new Hall probe bench prototype built at ALBA.

in operation mode, a stretching force of 5000 N is applied to maintain the frequency of vibration modes far from low frequencies. The ends of the tape are attached to a structure shaped in "C" through a mechanism allowing the horizontal alignment of the Hall probe as well as the stretching of the tape. The "C" structure is designed to allow a tension up to 20000 N, if needed, to shift the tape vibration modes at convenience.

The performance fulfils the desired specifications. It can measure a volume of 1.2 m long, 0.5 m wide and 0.25 m high with a global positioning accuracy of ~20 μm / 35 μrad, and repeatability of probe positioning of ~1 μm. Global accuracy of measured field is less than $1{\cdot}10^{-4}$ T in the range 0 – 2 T, and repeatability is < $0.5{\cdot}10^{-4}$ T. The new bench is fully described in J. Campmany, et al., *Physics Procedia,* 75 (2015) 1222-1229 [2].

Integral measurements at ALBA

Rotating coil bench to measure quadrupoles and sextupoles

The key element of this bench is the plate containing the coils. The accuracy depends on coil manufacturing. To avoid the uncertainties associated to conventional winding of thin wires, ALBA adopted multi-PCB technology.

A set of shafts with radial coils with diameters between 20 to 130 mm have been developed. The length of the coils are 0.5 m to 0.7 m. The positioning error of each coil with respect to the theoretical expected position is ±2 μm. An image of the multilayered coils is shown in Figure 40 left and the shaft with the coils assembled inside, in Figure 40 right.

Each shaft is provided with 5 coils in order to combine the output signals and perform compensated measurements of quadrupole magnets. According to the tests, the relative repeatability in the determination of the fundamental is better than $1{\cdot}10^{-4}$ and the repeatability in the determination of the higher order harmonics up to the 15th is better than 0.1%. One of the most relevant parameters of multipole magnets used in accelerators is the determination of the position of the magnetic axis of the device. Overall positioning error is within ±50 μm and the combined standard deviation is 17 μm / 43 μrad.

Long flipping coil

It has been developed at ESRF. It is a long coil that is rotated inside the gap of magnetic structures. The electromotive force induced is proportional to

Figure 39: Rotating coil bench at ALBA magnetic measurement laboratory.

Figure 40: Multilayered PCB with radial coils developed at ALBA outside and inside the shaft used for carrying out integral measurements of multipole magnets.

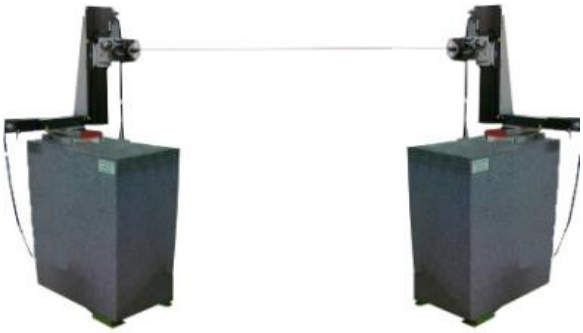

Figure 41: Flipping coil system at ALBA, with two motion stages on granite blocks.

the field integral. Length of the device is 4 m, and accuracy of first field integral measurements is < 10^{-5} T·m

It is particularly well suited to measure long (up to 2 or 3 m) and small aperture (down to ~4 mm gap) devices with field integral values close to zero. The horizontal and vertical scanning ranges are 240 mm and 250 mm, respectively.

Benches for pure permanent block characterization

Insertion devices are in general made of arrays of magnets. The laboratory is equipped with characterization benches specifically conceived to characterize PPM blocks.

Fixed stretched wire bench

ALBA's own stretched wire bench (figure 42, left) has been designed and built based on those developed at ESRF and BESSY. Overall accuracy is < 3 μT·m

Helmholtz coils bench

Helmholtz coil is known to produce a very flat field in its centre. In our case, a magnetic block placed in the centre is rotated 180º with respect to an axis perpendicular to the coils axis, and the magnetic flux change is proportional to the magnetization of the block along coils axis. The bench therefore provides the value of the average magnetization of the block. This bench (Figure 42, right) has been built by Sincrotrone Trieste Spa. In the usual case of magnetic blocks with uniaxial anisotropy, the bench relative accuracy is $\pm 5 \cdot 10^{-4}$ at easy axis, and $\pm 2.7 \cdot 10^{-2}$ for the other axes.

Figure 42: Fixed stretched wire bench (left) and Helmholtz coils (right) at ALBA.

Consistency of measurements

Given that we have different sensors for characterizing magnetic structures, the consistency of the results comparing Hall probe with Flippling coil measurements, as well as Hall probe with Rotating coil measurements for the same magnetic structure have been verified. The first comparison shows an agreement between the field integrals calculated from Hall probe data and those directly measured using flipping coil bench at the level of $10 \cdot 10^{-6}$T·m rms. Regarding the second comparison, in terms of integrated multipoles the use of Hall probe measurements is worst compared with those based on rotating coils, but still provides useful data with an accuracy of a few parts in 10^4.

Conclusion

The ALBA magnetic measurements laboratory is equipped with several characterization benches equipped to measure with high accuracy magnetic structures for accelerators. The main improvements implemented in the last years were: the new calibration method developed to calibrate 3D Hall probes, the cone system and the reference magnet made to increase the accuracy of referring the magnetic fieldmaps to mechanical fiducials, the new Hall probe bench equipped with a small sensor specially developed to measure closed magnetic structures, and the new shafts based on the multi-PCB technology developed to improve the accuracy of the Rotating coil bench.

Up to now, the authors have successfully characterized the combined bending magnets, quadrupoles and sextupoles as well as the elliptical undulators and conventional multipole wigglers of the ALBA Storage Ring and Booster accelerators, dipole magnets for ANKA Storage Ring (Germany), the combined bending magnets of the Canadian

Light Source Storage Ring, prototypes of wavelength shifters for E-XFEL (Germany), prototype quadrupoles for the European Spallation Source, ESS-Bilbao (Spain), and for the International Fusion Materials Irradiation Facility, IFMIF (Japan), a prototype superconducting sextupole for SLHC at CERN, and combined bending magnets for the SESAME Storage Ring (Jordan). They are currently measuring quadrupole permanent magnets for the Low Energy High Intensity Proton Accelerator, LEHIPA (India), and bending and quadrupole magnets for ThomX project (Paris).

OTHER REFERENCES

[1] J. Campmany, Ll. Ribó, C. Colldelram, F. Becheri, J. Marcos, V. Massana, New Improvements in Magnetic Measurements Laboratory of the ALBA Synchrotron Facility, ***Physics Procedia* 75**, 1214-1221 (2015)

[2] J. Campmany, Ll. Ribó, C. Colldelram, F. Becheri, J. Marcos, V. Massana, A New Bench Concept for Measuring Magnetic Fields of Big Closed Structure, ***Physics Procedia* 75**, 1222-1229 (2015)

[3] L.Ribó, C.Colldelram, L.Nikitina, Hall probe bench prototype for closed magnetic structures, Proceedings of the MEDSI Conference (2014)

CONTRIBUTIONS

J. Campmany coordinates the magnetic measurements laboratory. J. Marcos was in charge of performing data analysis of the mentioned projects. V. Massana performed magnetic measurements. L. Garcia participated as a team member. L. Ribó, J. Ferrer, L. Nikitina and C. Colldelram were responsible for the engineering mechanics design and implementation. F. Becheri, J. Andreu, D. Roldan and R. Homs were in charge of the development of the control system software. R. Petrocelli, T. Camps, D. Alloza and O. Matilla, were responsible for the electronics. M. Llonch and J. Ladrera were in charge of survey and alignment measurements. This was carried out with important contributions from transversal engineering and infrastructure sections in the engineering division and the electronics technicians and computing engineers. J. Campmany wrote the article.

2015 IN ALBA

JANUARY

The International Year of Light begins

2015 was designated by the UNESCO as the International Year of Light and Light-based Technologies to show the society how light directly affects every aspect of our lives. On 19th and 20th January 2015 the Opening Ceremony of the International Year of Light 2015 took place in Paris with more than 1,000 participants. Caterina Biscari, director of ALBA Synchrotron, took part in the thematic session "Light at the limits" standing in for the light source community with the talk on "Frontiers of synchrotron science".

FEBRUARY

SESAME magnets arrive to ALBA

In collaboration with the European Organisation for Nuclear Research (CERN), the magnetic measurements laboratory of ALBA validated the bending magnets that were installed at the Storage Ring of SESAME, the synchrotron facility built in the Middle East, by characterizing their magnetic field map.

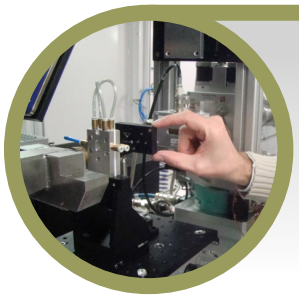

MARCH

Development of an X-ray detector

A team of researchers and engineers of the ALBA Synchrotron collaborated with members of the company Alibava Systems and the Institute of Microelectronics of Barcelona (IMB-CNM CSIC) to develop a radiation detector aimed at measuring the intensity of the beam with high precision when performing an experiment at a synchrotron facility. The new detector enables a correct development of the experiment, ensuring the quality of the obtained data and reducing the time of the experiment.

MARCH

Incorporation of floor coordinators

In 2015, five new positions of Floor Coordinators were opened in ALBA. Half of their time they work on shifts to cover all the beamlines dedicated time, and the rest in standard office hours. Their main activities are to provide immediate support to beamlines (basic troubleshooting in different areas from control, vacuum, cryogenics, mechanics,…) and laboratories and to give support to the operator in the control room.

MAY

Technology transfer agreement

The company SENER, devoted to engineering and construction, and the ALBA Synchrotron signed an agreement to commercialize a technological solution developed at ALBA: a new system to bend X-ray mirrors with higher precision than others available in the market and with a competitive price.

MAY

Synchrotron light for the pharmaceutical industry

More than forty people participated at the workshop organized by the Industrial Liaison Office of ALBA addressed to pharmaceutical companies. During the event the attendees were able to know in depth the available state-of-the-art techniques and the advantages that synchrotron light offers for the development and improvement of drugs.

JUNE

VII AUSE Congress and II ALBA User's Meeting

From June 16th till 19th 2015, the VII AUSE Congress (the association of synchrotron users from Spain) and the II ALBA User's Meeting were held at the ALBA facilities. During the event, more than 120 researchers from different scientific disciplines and national and international research institutions met to showcase their scientific results and debate synchrotron light capabilities.

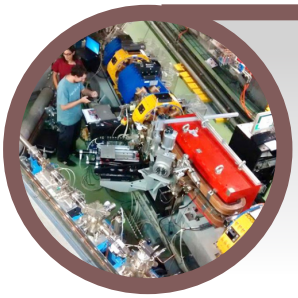

AUGUST

Installing the 8th beamline during the summer shutdown

The in-tunnel components of MIRAS were installed during the summer of 2015. The basic mechanical assembly for M1 mirror was installed and tested – including measurements for alignment and metrology-, along with cabling, plate supports and cable trays for all in-tunnel optics. M2, M3 and M4 mirror trays and MIRAS racks were also completed.

SEPTEMBER

Collaborating with international research facilities

In September, the ALBA Synchrotron signed a memorandum of understanding with two research facilities, the Elettra synchrotron facility (Trieste, Italy) and the Institute for Research in Fundamental Sciences (Teheran, Iran), for the design, development, construction and validation of components and systems in the field of particle accelerators and synchrotron beamlines.

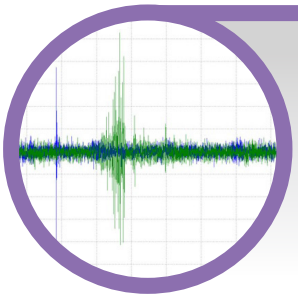

OCTOBER

Correction of the electron beam position after an earthquake

On the early morning of the 29th of October, the beam position monitors of the ALBA accelerators detected the seismic activity that occurred in the area of Alt Empordà (Catalonia) and corrected the beam position. This precision is possible thanks to the fast orbit feedback system, which, under normal conditions, keeps the electron beam oscillations below 100 nanometres.

NOVEMBER

A new ALBA Open Day

On the 21st of November 2015, 1,903 people attended the ALBA Open Day. On its 4th edition, the event has become a successful activity among families and the general public, thanks to the collaboration of 78 volunteers from the ALBA Synchrotron and 25 from Civil Protection.

DECEMBER

New young externally-funded staff in ALBA

Thanks to the positive resolution of the grant for young employment in R&D&i launched by the Spanish Ministry of Economy and Competitiveness (MINECO), ten new people under 30 years old started working at the ALBA Synchrotron. During two years, they will get experience and expertise in areas such as engineering, computing, accelerators, experiments, health & safety and user office.

MIRAS

The construction of MIRAS - the Infrared synchrotron radiation beamline at ALBA - was initiated in 2014, and continued rapidly during 2015. Most of the beamline components were installed and tested. The beamline achieved an important milestone in January 2016 by the successful commissioning of the first extraction optical element M1.

MIRAS is dedicated to infrared microspectroscopy, with the aim to deliver world class performance in terms of a bright and highly stable photon beam. The beamline will provide ALBA users with a modern infrared microspectroscopy facility covering a wavelength range from 0.4 to 100 μm. The design of the beamline optimizes performance in the mid-IR range and will give significantly enhanced efficiency, compared to a conventional source, in both far-IR and mid-IR regions.

The optical layout of MIRAS includes the option for splitting the extracted infrared beam in two parts, one of them containing the edge radiation of the beam. This configuration will enable the use of the two beams separately at different endstations or the use of a "combined single beam" for the experiments requiring maximum flux. The experimental cabin and transport optics are designed to accommodate two additional endstations as a future upgrade of the MIRAS beamline, one that will be based on a "bring your own equipment" concept (Figure 43). The FTIR microspectroscopy instrument at the first operational endstation is a Bruker system (Hyperion 3000 microscope coupled to a Vertex 70 spectrometer) equipped with an FPA detector for imaging (Figure 44). The FTIR microscope has been installed at the MIRAS hutch and is currently undergoing the commissioning process.

The installation process of the beamline in-tunnel components commenced during the shutdown of the machine, summer 2015. The mechanics of the first extraction mirror M1 were assembled and several tests were performed, including measurements for alignments and metrology, validation of the system functionality, in term of motors performance and vibration tests. Then thermocouples were installed on M1, two of them on the body of the mirror and six thermocouples of 1 mm diameter were installed on the back of M1 at the slot. The thermocouples are interlocked with the RF power supply for safety reasons.

Following the construction of the first mirror mechanics, the whole assembly has been placed inside the dipole chamber implementing a horizontal infrared beam extraction geometry using a laterally inserted M1 (Figure 45). M1 is made from aluminium, with 20 nm of electro-deposited gold layer that is tightly clamped onto a copper holder for heat dissipation. After the installation of the first mirror inside the tunnel, several steps have been followed, including the installation of the transport mirrors, chambers, ion pumps etc.

In parallel to the beamline components installation, the construction of the experimental users' hutch was initiated in September 2015. The full construction of the hutch including cabling, conditioning and lightning was accomplished by the end of November 2015.

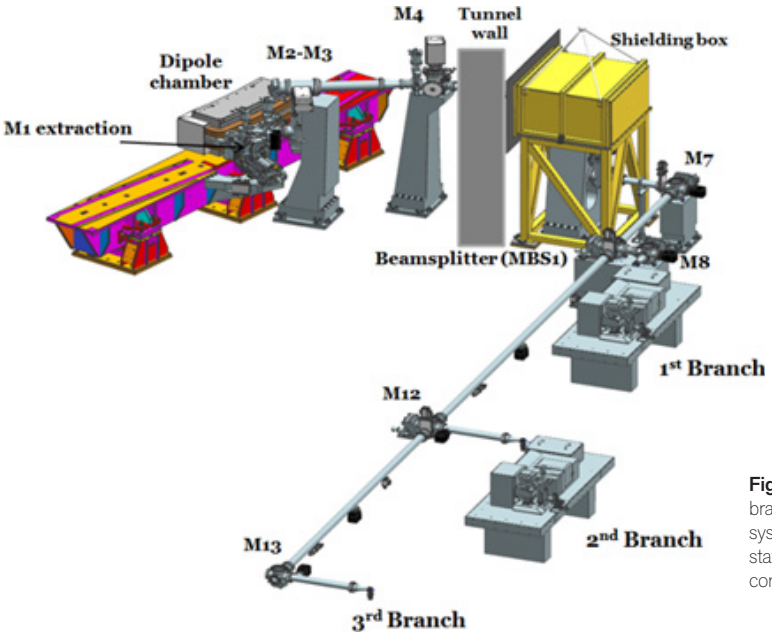

Figure 43: There are two endstations hosting the three branches. Two of these branches will be coupled to an FTIR system as indicated in the figure, the third branch will be free station, where the users can bring their own instrument and connect it to this branch.

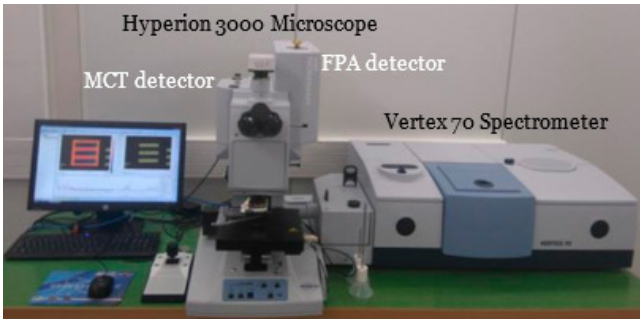

Figure 44: Hyperion 3000 Microscope coupled to a Vertex 70 Fourier transform IR spectrometer.

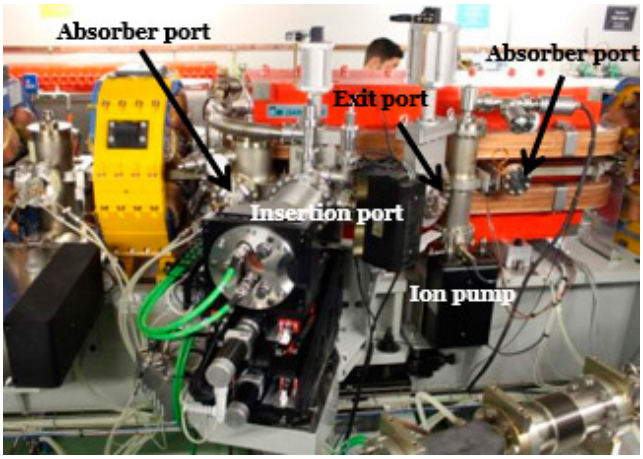

Figure 45: Installation of the extraction mirror assembly inside the tunnel in the dipole chamber.

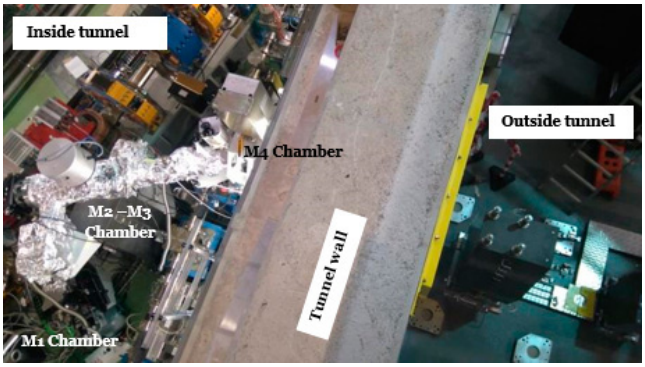

Figure 46: Installation process of the BL transport mirrors, chambers, ion pumps etc.

LOREA

The LOREA beamline will deliver photons with high resolution and high photon flux for Spin and Angle Resolved PhotoEmission Spectroscopy (S-ARPES). With this technique, the surface-parallel component of the dispersive electronic bands can be investigated in a very powerful way.

Usually, S-ARPES experiments are performed at low energies, 10-100eV, where the best energy and angle resolution can be obtained. However, such a small energy range can limit the quality of experiments, because the chemical analysis of samples (chemical composition and purity) cannot be performed with ARPES, and photons of higher energy are needed. The photon energy range in the original project was 10-350eV, which was subsequently increased to 600eV in order to have information on the occurrence of small amounts of Carbon or Oxygen in the samples (two of the most frequent "contaminants") and finally extended to 1000eV. In this way, a complete chemical analysis of samples with core level spectroscopy is possible, but also another ARPES technique, called soft X-ray (SX) ARPES, can be performed. SX-ARPES experiments are performed by scanning the photon energy in a wide range (about 200-300eV) and give information on the surface-perpendicular dispersion of the electronic bands. Thus, a complete set of measurements may deliver information on the electronic states both parallel and perpendicular to the surface. The increased photon energy range did not have any impact on the design of the insertion device (ID), since the same ID initially proposed for the low energy range could as well be used for photons up to 1000eV. The optical design, on the other hand, was adapted to guarantee the achievement of the large energy range (actually two order of magnitudes, from 10 to 1000eV) without any loss of performances at low energies.

In the last months, the project has advanced in two main directions. On one side, the assignment of the call for tenders for the purchase of the insertion device (an elliptically polarizing undulator with a period length of 125 mm – EPU125 – designed at ALBA by the ID section of the Accelerators division) and of the front end (FE) (also designed internally by the FE group of the Accelerators division) are on the way to be completed. Currently, the offers are being analyzed and discussed by all the sections involved and the contracts will be signed soon. Along with the schedule, the undulator should be installed in the straight section of BL20 during the shutdown of summer 2017, and the front end in the winter shutdown 2017/2018. The second major activity of the LOREA project is the design of the optical hutch and of the optical layout of the beamline. The optical hutch has been recently designed by the infrastructure section of the Engineering division in collaboration with the transversal section, the safety office and the optical section. The call for tenders for the optical hutch will start before summer 2016. The optical design is one of the most important and time-demanding activities of the first phase of the LOREA project, as it will influence the beamline performance and its daily utilization. After a careful evaluation of all possible optical solutions, the optical section of the experiments division completed a first design, which was sent to external experts for review. Afterwards, the call for tenders for the main optical items will be started.

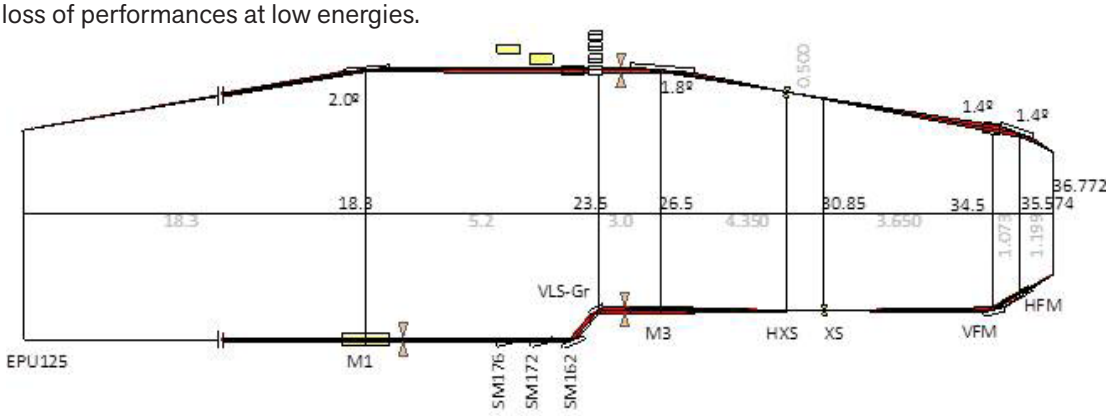

Figure 47: Sketch of the optical layout of the beamline. The first optical element (M1) is a flat mirror, whose function is to take most of the power from the beamline. This mirror will be installed inside the optical hutch. The following element is the monochromator, which includes three switchable spherical mirrors (SM176, SM172, and SM162) and four VLS plane gratings. Downstream from the monochromator is a plano-elliptic mirror (M3), which focuses the source horizontally at a plane (HXS) placed 0.5 m upstream from the exit slit. The beam is vertically focused by the monochromator mirrors at the exit slit plane (XS). Finally a KB mirror pair (VFM and HFM) refocuses the beam on the sample. Distances, sizes and incidence angles of the optical elements have been optimized by means of numerical simulations based on the analytic model of the beamline. The figure of merit for the optimization was to deliver maximum flux in a 10×10 μm2 spot at the sample position reaching the required energy resolution of 10000, still preserving reasonable sizes for mirrors, gratings and slits.

COLLABORATIONS, SEMINARS AND STUDENTS

The ALBA Synchrotron has continued its effort in 2015 to organize training activities and promote collaborations with external institutions with the aim of making progress in the development of science and technology.

COLLABORATIONS

ALBA is in close collaboration with other synchrotron facilities and research centres. Below are the most relevant new collaborations initiated in 2015.

Elettra Sincrotrone Trieste

Elettra Sincrotrone

Collaboration in the design and development of synchrotron components and beamline equipments.

Iranian Light Source Facility

ILSF (Iranian Light Source Facility) of the Institute for Research in Fundamental Sciences (Iran)

Design, development, construction and validation of components and systems in the field of particle accelerators and synchrotron beamlines.

CLIC-CERN

The Compact Linear Collider (CLIC) study is an international collaboration working on a concept for a machine to collide electrons and positrons head-on at energies up to several Teraelectronvolts (TeV). ALBA is involved in damping ring technologies, design and prototyping and test of the final equipment.

EuroCirCol A key to New Physics

EuroCirCol

This H2020 project is a conceptual design study for a post-LHC research infrastructure based on an energy-frontier 100 TeV circular hadron collider. ALBA's role is to contribute to managing accelerator developments, organising international events and to the vacuum chamber design.

Other ongoing collaborations

Also during 2015, ALBA has continued other collaborations established in previous years: CIEMAT-IFMIF, SESAME synchrotron facility - CERN, INFN - ELI-NP Romania, the Spanish Pulsed Lasers Centre, etc.

SEMINARS

One of the commitments of the ALBA Synchrotron is to share the knowledge and scientific outputs of synchrotron-based research and technology. In 2015, ALBA has been involved in the organisation of 53 events (30% more than in 2014).

ALBA hosted 25 invited speakers from other synchrotron facilities and research institutions. 10 workshops were organized in the area of accelerators, experiments, industrial applications or teaching resources for high schools. 5 internal events were organised for the ALBA staff. The events outside the ALBA facilities (13) considerably increased because of the celebration of the International Year of Light 2015.

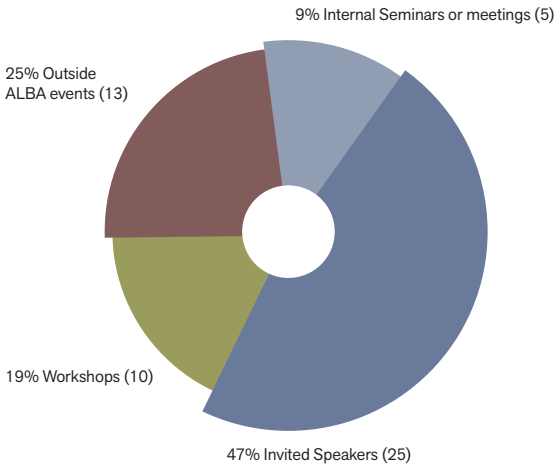

List of workshops organised or hosted by ALBA

21/04/2015	EuCARD-2 2nd Annual Meeting
7/05/2015	Industrial applications of synchrotron light for pharmaceutical companies
22/05/2015	Characterisation and analysis of cultural heritage material
15-16/06/2015	Diagnostics Experts of European Light Sources
16-19/06/2015	VII AUSE Congress and II ALBA User's Meeting
19/06/2015	Workshop on X-ray Photoemission Electron Microscopy (X-PEEM) at ALBA
19/06/2015	Workshop on High pressure powder diffraction at ALBA
21-23/10/2015	Specialization course for high school teachers
16-20/11/2015	WIEN2k & Turbomole Workshop
30/11/2015 - 02/12/2015	Joint MxCuBE & ISPyB meeting

STUDENTS

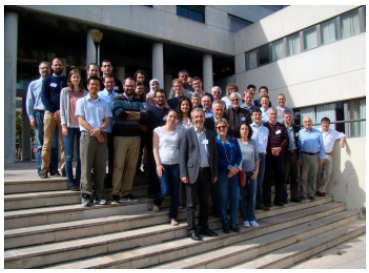

Photo of the poster session at the VII AUSE Congress and II ALBA Users' Meeting. Next, presentation of Ana Joaquina Pérez, from the MISTRAL beamline, during the industrial workshop. Group photo of the participants at the EuCard-2 meeting.

Check the complete list of events at http://www.albasynchrotron.es/en/media/events012

Training programs for students have been settled and systematized in the last years in ALBA. Four categories are identified, with gradual growth year after year.

Undergraduate internships

A total of 14 university undergraduate students had the opportunity to do internships at ALBA during 2015. They were trained in different disciplines: accelerators' technologies, scientific applications of synchrotron light, health & safety, engineering, computing and control and science communication and outreach.

Vocational training

Students from eight technical schools of the neighbouring area are trained in ALBA for the whole academic year sharing the time between the classroom and hands-on activities in the facility. Eight students took part during the course 2014-2015 and 9 during the course 2015-2016.

PhD students

Six students have been performing their PhD at ALBA during 2015. Three of them are working in the Experiments division in radiation damage in X-ray crystallography, RF plasma sources for optical surface cleaning and graphene/nanosystem thin film deposition and surface properties of metal nanoparticles under reaction conditions in the NAPP endstation. The other three students are working in the Accelerators division in electron beam diagnostics, linear and non-linear beam dynamics and radiofrequency.

Teaching activities

Members of the ALBA staff also do university teaching activities related to accelerators' physics and scientific applications of synchrotron light: Physics degree at the Universitat Autònoma de Barcelona (UAB), master on Nanoscience and Nanotechnology also from UAB and tutoring final grade projects at Universitat Politècnica de Catalunya (UPC).

Some of the undergraduate and vocational training students in 2015.

OUTREACH

2015, the year of Light

Since 2015 was designated by the UNESCO as the International Year of Light and Light-based Technologies (IYL2015), the outreach activities developed by ALBA in this period have been especially intense in order to communicate to the society as a whole the impact of light in areas such as energy, education, health or communications.

The ALBA Synchrotron has been an active member of the Spanish Committee for the IYL2015, which was in charge of coordinating and promoting different events to celebrate light in the country. In close collaboration with the president and other members of the Spanish Committee, ALBA has actively participated in the Spanish opening and closing ceremonies.

The involvement of ALBA in the organization of many activities to promote the IYL2015 has taken place at international, national and local levels. Different members from ALBA had the opportunity to deliver talks about the nature of light, the study of matter with (synchrotron) light, and many other related topics. These conferences have been addressed to different targets of non-experts, and took place in libraries, universities, science festivals but also in pubs or museums, reaching more than 3,000 people. The presence in mainstream media has also been remarkable, bringing the general public closer to the outstanding capabilities of light as a research instrument. Consolidated outreach activities like the Visits Program (which hosted more than 4,500 people in 2015, half of them high school students) or another successful edition of the ALBA Open Day (with 1,903 participants) included new activities specially designed to explain light and its properties. The celebration of light in 2015 has been horizontally shared among the staff, with a nice collection of photographs taken by members of the facility.

ALBA organized for the second year in a row the European Researchers' Night on the last Friday of September in order to bring the science of synchrotron light to the city of Cerdanyola del Vallès, where our facility is located. The event gathered 650 people who enjoyed an evening of free outreach activities organized in recognition of the IYL2015.

As part of the effort to get closer to people who are not familiar with synchrotron facilities, a new exhibition about the ALBA Synchrotron was launched in 2015 at Cosmocaixa, the science museum of Barcelona managed by "la Caixa" Foundation. About 750,000 people have had the opportunity to visit the exhibition in 2015.

The celebration of the International Year of Light and Light-based Technologies in 2015 has been the central issue of the different outreach initiatives of the ALBA Synchrotron. Coincidence or not, ALBA's new address is, from 2015, Carrer de la Llum (Light Street in Catalan).

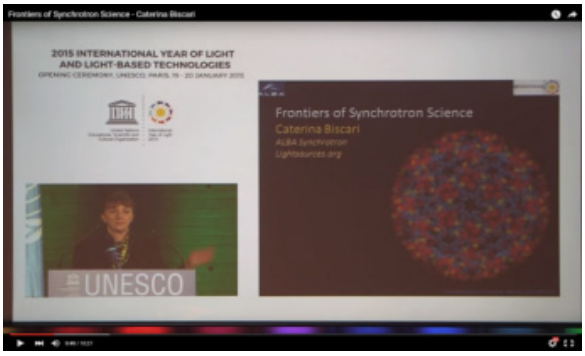

Conference of Caterina Biscari during the opening ceremony of the International Year of Light 2015 on 19th and 20th January in Paris.

The Spanish Opening Ceremony of the International Year of Light took place in Barcelona on the 16th of February with the participation of 500 attendees.

El País – Materia - http://elpais.com/elpais/2015/07/31/ciencia/1438353280_918260.html

UNED – LA 2 - https://www.youtube.com/watch?v=Pj2wy-HTUVw&feature=youtu.be

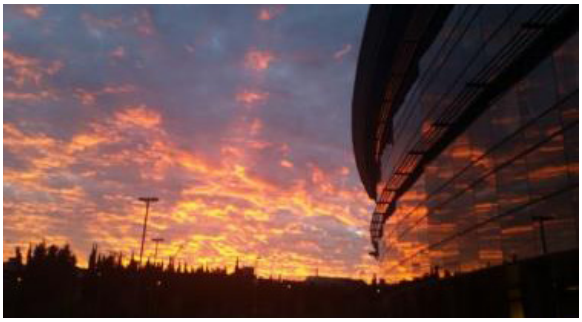

Picture from Laura Campos (Administration division) to celebrate light in 2015.

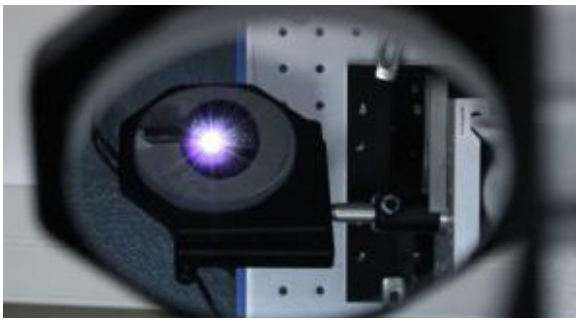

Picture from Jon Ladrera (Engineering division) to celebrate light in 2015.

MACHINE OPERATION

	2012	2013	2014	2015
Scheduled hours for BLs	3112.0 h	3539.5 h	3740.0 h	4320.0 h
Delivered hours for BLs	2387.3 h	2971.5 h	3621.2 h	4201.5 h
Beam availability	76.7%	84.0%	96.8 %	97.3 %
Hours for machine development	1144.0 h	1368.0 h	1352.0 h	1408.0 h
Mean time between failures	21.0 h	25.0 h	33.7 h	51.0 h
Mean time to be back	1.0 h	0.8 h	1.1 h	1.4 h

The ALBA Storage Ring has run more than 4300 h for users in 2015 with a beam availability of 97.3%. The Storage Ring runs on a 24 h a day, 7 days a week basis, for periods that usually are 4 to 5 weeks long. About 1400 h have been dedicated to the optimization of the accelerators for the users as well as to test new developments.

In 2015, the injection in top-up mode has been consolidated at 130 mA. In agreement with the beamlines, new injections to refill are scheduled every 20 min. The amount of current injected is 1-2% of the nominal current and it takes 10 s or less to complete the refilling.

In May 2015, a fast orbit feedback system (FOFB) came into regular operation, stabilising the photon beam at the source location at frequencies up to 100 Hz. More details about the FOFB development can be found elsewhere in this annual report. The immediate conclusion of this development is that now the orbit in the Storage Ring is stable to better than 600 nm(rms) in the horizontal plane and 100 nm(rms) in the vertical plane; in other words, the electron beam is stable to less than 1% of its beam size (at the medium straight), making ALBA one of the most stable synchrotron facilities worldwide.

An additional development, a bunch-by-bunch transverse feedback system, has also started operating in 2015. Figure 49 shows a schematic overview of the feedback system, which has been set up in collaboration with Diamond Light Source.

This system fights electron beam instabilities on a bunch-by-bunch basis, acting directly on the individual bunches by damping high frequency oscillations (up to 250 MHz) that may affect the brilliance of the photon beam.

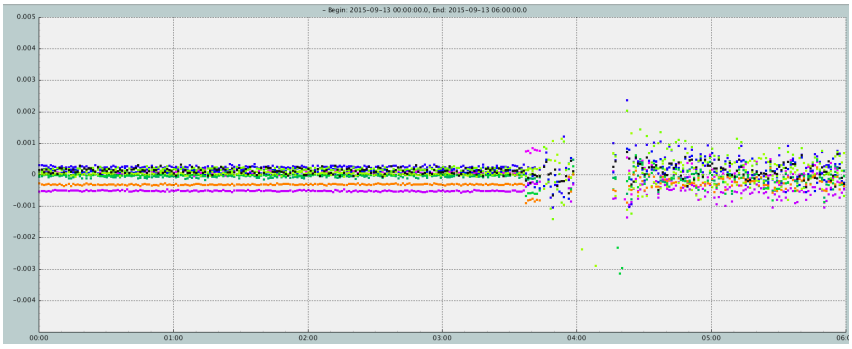

Figure 48: Storage Ring beam position during 6 h, as read by the BPMs, to the left while the FOFB is running (between 00:00 and 03:00), to the right while the previous correction system (SOFB) is running (between 04:00 and 05:00).

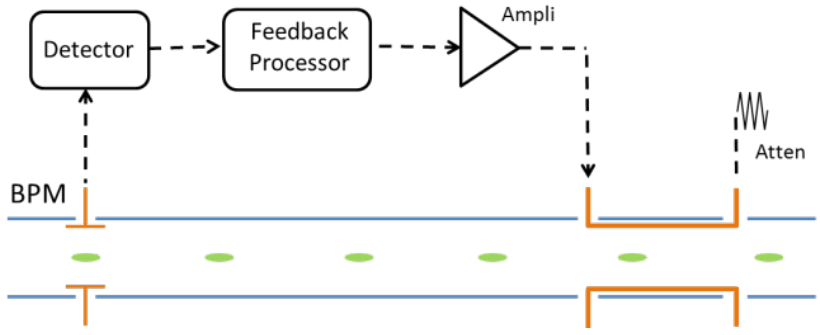

Figure 49: schematics of the BbB transverse feedback system.

USERS

In 2015 the ALBA Synchrotron has started two allocations periods per year covering the first and second semester. 2015-I call was launched from 5th June 2014 till 7th July 2014 and covered the period from January to June 2015 (with the exception of BL13-XALOC which covered the full year, from January to December 2015). 2015-II call was opened from 26th January till 23rd February 2015 and covered the period July to December 2015.

Again this year, the number of proposals and shifts has increased. A total of 335 proposals were submitted (34% more than in 2014) and 4980 shifts were requested (58% more than in 2014). All the proposals for experiments are peer reviewed. They are evaluated by a panel, composed of international experts from different research areas. As a result of a ranking based on scientific excellence criteria, 187 proposals and 2148 shifts were awarded, representing an oversubscription factor of 2.35.

In 2015, according to the number of proposals and shifts requested, the most demanded beamline was BL24- CIRCE, the Photoemission Spectroscopy and Microscopy beamline. The largest number of granted proposals and awarded shifts was for BL04-MSPD, the Materials Science and Powder Diffraction beamline.

Most of the granted proposals correspond to Spanish institutions (65%). European institutions represent 31% and non-European countries 4%. The Spanish granted proposals are distributed as follows: 39% Catalonia, 27% Madrid, 16% Comunitat Valenciana, 8% Basque Country, 5% Andalusia and other regions from Spain (5%).

Regarding the research areas of the granted shifts, experiments from Hard Condensed Matter and Electronic and Magnetic properties have been the most granted (26%), followed by Materials Science and Structure (21%), Chemistry (19%), Macromolecular Crystallography (13%), Biology (12%), Soft Condensed Matter and Biomaterials (6%) and Environment and Cultural Heritage (3%).

COMPARISON OF SUBMITTED AND GRANTED PROPOSALS AND SHIFTS

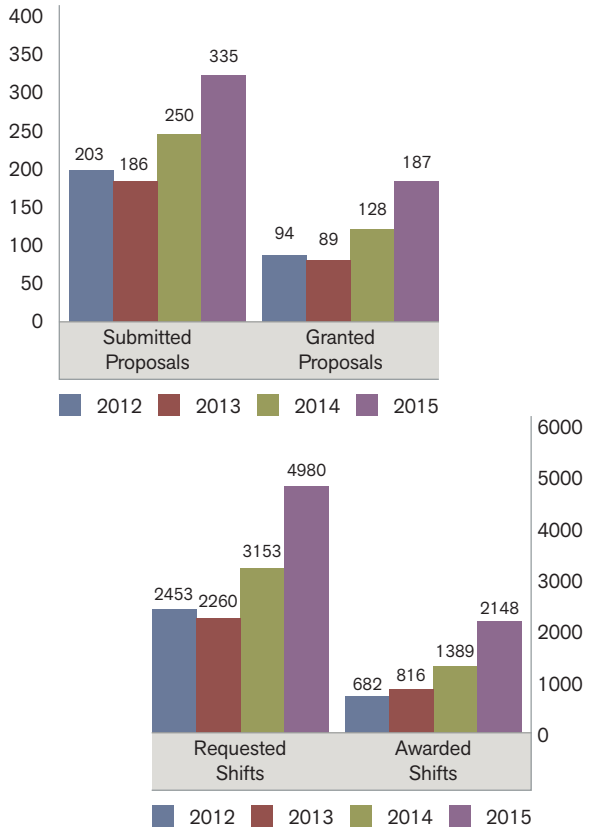

2015 PROPOSALS

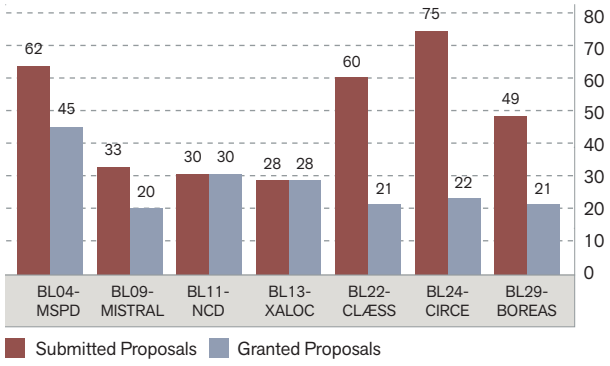

2015 SHIFTS

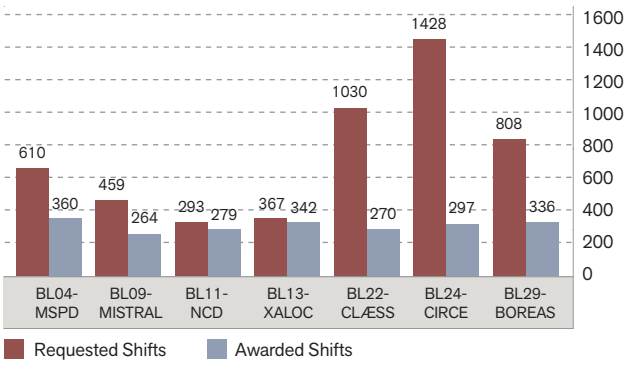

COUNTRY OF ORIGIN OF 2015 PROPOSALS

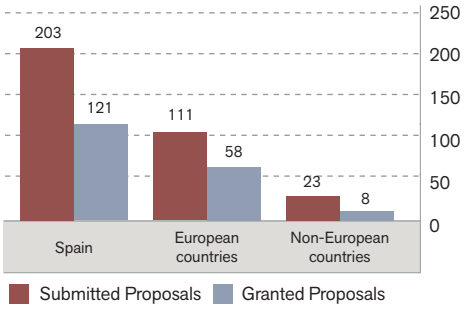

COUNTRY OF ORIGIN OF 2015 SHIFTS

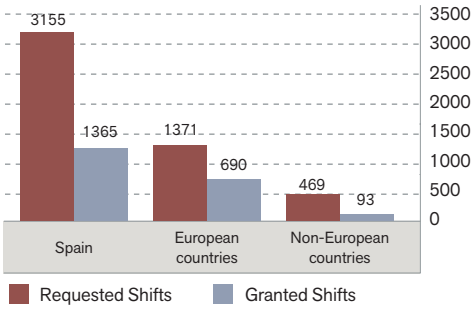

EVOLUTION OF INTERNATIONAL USERS %

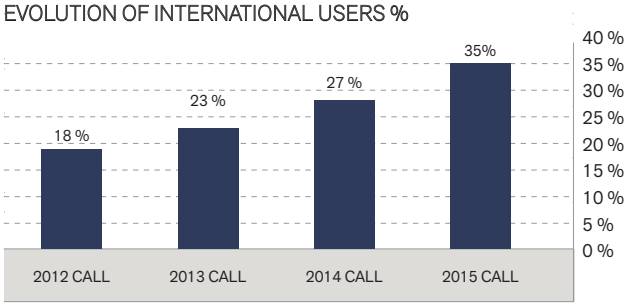

2015 SPANISH GRANTED SHIFTS BY REGION

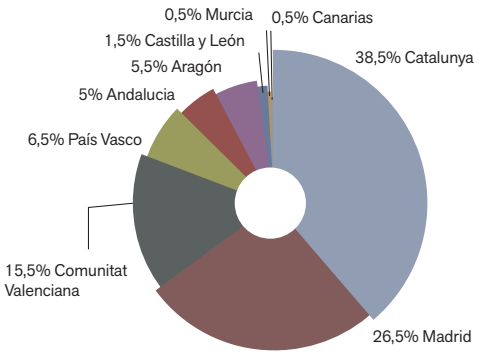

2015 RESEARCH AREAS OF ALL GRANTED SHIFTS

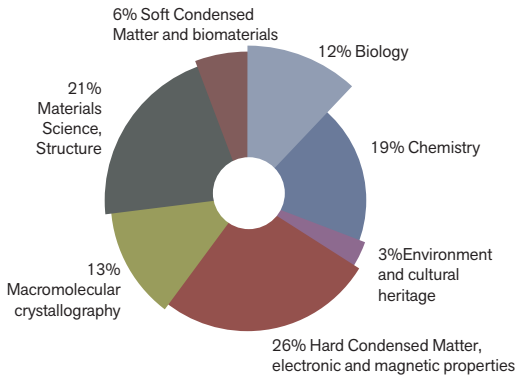

EVOLUTION OF NUMBER OF VISITS / EXPERIMENTS

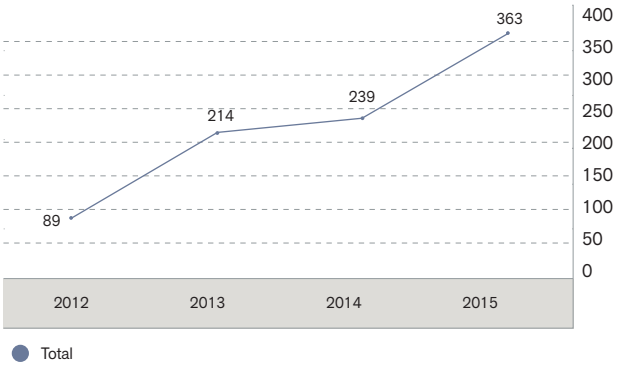

PUBLICATIONS

Since the start of the operation of the ALBA Synchrotron in May 2012, the number of publications has been growing steadily. In 2015, a total of 90 papers have been registered which involved beamtime at ALBA. Some of them have been published in the most renowned journals such as Science. 2015 has also witnessed the first publications from industrial users.

ALBA ACADEMIC BEAMTIME PUBLICATIONS

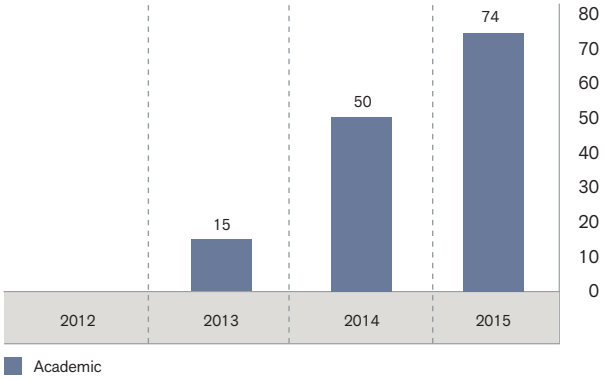

ALBA BEAMTIME PUBLICATIONS

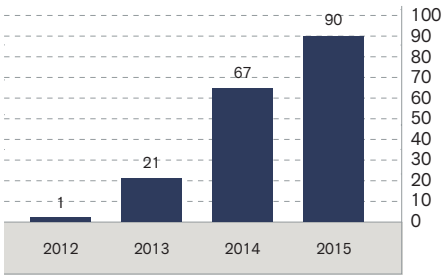

The updated complete list of publications is available at: www.albasynchrotron.es/en/science-at-alba/publications

HEALTH & SAFETY

During 2015 several changes have occurred in ALBA's Health & Safety Office. A reorganization of the two groups of the Health & Safety Office (the Radiation Protection Service and the Occupational Health and Safety Group) has been carried out, including the appointment of a new Safety Officer to cover the vacancy of the former head of office and a new Radiation Protection Officer by the Spanish Nuclear Safety Council (NSC) and by the ALBA Synchrotron.

Regarding the radioprotection service, radiation levels produced at the facility have not surpassed the public access area level for ionising radiation during 2015. The first part of the year was devoted to the shielding calculation and licensing process for the eighth ALBA Beamline, MIRAS, the authorisation to start the commissioning of which was successfully obtained in May. In turn, the calculations for the LOREA beamline, to be constructed during 2017, also started.

A new External Prevention Service was contracted at the beginning of January, and an Audit was programmed to determine the Occupational Health and Safety aspects that have to be improved and changed in order to more accurately follow the principles established by the current Spanish legislation. An Action Plan has been established and approved by our technical staff and the ALBA management board, respectively, to introduce the priorities resulting from the Audit.

In the last part of 2015 Good Laboratory Practices have been introduced (preparation of Work Instructions, Risk Evaluation, Working Norms in the Laboratories as a support for the daily activity, and the establishment of a method to make this information available to everybody related to the work areas) in the Biology Laboratories and in the Materials Science Laboratory.

It has also been proposed, accepted and carried out, to place in the control hutch doors a signal indicating the colour flag of the experiments being conducted at each moment (for the yellow and red-labelled experiments) as well as the "Safety Lab Access Register" to offer the information about the ongoing experiment.

Different training activities have been performed during the year, including 10 new operators and the first 6 floor coordinators.

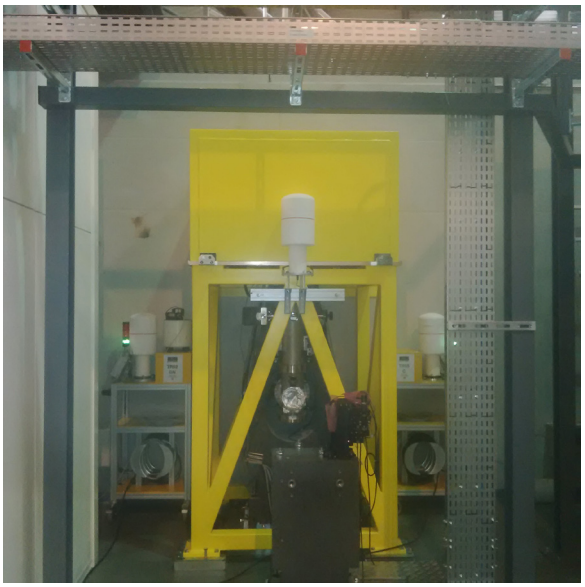

MIRAS shielding and radiation monitors.

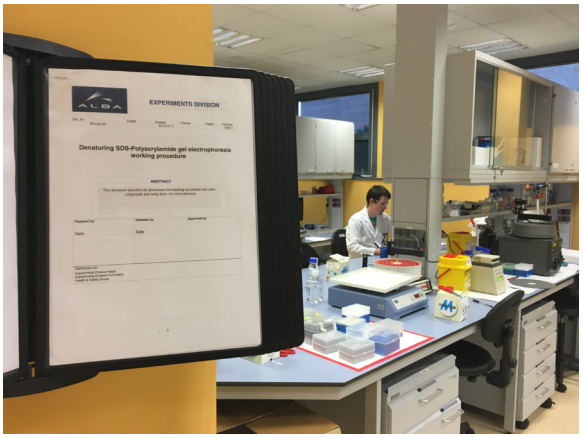

Example of Good Laboratory Practice in the Biology laboratory.

HUMAN RESOURCES

As of 31st December 2015, the staff of the ALBA Synchrotron is composed of 195 members, organized in five different divisions: Accelerators (14%), Administration (8%), Computing & Control (25%), Experiments (25%), and Engineering (19%). In addition, there is a Director's Office (9%) and the president of the ALBA Executive Committee.

56% of ALBA staff are technologists, 29% scientists, 15% administrative, management staff and health and safety staff.

Although some minor improvements have been achieved in this area, still today gender distribution is not proportional in the ALBA Synchrotron. Women represent 26% of ALBA staff. As in previous years, areas like administration or the director's office have more women, while, in technical and scientific divisions, they are underrepresented.

Regarding the nationality of the staff, 81% is Spanish – in some cases people who used to work in other synchrotron facilities and have come back from foreign countries -, 16% are from European countries and 3% from other countries, with people from Asia, Africa and America.

ALBA STAFF - DISTRIBUTION OF CATEGORIES

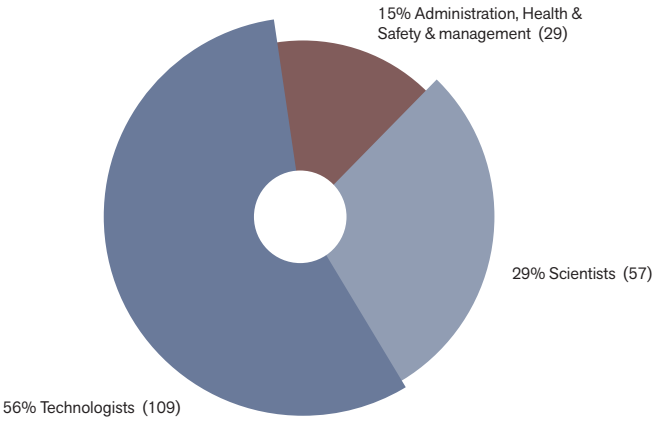

ALBA STAFF - DISTRIBUTION OF DIVISIONS AND GENDER

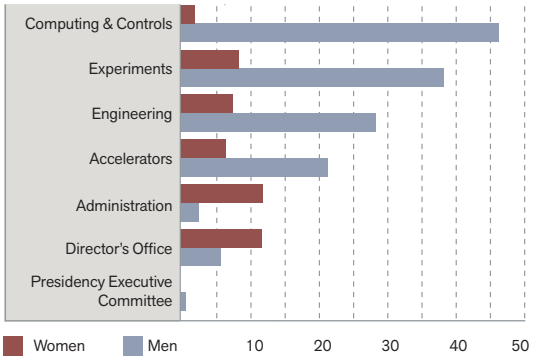

ALBA STAFF - DISTRIBUTION OF DIVISIONS

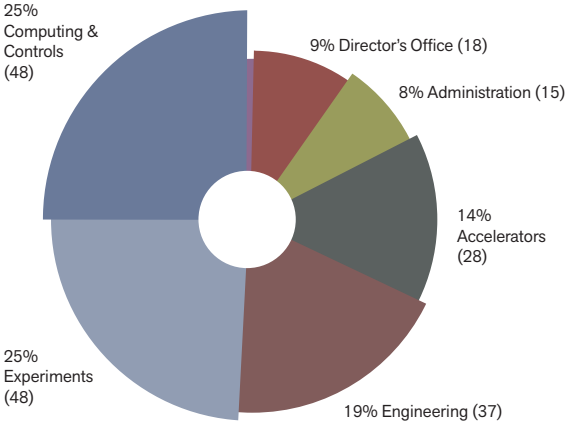

ALBA STAFF - DISTRIBUTION OF NATIONALITIES

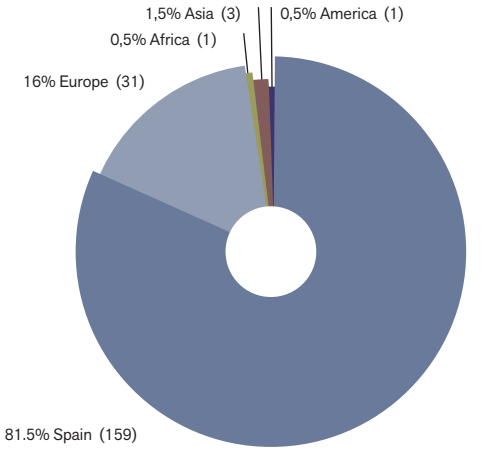

2015 SCIENTIFIC ADVISORY COMMITTEE

The ALBA Scientific Advisory Committee (SAC) is a board of internationally renowned experts in the field of synchrotron radiation, which participates in the strategic scientific management of the ALBA Synchrotron with the aim of ensuring the quality and relevance of the research developed in ALBA. The ALBA SAC meets twice per year including an open session for the staff. The 20th meeting of the SAC was held the 20th of June 2015. The 21st meeting of the SAC was held the 10th of December 2015. These were its members in the 21st meeting:

IAN ROBINSON, CHAIR

Full permanent professor at the London Centre for Nanotechnology

WIM BRAS

Project leader of DUBBLE CRG-BL at the European Synchrotron Radiation Facility (ESRF)

ANDREAS JANKOWIAK

Director of the Institute of Accelerated Physics at the Helmholtz Zentrum Berlin

PETER GUTTMANN

X-ray microscopy beamline scientist at U41-XM (BESSY II)

MARTÍN MARTÍNEZ RIPOLL

Research Professor at the Institute of Physical-Chemistry "Rocasolano", Department of Crystallography

AMOR NADJI

Director of Sources and Accelerators Division at Soleil Synchrotron

ENRIQUE ORTEGA

Full permanent professor at the Universidad del País Vasco, Department of Applied Physics I

SAKURA PASCARELLI

Head of ID24 beamline Energy dispersive X-ray absorption spectroscopy of the European Synchrotron Radiation Facility (ESRF)

NICK TERRILL

Principal Beamline Scientist of the Small Angle beamline I22 of Diamond Light Source, UK

TRINITAT PRADELL

Full permanent professor at the Universitat Politècnica de Catalunya, Physics Department and Centre for Research in NanoEngineering (CRNE)

FINANCIAL INFORMATION

INCOME		
Capital funding	18,040,399 €	76.61%
Services revenue	449,708 €	1.91%
Agreements	182,628 €	0.78%
National grants	137,100 €	0.58%
European grants	169,000 €	0.72%
Other	4,568,783 €	19.40%
TOTAL	23,547,618 €	100.00%
EXPENDITURE		
Staff	7,732,736 €	32.84%
Social costs	2,018,837 €	8.57%
Equipment and maintenance	1,083,848 €	4.60%
Recurrent costs	4,675,899 €	19.86%
Taxes	40,071 €	0.17%
Financial costs	8,870 €	0.04%
Users' support	291,693 €	1.24%
Students grants	63,927 €	0.27%
Expenses	336,179 €	1.43%
Other operational expenses	2,003,287 €	8.51%
Investments	5,292,271 €	22.47%
TOTAL	23,547,618 €	100.00%

2015 INCOME

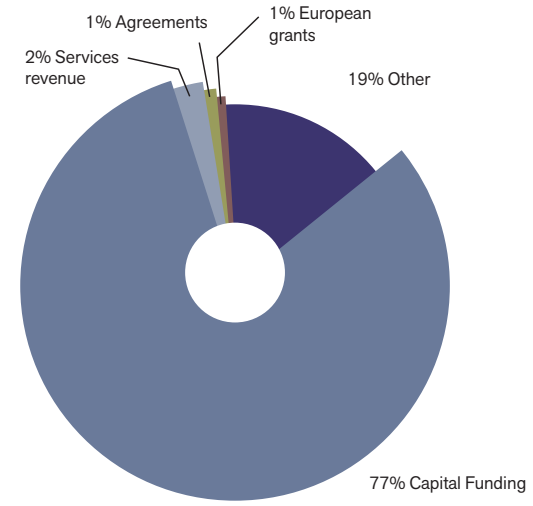

2015 EXPENDITURE